Primary and Secondary Frequency Control Techniques for Isolated Microgrids

by

Mostafa Farrokhabadi

A thesis
presented to the University of Waterloo
in fulfillment of the
thesis requirement for the degree of
Doctor of Philosophy
in
Electrical and Computer Engineering

Waterloo, Ontario, Canada, 2017

I hereby declare that I am the sole author of this thesis. This is a true copy of the thesis, including any required final revisions, as accepted by my examiners.

I understand that my thesis may be made electronically available to the public.

Abstract

Isolated microgrids have been shown to be a reliable and efficient solution to provide energy to remote communities. From the primary control perspective, due to the low system inertia and fast changes in the output power of wind and solar power sources, isolated microgrids' frequency can experience large excursions and thus easily deviate from nominal operating conditions, even when there is sufficient frequency control reserves; hence, it is challenging to maintain frequency around its nominal value. From the secondary control perspective, the generation scheduling of dispatchable units obtained from a conventional Unit Commitment (UC) are considered fixed between two dispatch time intervals, yielding a staircase generation profile over the UC time horizon; given the high variability of renewable generation output power, committed units participating in frequency regulation would not remain fixed between two time intervals. The present work proposes techniques to address these issues in primary and secondary frequency control in isolated microgrids with high penetration of renewable generation.

In this thesis, first, a new frequency control mechanism is developed which makes use of the load sensitivity to operating voltage and can be easily adopted for various types of isolated microgrids. The proposed controller offers various advantages, such as allowing the integration of significant levels of intermittent renewable resources in isolated/islanded microgrids without the need for large energy storage systems, providing fast and smooth frequency regulation with no steady-state error, regardless of the generator control mechanism. The controller requires no extra communication infrastructure and only local voltage and frequency is used as feedback. The performance of the controller is evaluated and validated using PSCAD/EMTDC on a modified version of the CIGRE benchmark; also, small-perturbation stability analysis is carried out to demonstrate the contribution of the proposed controller to system damping.

In the second stage of the thesis, a mathematical model of frequency control in isolated microgrids is proposed and integrated into the UC problem. The proposed formulation considers the impact of the frequency control mechanism on the changes in the generation output using a linear model. Based on this model, a novel UC model is developed which yields a more cost efficient solution for isolated microgrids. The proposed UC is formulated based on a day-ahead scheduling horizon with Model Predictive Control (MPC) approach. To test and validate the proposed UC, the realistic test system used in the first part of the thesis is utilized. The results demonstrate that the proposed UC would reduce the operational costs of isolated microgrids compared to conventional UC methods, at similar complexity levels and computational costs.

Acknowledgement

First and foremost, I would like to express my sincere gratitude to my supervisors, Professor Claudio A. Cañizares and Professor Kankar Bhattacharya for their guidance, patience, and support throughout my PhD studies. Under their supervision, I have learnt beyond the boundaries of power and energy systems. It has been my privilege to have completed my studies under their supervisions, and they continue to be my role model in professionalism and class throughout my life.

I would like to acknowledge the following members of my committees for their valuable support: Professor Mehrdad Kazerani, Professor Christopher Nielsen, and Prof. Tarek El-Fouly from the Department of Electrical and Computer Engineering, University of Waterloo; Professor Jatin Nathwani from the Department of Civil and Environmental Engineering and Management Sciences, University of Waterloo; and Professor Reza Iravani from the Department of Electrical and Computer Engineering, University of Toronto.

I wish to acknowledge the University of Waterloo, Natural Sciences and Engineering Research Council (NSERC) Strategic Grants and NSERC Smart Microgrid Research Network (NSMG-Net) for providing the funding necessary to carry out this research.

I am always grateful for the support of my friends through the up and downs of these past few years. Special thanks to Aref, Bahare, Ehsan, Hootan, Mehrdad, and Mauricio for being great friends throughout the years. I also acknowledge my officemates for their friendship in the EMSOL lab: Summit, Behnam, Daniel, Mariano, Isha, Nafeesa, Indrajit, Amir, Bharat, Fabian, Ivan, Juan Carlos, Edris, Victor, Edson, David, Sofia, Chioma, Alfredo, Akash, Dario, Fabricio, Felipe, Jose, Rajib, Rupali, and Shubha for all technical discussions, and for all the fun we have had during the last few years. Thank you all for creating a pleasant and friendly working environment in the lab.

Finally, I would like to thank my family and dedicate this thesis to my mom Zari, my dad Mohammad, my sister Maryam, and my brother-in-law Saeed for their unconditional love and support through all these years. Thank you for all the sacrifices you made, the life principles you taught me and the comfort you provided me.

You can know the name of a bird in all the languages of the world, but when you're finished, you'll know absolutely nothing whatever about the bird... So let's look at the bird and see what it's doing, that's what counts. I learned very early, the difference between knowing the name of something and knowing something.

- R. P. Feynman

Table of Contents

List of Tables

List of Figures

Nomenclature

Chapter 2, Chapter 3, and Chapter 4

C_f Inverter output filter capacitor (F)

C_{max} Maximum servo Position (gorvernor) (pu)

C_{min} Minimum servo position (gorvernor) (pu)

D Damping coefficient (pu)

Δf System frequency deviation (pu)

ΔP_D Net electrical power demand (pu)

ΔP_g Governor input power changes (pu)

ΔP_{in} System electrical generation (pu)

ΔP_L Changes in the system electrical load (pu)

ΔP_{ref} Synchronous machine reference power (pu)

ΔP_v Changes in the turbine valve position (pu)

δ Power angle (rad)

δ_n Nominal voltage angle (rad)

δ_o Operating voltage angle (rad)

H Inertia constant (s)

I_p Constant current load coefficient

i_o Inverter line current

K_A Amplifier gain

K_E Exciter gain

K_G Synchronous machine gain

K_g Inverse of droop (governor) (pu)

K_I VFC integrator gain

K_{I_c} Inverter current controller integrator gain

K_{I_v} Inverter voltage controller integrator gain

K_P VFC proportional gain

K_{P_c} Inverter current controller proportional gain

K_{P_v} Inverter voltage controller proportional gain

K_R Sensor gain

K_{VFC} VFC gain

L_f Inverter output filter inductor (H)

$\hat{m}_p$ Transient active power droop coefficient in inverter control (pu)

m_δ Angle droop coefficient in inverter control (pu)

m_p Active power droop coefficient in inverter control (pu)

$\hat{n}_q$ Transient reactive power droop coefficient in inverter control (pu)

n_P Load voltage index for active power

n_Q Load voltage index for reactive power

n_q Reactive power droop coefficient in inverter control (pu)

P Inverter fundamental frequency active output power (pu)

p Inverter instantaneous active output power (pu)

P_e Synchronous Machine output electrical power (pu)

P_L Load active power demand (pu)

P_{L0} Load rated active power demand (pu)

P_m Synchronous Machine driving mechanical power (pu)

P_p Constant power load coefficient

P_{up} Maximum opening rate (governor) (pu)

P_{down} Maximum closing rate (gorvernor) (pu)

Q Inverter fundamental frequency reactive ourpur power (pu)

q Inverter instantaneous reactive output power (pu)

Q_L Load reactive power demand (pu)

Q_{L0} Load rated reactive power demand (pu)

R Speed droop regulation (pu)

R_a Stator resistance (synchronous machine) (pu)

$\bar{R}_i$ Output residue of mode i

R_f Inverter output filter resistor (Ω)

V_e Amplifier input voltage (pu)

V_F Synchronous machine field voltage (pu)

V_L Load operating voltage (pu)

V_{L0} Load nominal operating voltage (pu)

V_n Nominal voltage magnitude (pu)

v_o Inverter output voltage (pu)

V_R Exciter input voltage (pu)

V_S Sensor measured voltage (pu)

V_t	Synchronous machine terminal voltage (pu)
X	Synchronous reactance (synchronous machine) (pu)
X_l	Stator leakage inductance (synchronous machine) (pu)
X'	Transient reactance (synchronous machine) (pu)
X''	Sub-transient reactance (synchronous machine) (pu)
T'_0	Transient time constant (synchronous machine) (pu)
T''_0	Sub-transient time constant (synchronous machine) (pu)
Z_p	Constant impedance load coefficient
α_i	Real part of eigenvalue i
β_i	Imaginary part of eigenvalue i
ω	System electrical angular velocity (Rad/s)
ω_{FL}	Full-load steady-state speed (Rad/s)
ω_n	Reference angular velocity (Rad/s)
ω_{NL}	No-load steady-state speed (Rad/s)
ω_o	Inverter output angular velocity (Rad/s)
ω_s	Synchronous machine electrical angular velocity (Rad/s)
λ_i	Eigenvalue i
τ_1	VFC lead time constant (s)
τ_2	VFC lag time constant (s)
τ_A	Amplifier time constant (s)
τ_E	Exciter time constant (s)
τ_T	Turbine mechanical delay time constant (s)
τ_G	synchronous machine time constant

τ_g Governor time constant (s)

τ_R Sensor time constant (s)

τ_{SR} Speed relay time constant (governor) (s)

τ_{SM} Gate servo time constant (governor) (s)

Chapter 5

Indices and Superscripts

g Generation units

i, j Microgrid asset

k Time step

r Renewable generation units

s ESS units

Sets

$\mathcal{F}$ Dispatchable units that participate in frequency control

$\mathcal{G}$ Generation units

$\mathcal{P}$ Dispatchable units that do not participate in frequency control

$\mathcal{R}$ Renewable generation units

$\mathcal{S}$ ESS units

$\mathcal{T}$ Time steps

$\mathcal{T}_1, \mathcal{T}_2$ Subsets of $\mathcal{T}$

$\mathcal{T}^*$ Time steps excluding the first step

Parameters

a_i Quadratic term of cost function of diesel engine i (\$/kW^{2}h)

b_i Linear term of cost function of diesel engine i (\$/kWh)

c_i Constant term of cost function of diesel engine i (\$/h)

Csh_i^g Shut-down cost of diesel engine i (\$)

Cst_i^g Start-up cost of diesel engine i (\$)

D_k Net demand at time step k (kW)

E_k Required energy for dispatch time interval k (kWh)

ID_i Inverse of droop of dispatchable unit i (kW/Hz)

MD_i^g Minimum down-time of dispatchable unit i (h)

MU_i^g Minimum up-time of dispatchable unit i (h)

$P_{i,k}^r$ Forecasted power output of renewable unit i at time step k (kW)

$P_{L,k}$ Loading at time step k (kW)

$\bar{P}_i^g$ Maximum output power of generation unit i (kW)

$\underline{P}_i^g$ Minimum output power of generation unit i (kW)

$\bar{P}_i^s$ Maximum charging/discharging power of storage unit i (kW)

$\bar{R}_i^g$ Maximum ramp-rate of dispatchable unit i (kW/5-min)

$\underline{R}_i^g$ Minimum ramp-rate of dispatchable unit i (kW/5-min)

R_i Droop of dispatchable unit i (Hz/kW)

RES_k Spinning-up reserve limit at time step time k (kW)

$\overline{SoC}_i$ Maximum state of charge of ESS i (kWh)

$\underline{SoC}_i$ Minimum state of charge of ESS i (kWh)

$\Delta\tau$ Dispatch interval (5 min.)

ΔP_L Load change (kW)

ΔP_i^r Power output change of renewable generation unit i (kW)

ΔP_{ref} Reference power change of the dispatchable unit i

η_i Charging/discharging efficiency of ESS i

Variables

$\alpha_{i,j,k}^g$ Auxiliary variable for diesel engines i and j at time step k (kW)

$\omega_{i,k}^g$ Binary variable for unit commitment decision of dispatchable unit i at time step k

$d_{i,k}^s$ Binary variable for ESS i representing the discharging(1)/charging(0) status at time step k

$u_{i,k}^g$ Start-up decision binary variable for diesel engine i at time step k

$v_{i,k}^g$ Shut-down decision binary variable for diesel engine i at time step k

C_i^g Cost function of dispatchable unit i (\$/h)

$C\tau_i^g$ Cost of energy delivered by dispatchable unit i during dispatch time interval k (\$)

$P_{i,k}^g$ Power output of diesel engine i at the beginning of time step k (kW)

$P_{i,k}^{s,chg}$ Charging power of ESS i at time step k (kW)

$P_{i,k}^{s,dch}$ Discharging power of ESS i at time step k (kW)

$P_i^g(t)$ Time-domain function of power output of diesel engine i over a certain dispatch interval (kW)

$Pa_{i,k}^g$ Auxiliary variable for power output of diesel engine i at the end of the time step k (kW)

$PE_{i,k}^g$ Power output of diesel engine i at the end of the time step k (kW)

$OC_{i,k}^g$ Total operating cost of dispatchable unit i during dispatch time interval k (\$)

$SoC_{i,k}$ SoC of ESS i at time step k (kWh)

Δf_k Frequency change during during dispatch time interval k (Hz)

$\Delta P_{i,k}^{g}$ Power output change of diesel engine i at the end of dispatch time interval k due to changes in D_k (kW)

List of Acronyms

AVR	Automatic Voltage Regulator
CCM	Current Control Mode
CERTS	Consortium for Electric Reliability Technology Solutions
DDC	Dynamic Demand Control
DERs	Distributed Energy Resources
DG	Distributed Generation
EMS	Energy Management Systems
ESS	Energy Storage Systems
FC	Fuel Cell
GPS	Global Positioning System
ILS	Isochronous Load Sharing
MGCC	MicroGrid Central Controller
MILP	Mixed Integer Linear Programming
MIQP	Mixed Integer Quadratic Programming
MINLP	Mixed Integer Non-Linear Programming
MPC	Model Predictive Control
MPPT	Maximum Power Point Tracking
OPF	Optimal Power Flow
PCC	Point of Common Coupling
PSS	Power System Stabilizer
PV	Photovoltaic

RES	Renewable Energy Resources
SCADA	Supervisory Control and Data Acquisition
SoC	State-of-Charge
SPWM	Sinusoidal Pulse Width Modulation
UC	Unit Commitment
VCM	Voltage Control Mode
VSC	Voltage-Sourced Converter
VFC	Voltage-based Frequency Controller

Chapter 1

Introduction

1.1 Motivation

Traditionally, electricity is produced in a few central generation plants of significant capacity of a few gigawatts, and transmitted and distributed to local consumers. With the arrival of renewable energy technologies, this generation paradigm is gradually changing, and the focus is shifting toward small generators at the distribution system level, closer to the loads. In this context, the concept of microgrids was initially introduced by the Consortium for Electric Reliability Technology Solutions (CERTS) in 1998 in [1] and [2], where, a microgrid is defined as a cluster of distributed generation (Distributed Generation (DG)) units such as diesel generators, solar panels, wind turbines, and Fuel Cell (FC) units, which can operate in grid-connected and/or in isolated/islanded mode.

Isolated/islanded microgrids play two important roles in shaping the present and future of power and energy systems. First, they have been shown to be a reliable and efficient solution to provide energy to remote communities or those with no access to electricity [3]. Currently, 17% of global population lack access to electricity, and 38% lack clean cooking facilities [4]; isolated microgrids have been shown to be a feasible solution to the problem of energy poverty. Aboriginal Affairs and Northern Development Canada reports that there are approx. 200 thousands Canadians live in 280 distant off-grid communities, whose energy needs are currently satisfied by local isolated microgrids [5].

The second significant role of isolated microgrids is their potential to integrate distributed Renewable Energy Resources (RES) that contribute to the reduction of greenhouse gas emission, hence mitigating the adverse impacts of climate change. In this context, in

the last decade, driven by the need for clean energy and cheaper wind and solar technologies, RES such as wind and solar have proliferated all over the world. Thus, Distributed Generation (DG) is growing rapidly, with attractive feed-in tariffs and carbon-emission tax policies, thereby increasing the penetration of RES. Most recently, with the IEEE 1547 Standard permitting the islanded operation of distribution networks [6], isolated/islanded microgrids are becoming more prevalent, potentially improving the reliability of electricity supply and allowing better integration of RES [7].

In comparison to the large interconnected systems, an isolated micorgid has a smaller size but could have a significantly higher share of RES. However, similar to traditional systems, an isolated microgrid should also meet reliability and adequacy standards, which require all the controllable units to be actively involved in maintaining the system voltage and frequency within acceptable ranges. Hence, the power system controls may need to be modified in different control hierarchies to account for the intrinsic microgrid characteristics, in particular the impact of significant levels of non-dispatchable variable RES on system voltage and frequency. Therefore, the focus in this thesis is on primary and secondary control of frequency.

1.1.1 Primary Frequency Control

From the primary control perspective, the system frequency is traditionally controlled using frequency droop characteristics [8], [9]. However, the system inertia in an isolated microgrid is considerably lower compared to that of a large interconnected system, and thus the power generation may experience fast changes due to the high penetration of RES. Consequently, in such a situation, conventional control mechanisms may not be fast enough to overcome the rapid changes in the output power of RES, resulting in the system frequency experiencing large excursions and easily deviating from its nominal operating point [10]. In fact, in the case of a disturbance such as a generator outage, the rate of change of frequency can be as high as 1 Hz/s because of the negligible inertial response of RES, that can be attributed to the presence of electronically coupled Photovoltaic (PV) panels and wind turbines [10], [11]. Therefore, it is a challenging task to maintain the system frequency around the nominal operating point in isolated microgrids with significant penetration of RES [12].

In this thesis, first, a new frequency control mechanism is developed which makes use of the load sensitivity to operating voltage and can be easily adopted for various types of isolated microgrids. The proposed controller offers various advantages, such as allowing the integration of significant levels of intermittent RES in isolated/islanded microgrids without

the need for large energy storage systems, providing fast and smooth frequency regulation with no steady-state error, regardless of the generator control mechanism. The controller requires no extra communication infrastructure and only local voltage and frequency are used as feedback. The performance of the controller is evaluated and validated through various simulation studies in the PSCAD/EMTDC based on a a modified version of a CIGRE benchmark test system [13]. Small-perturbation stability analysis is carried out to demonstrate the positive impact of the proposed controller on system damping.

1.1.2 Secondary Frequency Control

In isolated microgrids, the Unit Commitment (UC) problem ensures reliable and economical operation [14]. The generation scheduling of dispatchable units obtained from a conventional UC are considered fixed within a dispatch time interval, yielding a staircase generation profile over the UC time horizon. This approach is reasonable in large interconnected systems, where UC and frequency regulation are treated separately; however, the staircase schedule of generation outputs is shown in [15] to create large frequency deviations at the beginning and end of each dispatch interval. Since, in isolated microgrids all DG units participate in frequency regulation, especially if RES are present, given their high output-power variability, the DG units would not remain at fixed operating points within one dispatch time interval. Hence, a UC model should be developed to consider the impact of frequency control mechanism on the DGs power output.

In the second stage of this thesis, a mathematical model of frequency control in isolated microgrids is proposed and integrated into the microgrid UC problem. The proposed formulation considers the impact of the frequency control mechanism on the changes in the generation output, resulting in a novel UC model that yields a more cost efficient solution for isolated microgrids. The proposed UC is formulated based on a day-ahead horizon with a Model Predictive Control (MPC) approach, and is tested and validated using a modified CIGRE benchmark test system. The results demonstrate that the proposed UC would reduce the operational costs of isolated microgrids compared to conventional UC, at similar complexity levels and computational costs.

1.2 Literature Review

This section presents a summary of some relevant works, pertaining to the issues addressed in this thesis.

1.2.1 Operation and Primary Control of Microgrids

Recently, the IEEE 1547 Standard [6] has defined a microgrid as an electric power system that has distributed resources and loads, has the ability to work in connected and isolated modes, and is intentionally planned to serve nearby loads. From the grid point of view, four modes of operation are defined for microgrids [3]: grid connected, transition-to-islanding, isolated, and reconnection mode. Each mode of operation has its own rules and challenges.

Compared to large interconnected power systems, isolated microgrids have lower system inertia, and they may have a high penetration of RES. Hence, they have a lower ability to deal with disturbances in the system, with frequency instability being a significant concern in isolated microgrids. In traditional power systems, power mismatch between generation and load is compensated by adjustment of generation; this is called primary frequency regulation, i.e. the adjustment of the mechanical input power of the conventional generators using their governors [16], with an extensive number of strategies proposed and implemented for traditional primary frequency control as discussed in [17].

In the context of microgrids, the deficiency of traditional control functions in the system was highlighted during an event in the Danish Bornholm Island [18], where, on December 22, 2005, the island distribution system was isolated due to a failure in the high voltage cables that connect the system to the main transmission grid. During that period, local regulators were not able to keep up with the fast fluctuations of output power of the wind generators, and as a result the whole distribution system was forced to shut down. An extensive number of control methodologies have been proposed for the operation of microgrids to mitigate some of the aforementioned problems [19–22]. These can be categorized in two groups, namely, decentralized and centralized controls [14]. For each category, many different control strategies have been proposed [23]. The focus of this section is on decentralized control techniques, with centralized controls briefly discussed.

In [24], three levels of centralized control are proposed as follows: local DG and load controls (decentralized), MicroGrid Central Controller (MGCC), and energy management system; thereafter, it introduces a demand side and production side bidding scheme in the context of MGCC. The aim is to optimize the production from the local DG units and power exchanges with the main grid. In [25], a secondary (as well as tertiary) control scheme is proposed based on minimization of a "potential function" that corresponds to the control goal. Both strategies in [24] and [25] require different components of the system to be able to communicate and share data, which is an essential part of centralized hierarchical control techniques. The need for a communication infrastructure may expose the system operation to several drawbacks and risks such as communication delay and data reliability. Additionally, in the presence of a communication infrastructure, reconfiguration of the

network and adding/removing a component, which could be relatively frequent event in microgrids, is challenging.

Substantial efforts have been made on the development of local decentralized controllers, which is specifically possible in microgrids because of the presence of an abundant amount of modern power electronic devices [26]. In a microgrid, DERs are interfaced via power electronic inverters that can be controlled locally without requiring data from other inverters or locations [27]. Such DERs should be dispatchable, i.e. they should be able to adjust their injected active and reactive power. In this context, Energy Storage Systems (ESS) are a practical and viable option for isolated/islanded microgrids with high penetration of RES, allowing for proper frequency and voltage control. Thus, in [10], it is demonstrated that fast acting ESS considerably reduces the impact of wind and solar generation on isolated microgrid inertia. In [28], ESS performs the primary voltage and frequency control in an inverter-based isolated microgrid, and is shown to be effective in maintaining the voltage and frequency within acceptable ranges.

Control strategies based on droop controllers are the most common for dispatchable DERs [29]. These controllers allow generators to properly share active and reactive powers among themselves by controlling frequency and voltage magnitude with no need for intercommunication between the units, as discussed in [30], where a control strategy is proposed to emulate the conventional droop control mechanism, providing the ability to distribute the total demand amongst DG units using local feedback signals, without the need for communications. This makes the droop mechanism one of the most appropriate **primary** controls for isolated microgrids, where access to communication infrastructure is limited, with many papers discussing and demonstrating the application of droop controllers; hence, droop controls are extensively discussed next.

There are some drawbacks associated with conventional droop controllers. First, in a system with a frequency droop controller, a load perturbation results in the steady-state frequency change; hence, secondary frequency regulation is required as proposed in [31]. Second, the load sharing control affects the stability of the system because it requires a change in the demand power of each inverter. Although increasing the droop gains improves the power sharing, the trajectories of the low-frequency modes will be shifted, which adversely affects the overall system stability; this issue has been fully explored in [32] and [33]. In addition, there are limitations in the use of frequency deviation as a control signal, as measuring the instantaneous frequency accurately is not a straightforward task [34]. Furthermore, droop controllers may exhibit poor frequency regulation due to rapid changes in the output power of the DG units [11]. Thus, there is a need for additional frequency control, especially in islanded microgrids with high penetration of RES.

In view of the limitations of droop control, numerous strategies have been proposed for frequency control and power sharing in isolated/islanded microgrids. In [35, 36], the conventional drooping mechanisms are revised and supplemental transient droop characteristics are added via PID controllers. While this mechanism improves the transient response of the system, it has a few drawbacks: first, the output impedance of the converter is neglected and is emulated by a high-pass filter; second, the PID controller needs careful tuning and is very sensitive to the X/R ratio of the system, a fact which is problematic in microgrids with frequent reconfiguration. In [37, 38], a simple PI controller is proposed that works based on transient drooping of active and reactive power; while this implementation improves the transient response and stability of the system, it has the same drawbacks of [35], with inferior performance, and presents the problem that calculation of adaptive droop coefficients are sensitive to measurement noises and inaccuracies, which may jeopardize the system stability.

All the methods proposed in [35–38] are built on top of the conventional drooping mechanism, which results in steady-state frequency error. To overcome this drawback, a load-angle droop is introduced to replace the traditional frequency droop in [39, 40]. In this methodology, the active power sharing is done by drooping the converter output voltage angle instead of frequency, which is referred to as "angle droop". In [39], it is shown that the standard deviation of the frequency in a system with angle droop controllers is less than the one in a system with conventional frequency droop controllers. Also, the steady-state frequency deviation is improved, which decreases the dependency on secondary frequency regulation. However, the major drawback of this methodology is that it requires signals from a Global Positioning System (GPS) for angle referencing, which is an issue for the reliability of the system, since the GPS signal might not be always available. In addition, to ensure proper load sharing, high values of angle droop gains are required, which negatively affect system stability, as illustrated in [40]. Also, it is important to mention that all the methods in [35–40] rely on microgrids with dispatchable, electronically interfaced Distributed Energy Resources (DERs), while the majority of isolated micorgrids, specially in remote communities, rely on synchronous machines with diesel engines [5].

In low-voltage microgirds, lines are mainly resistive, which expose the droop controllers to poor and slow transient response due to real and reactive power coupling. To overcome this problem, a virtual real and reactive power frame transformation is proposed in [41]. However, the proposed method cannot directly control actual real and reactive powers and instead relies on controlling the active and reactive currents. In addition, the efficiency of the proposed methodology highly depends on the accuracy of the estimation of the X/R ratio of the system. In [42], power droop controllers with virtual impedances are proposed to improve the active and reactive power decoupling; however, this methodology

increases the impedance voltage drops and consequently affects the reactive power control and sharing error.

Generally, and in addition to previously highlighted shortcomings, droop controllers may exhibit poor frequency regulation due to rapid changes in the output power of the DGs [11]. Thus, there is a need for additional frequency controls, especially in islanded microgrids with high penetration of RES. For example, in view of the need for additional frequency controls in isolated microgrids, in [43,44], a supplementary loop is introduced in the control system of variable-speed wind turbines to extract power from the rotating mass of the turbines in islanded systems. This strategy emulates the response of a conventional synchronous generator, and adds virtual inertia to the system, but this is limited by the speed and power rating of the turbines and introduces delays into the recovery period of the turbine.

A long-established strategy in conventional systems to help with frequency regulation is Dynamic Demand Control (DDC), i.e. reducing the consumption of the loads by directly turning them off or switching their operating voltage [45]. For example, the Pacific Northwest National Laboratory (PNNL) has developed a load controller that detects major deviations in the grid frequency and turns off appliances accordingly [46]. Various other centralized and decentralized DDC approaches have been reported in the literature [47–49]. However, these techniques are not viable for isolated microgrids, especially those in remote communities, as DDC requires significant communication infrastructure and controllers to be installed at each individual appliance.

The idea of reducing the system load during major under-frequency events by manipulating the grid voltage is introduced in [50,51], with operating voltages remaining within acceptable limits to not affect customers. Since the load response in this case would be almost instantaneous, this approach would improves the overall system frequency response, and in the case of droop controllers, there is no need for any inter-communication between the controllers thereby improving the reliability of the system. However, the idea presented in this paper is not of a dynamic controller, but it is a simple constant step-change in the system operating voltage activated by a certain threshold in the rate of change of frequency, imposed by changing the excitation reference set point; moreover, the issues pertaining to measuring the rate of change of frequency in the system is not discussed.

The review of the major works in the area of frequency control in isolated microgrids discussed in this section reveals the need for further improvements to ensure a reliable and stable operation of the system. Hence, a state-of-the-art Voltage-based Frequency Controller (VFC) is proposed in this thesis for both diesel-based and inverter-based isolated microgrids that acts as a primary controller providing frequency regulation support through

voltage regulators in parallel with the system conventional primary controls. In particular, the proposed VFC is based on the principle that, in microgrids, load powers are sensitive to voltage variations and, given the network size, voltage changes at diesel generator exciter systems and DERs inverters directly affect load voltages.

1.2.2 Unit Commitment in Isolated Microgrids

The Unit Commitment (UC) problem determines the optimal generation schedule to supply demand, while ensuring that the system operates within certain technical constraints [52]. In isolated microgrids, the UC problem functions as a secondary control to ensure its reliable and economical operation [14]. For microgrids with high penetration of RES, UC and its corresponding controls should be properly designed to take into account various challenges such as high supply and demand variability in the system, thus ensuring a reliable and economical operation of microgrids.

Several researchers have proposed UC models for microgrids with different configurations and constraints. In [53], an off-line UC technique is proposed for small-scale isolated microgrids with a low penetration of DERs. The optimal dispatch is pre-calculated for a range of different loading levels in the system; the obtained solutions are stored in a look-up table to be used in real-time based on the system loading condition. However, the proposed method is not appropriate for isolated microgrids with a significant number of dispatchable DERs, because, as the number of units increases, the number of possible operating scenarios grows exponentially. In addition, this approach presents a problem in systems with ESS, because the State-of-Charge (SoC) of a battery is a time-dependent variable that depends on the time-steps and the dispatch horizon. Finally, this model neglects some important operational constraints such as ramp up/down limits and minimum up/down times.

In view of the limitation of the aforementioned approach and other similar off-line UC techniques, the focus here is on on-line methodologies where the optimal dispatch is calculated based on the system conditions and forecasts over a given time horizon. Thus, in [54], a UC model that includes operational constraints pertaining to DERs and ESS such as ramp-up, ramp-down, and minimum up/down-time constraints is proposed. However, the accuracy of the solution obtained by deterministic methods such as the one in [54] directly depends on the accuracy of the forecast of RES and demand. To mitigate the negative impacts of forecast inaccuracy, Model Predictive Control (MPC) theory [55] has been applied to UC. In MPC-based approaches, the optimal dispatch solutions are obtained in each time step for a pre-defined horizon and is only applied to the next time interval; then

the problem is re-solved in the next time step with the updated forecast, repeating the process untill the end of the time horizon. For example, in [56], the dispatch is re-calculated hourly for the next 48 hours, updating the forecast of RES and demand. However, MPC-based approaches might not be sufficient to ensure the reliability of the isolated microgrids due to critical demand-supply balance [57]. Therefore, more detailed modelling techniques for uncertainties in the system can be combined with conventional MPC-based UC problems to obtain a more reliable dispatch solution. Examples of these techniques are robust optimization, stochastic optimization, and chance constrained optimization [57–60]

Generally, UC models for isolated microgrids are formulated as Mixed Integer Linear Programming (MILP) problems. However, Mixed Integer Non-Linear Programming (MINLP) formulations are also proposed where conventional UC is combined with more complex network load flow constraints. In [58], the problem of optimal energy management in microgrids is decomposed into UC and Optimal Power Flow (OPF) problems, incorporating the distribution system constraints such as acceptable voltage ranges within the UC problem while keeping the problem linear. In [61], a combined UC and OPF problem with smart loads in microgrids is proposed to obtain the optimal dispatch decisions of generation units. While such methods increase the accuracy of the optimal dispatch, the problem should be carefully formulated to ensure reasonable computation performance.

So far, none of the above mentioned works account for the impact of frequency regulation on DG units output, assuming that the generation outputs are fixed between two dispatch intervals. There are some works that consider constraints related to frequency control within the framework of UC for microgrids, with the majority focusing on reserve-related constraints. For example, in [62], the reserve required for frequency regulation is modelled as a decrease in the minimum limit and an increase in the maximum limit of the largest generator involved in the control process. In [63], a new constraint is introduced to control the frequency levels, which determines the minimum frequency reached if the system loses the largest generator; reserve levels are then adjusted through an iterative process until the frequency constraint is satisfied. In [64], a frequency-regulating reserve constraint and a load-frequency sensitivity index are introduced to calculate the proper amount of reserves required to keep the system frequency higher than the minimum acceptable value. In [65], the isochronous mode of generation is modelled and integrated into the UC problem, with particular emphasis on the microgrid reserve requirements. None of these references model or consider the impact of the frequency control mechanism on the generation output, and hence on the UC objective function; the primary assumption of these works remains that the generation power outputs are fixed between two dispatch time intervals.

The idea that dispatchable units' power outputs would not be fixed between two dis-

patch intervals has been investigated in [66–68] for bulk power systems. In [66], it is demonstrated that considering generation levels in UC problems as hourly energy blocks may not be realizable in practice. To address this problem, the UC problem is reformulated in [67] to incorporate energy delivery constraints based on a sub-hourly energy demand profile. In [68], a UC-based market clearing model is proposed, considering the difference between power and energy, and accounting for start-up and shut-down power trajectories and ramping constraints; in this case, demand and energy are modelled as piecewise-linear functions representing their power trajectories. The methods proposed in these works have not been applied to microgrids with various DERs; in addition, none of these works investigate the impact of frequency control on power trajectories of dispatchable units.

Based on the aforementioned literature review, there is a need for state-of-the-art UC models for isolated microgrids that considers the impact of frequency control on generation outputs, and hence integrates the corresponding frequency control model into the UC problem formulation. Hence, in this thesis, a novel UC is proposed that integrates the mathematical formulation of various frequency control techniques, thus considering for the impact of these techniques on dispatchable DERs output.

1.3 Research Objectives

The review of the current technical literature reveals the need to improve the primary and secondary frequency control techniques for isolated microgrids. In this context, the main objectives and contributions of this thesis are as follows:

1. Develop a state-of-the-art VFC for both diesel-based and inverter-based units in isolated micorgirds. The controller utilizes a load voltage regulation mechanism to manipulate the system demand, and consequently balance the power mismatch. The load voltage regulation will be performed via diesel generator exciter systems and DERs inverters, without the need for communication between different components of the system.

2. Investigate the impact of various frequency control mechanisms such as single unit control, droop control, or isochronous load sharing (ILS) control mode on optimal dispatch solution, using the developed UC model.

3. Develop a hybrid droop-based frequency controller for inverter-based isolated microgrids and investigate the impact of various droop-based frequency control mechanisms on the transient response and stability of such systems.

4. Develop a novel mathematical formulation of the frequency control mechanism integrated within a UC framework for isolated microgrids, yielding a more economical dispatch solution, and introducing a new reserve power constraint in the UC model to represent the corresponding frequency control mechanism that yields a more realistic dispatch solution.

5. Develop a comprehensive dynamic and static simulation model of the CIGRE benchmark system [13] for medium voltage distribution networks to carry out time-domain and steady-state simulations to test and demonstrate the proposed frequency control paradigms. Detailed Models voltage and frequency control systems, both for synchronous machines and inverters, will be developed.

1.4 Outline of the Thesis

The rest of the thesis is structured as follows: Chapter 2 provides a background review on the main concepts, models and tools used in this thesis. It discusses microgrids in detail, with a focus on voltage and frequency control and Energy Management Systems (EMS) in isolated microgrids. Different types of DERs are also presented, and their benefits and shortcomings are briefly discussed.

Chapter 3 compares the performance of different droop-based control techniques in an inverter based isolated microgrid. Specifically, the following techniques are compared: conventional droop-based control including a Sinusoidal Pulse Width Modulation (SPWM)-based Voltage-Sourced Converter (VSC) with power, voltage and current controls, transient decentralized droop controls, and angle droop controls. Finally, it proposes a hybrid controller that merges the advantages of both the transient decentralized droop controller and the angle droop controller. The performance of these control techniques in an isolated microgrid is evaluated through time domain simulations on a simple test system.

Chapter 4 describes the proposed VFC controller in detail. The microgrid test system, based on a CIGRE bench-mark system, and its components used to study and validate the presented controller are also discussed, including the models of DERs and their corresponding controls. Finally, simulation results are presented both for diesel-based and inverter-based test systems, and analyses are carried out to demonstrate the positive impact of the proposed controller.

Chapter 5 proposes a novel UC that integrates the mathematical model of frequency control in isolated microgrids. A MILP problem is formulated to model the changes in the DERs output according to the system frequency control mechanism. A modified version

of the CIGRE benchmark test system is used to demonstrate and validate the proposed UC for isolated microgrids.

Finally, Chapter 6 summarizes the main conclusions and contributions of this thesis, and suggests possible future research work. Appendix A presents detailed data of the test system components and their corresponding controls used for simulations.

Chapter 2

Background Review

2.1 Introduction

This chapter presents a background review of the concepts, models and tools that are used in this thesis. First, microgrids are discussed in detail, with a general discussion on the stability these systems, concentrating on frequency stability and the frequency control problem formulation. Then, voltage/frequency control and EMS in isolated microgrids are reviewed in detail.

2.2 Microgrids

Generally, a microgrid is defined as a cluster of DG units and loads such as diesel generators, solar panels, wind turbines, etc., connected to the main grid at the Point of Common Coupling (PCC) [1,3]. Depending on the size and configuration, microgrids can be as large and complex as a full substation, or as small and simple as a single customer microgrid, as shown in Figure 2.1.

Microgrids can operate both in grid-connected and islanded modes and are also able to transit between these two modes of operation [69, 70]. Some microgrids may have no connection available to the main grid, such as those built for remote communities [5] or industrial sites; these microgrids always operate in islanded mode, and are referred to as isolated microgrids[1]. In the grid-connected mode of operation, the voltage and

[1]In this thesis, the terms *islanded* and *isolated* microgrids are used interchangably.

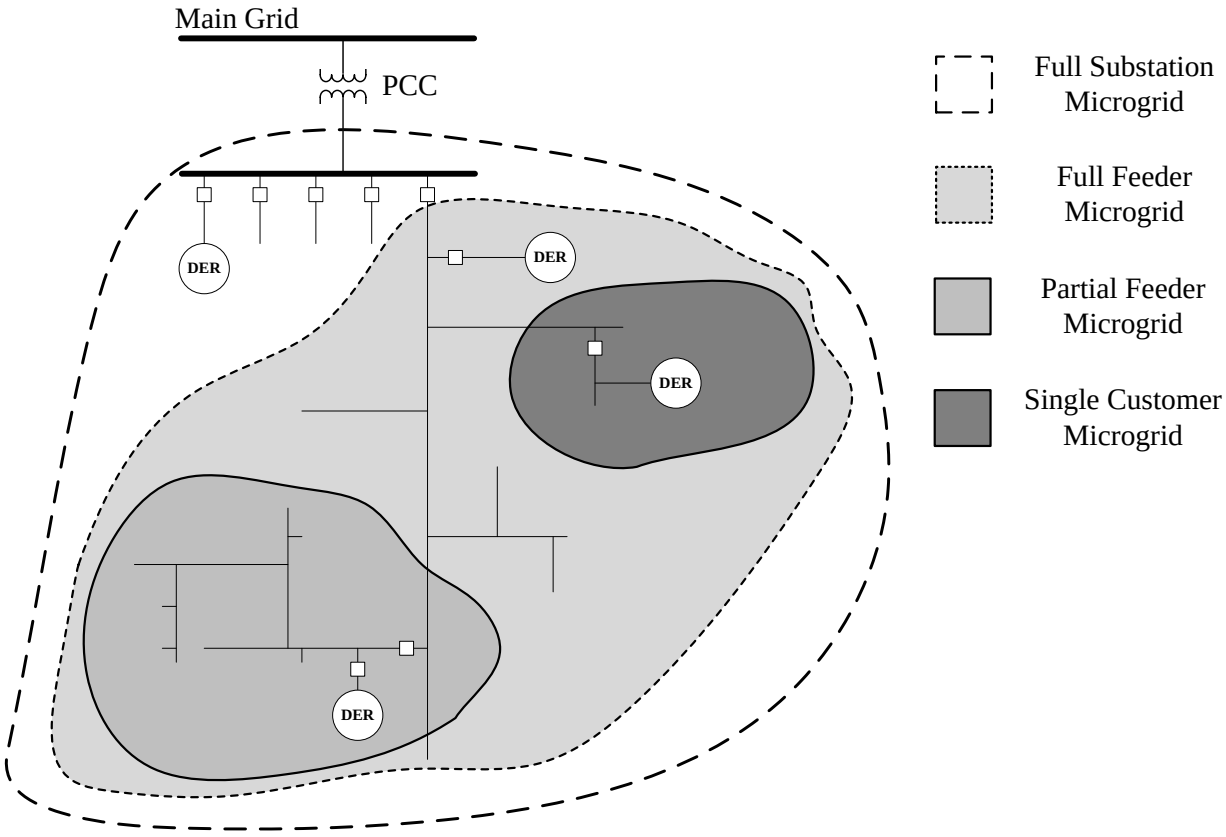

Figure 2.1: Different sizes and configurations of microgrids.

frequency are imposed by the main grid, and the microgrid only performs pre-defined ancillary services. On the other hand, in islanded operation, various DERs are in charge of controlling the voltage and frequency.

Controlling microgrids in islanded mode of operation is challenging due to the critical demand-supply balance that should be locally satisfied. Furthermore, the system inertia is lower compared to traditional power systems, especially in the case of high penetration of intermittent RES with the majority of DERs being electronically interfaced with the system, in which case the uncertainty of generation is significant, requiring accurate and fast control mechanisms to ensure stable and reliable operation.

Stable operation in microgrids refers to the formally accepted definition of power system stability, which is "the ability of an electric power system, at a given initial operating condition, to regain a state of operating equilibrium after being subjected to a physical disturbance, with most system variables bounded so that practically the entire system

remains intact" [71]. Disturbances in isolated microgrids occur in many different forms, and are generally categorized into large and small disturbances. For example, continuously changing loads represents small disturbances, while the loss of generators or loads or short circuits on feeders can be categorized as large disturbances. In both cases, the isolated microgrid should be able to remain stable, i.e. to damp the fluctuations in the system operating state and return to a new satisfactory equilibrium point.

Instability may be manifested in different ways and/or affect different states of the system. By states of the system one refers to those variables that define the system operating point, in particular voltages and system frequency. Hence, there is a need to identify different types of instability that may occur in an isolated microgrid; however, this is work currently underway and being lead by an IEEE Power & Energy Society (PES) Task Force, and thus there is not yet relevant literature in this topic. Therefore, in this thesis, the definitions and concepts introduced in [71] are used as a starting point. In this paper, power system instabilities are categorized based on the following factors:

- The physical origin of the instability
- The relative size of the disturbance
- The components that are involved in the process, and the time span that determines the instability
- The numerical methodology to calculate or predict the instability

Accordingly, instabilities can be classified into different categories as shown in Figure 2.2. In an event of instability, more than one type of instability may be triggered. In fact, in many cases one form of instability may result in another form. Hence, careful studies should be carried out to understand all types of instabilities in isolated microgrids in order to develop proper controls.

The focus of this thesis is on frequency stability of isolated microgrids. Frequency instability is a major concern in isolated/islanded systems, where there might not be enough inertia of rotating mass required to reduce the rate of change of frequency. Additionally, in such systems, the number of generation units are relatively low, resulting in severe power mismatches in the event of a generator outage. In [71], frequency stability is defined as "the ability of a power system to maintain steady frequency following a severe system upset resulting in a significant imbalance between generation and load". Frequency instability is usually manifested in the form of sustained frequency swings that result in tripping of generators. In the case of a sudden outage of a generator or load variations, the

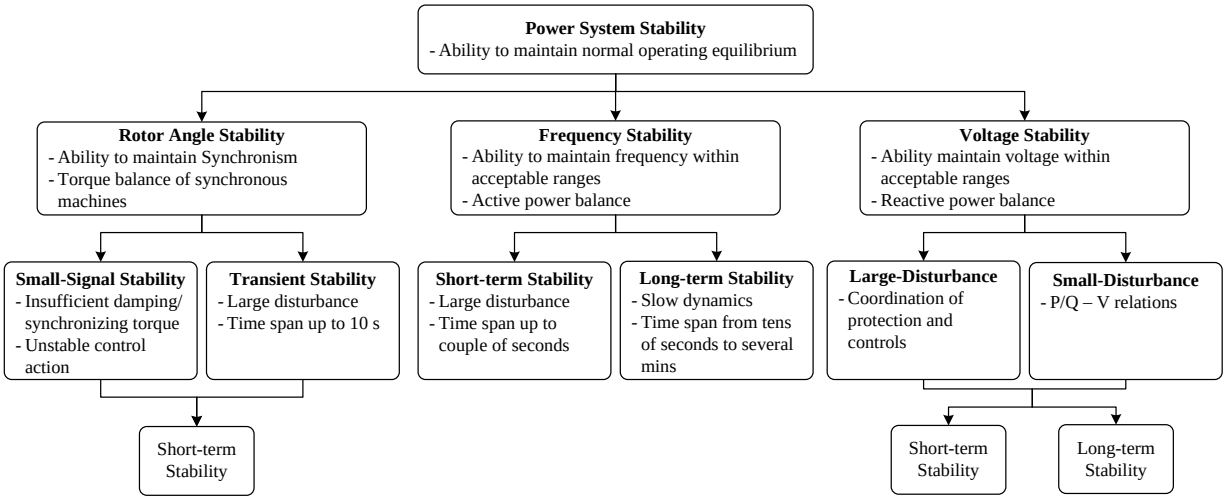

Figure 2.2: Classification of bulk power system stability [71].

system should be able to restore the balance between generation and load, with minimal unintentional loss of load. As shown in Figure 2.2, frequency stability can be either a short-term or long-term phenomenon depending on the duration of the process and activation time of the control and protection devices. A short-term frequency instability has a time frame from a fraction of a second to a few seconds; it occurs when the equilibrium between the generation and the load is severely disturbed, resulting in a high rate of change of frequency. Such a disturbance may result in a system blackout within a few seconds if timely corrective actions are not taken (e.g., under-frequency load shedding). On the other hand, long-term frequency instability is the result of situations in which the dynamics of the turbine overspeed controls and/or governor protection and controls are involved [72]. Long-term frequency instability has a time frame from tens of seconds to several minutes.

The frequency response of an isolated microgrid, and more specifically the rate of change of frequency, is a function of its frequency control mechanisms. Any change in the generator and DERs output power and/or loads in the system will affect the frequency. However, even if the load changes instantaneously, the frequency will change smoothly due to the controls in the system. This behaviour is modelled with a damping coefficient D relating the changes in the electric power to the changes in the system frequency. Thus, any change in the generation input power ΔP_{in} and/or net electrical power demand ΔP_D will result in a frequency change Δf, which can be modelled linearly as follows [52]:

$$G(s) = \frac{\Delta f}{\Delta P_{in} - \Delta P_D} = \frac{K_S}{1 + sT_S} \tag{2.1}$$

where K_S is a gain in reverse proportion to the amount of frequency sensitive loads, and T_S is a time delay in the order of fractions of a second. The notation used in this equation and others throughout this thesis are defined in the nomenclature section found in page xi. Equation (2.1) models the rate of change of frequency with respect to a power imbalance in the system under the assumption that the frequency variation propagates through the system uniformly.

In an isolated microgrid, there are several controllers with different time constants and hierarchies to keep the system in a steady-state operating point, maintaining the system voltage and frequency within acceptable limits during disturbances, and ensuring a reliable and economic operation. Such control functions range from automatic localized actions with fast dynamics to slower dynamic controls such as optimal dispatch. Large isolated microgrids may be equipped with Supervisory Control and Data Acquisition (SCADA) systems that gather and monitor different signals from all over the system and perform signal processing tasks to take proper actions.

Based on the implementation (centralized or decentralized), time frame, and required infrastructure, the controller can be categorized into three hierarchies: primary, secondary, tertiary, as shown in Figure 2.3 [14,73]. Primary level controls are usually autonomous and designed to react instantaneously to local feedback signals; examples of primary control are voltage and frequency regulation in the system. Secondary controls are designed to supervise and coordinate primary controls; they function within a time frame of several minutes, with EMS falling under the secondary control category. Tertiary controls are used to coordinate a cluster of interconnected microgrids or supervise the microgrid interaction with the main grid. Hierarchical controls are essentially an extended version of autonomous controls, in which the control functions are shared among different levels of hierarchy that have different time frames and functions, as illustrated in Figure 2.3 [74] [75].

Apart from certain pre-dispatch tasks and urgent intentional corrective actions, a bulk power system is mostly controlled by changing the active and reactive power flows via automatic localized controllers. Active power changes mainly affect the system frequency, while reactive power changes dominantly affect the system voltage; hence, two separate controllers are responsible for controlling real and reactive powers. In this context, frequency control takes care of the real power generation and frequency, while voltage control regulates the reactive power and the bus voltage magnitude. However, in the case of isolated microgrids, especially those operating at low-voltage levels, the feeder is dominantly resistive, and thus relying on conventional controls may deteriorate system transient-response and steady-state performance [76]. Hence, for these systems, there is a need to also consider the impact of voltage magnitude on active power and voltage angle on reactive power.

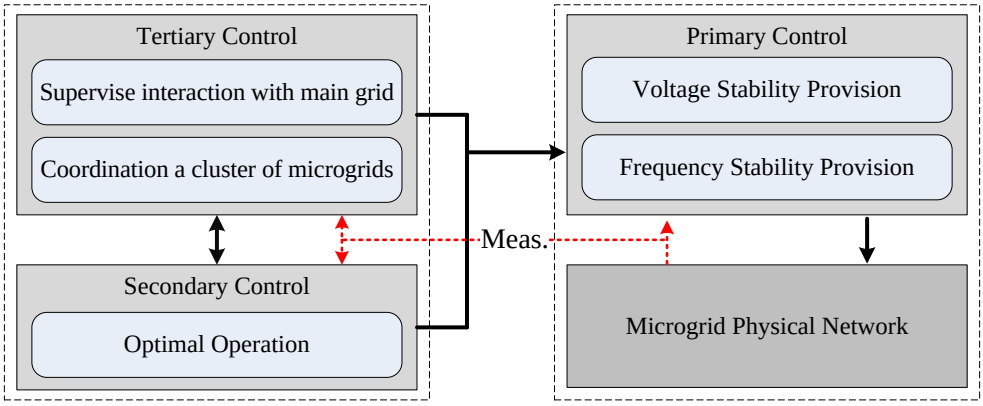

Figure 2.3: Frame for hierarchical control of a microgrid.

2.3 Frequency and Voltage Control in Isolated Microgrids

The objective of frequency control is to maintain the frequency within an acceptable limit by properly sharing the loads among the generation units. This is done by measuring the error signal Δf, and controlling the output power of DERs that participate in frequency control. In this section, General load sharing techniques in isolated microgrids are described and then technical details of frequency control in synchronous machines and inverter-based DERs are discussed.

The purpose of voltage control is to maintain the system operating voltage and consequently to manage the reactive power generation. As reactive power plays a considerable role in determining the overall system stability, voltage control is of paramount importance in power systems.

Different components produce or absorb reactive power in a power system. For example, synchronous generators can either generate or absorb reactive power depending on their excitation level. Inverter based ESS can also produce or absorb reactive power depending on the system condition and controls. In isolated microgrids, transformers and feeders are sinks of reactive power, and loads also consume reactive power in the system.

There are different methods for voltage control in isolated microgrids that involve various devices and mechanisms. A combination of these methods ensures a properly functioning voltage control. Technical details of voltage control in synchronous machines and inverter-based DERs are also discussed in this section.

2.3.1 Load Sharing Techniques in Isolated Microgrids

Load sharing between DERs can be done autonomously or via proper communication channels. The focus here is on autonomous load sharing controls.

Isochronous Control

In this control mode, a single generation unit is in charge of restoring the active power balance in the system, while the rest of the generation units' outputs remain fixed; hence, the system steady-state frequency error is zero. This type of frequency control is usually suitable for small isolated microgrids with low penetration of RES, where a single DG unit provides a significant share of the active power demand of the system and changes in active power mismatch are not significant. For larger isolated microgrids with higher penetration of RES, the active power mismatch can be substantial, and hence one single controllable unit may not be able to properly regulate the system frequency; this may result in the system frequency deviating from its acceptable range of operation. In such a case, frequency control tasks should be divided amongst multiple generators.

Droop Load Sharing Control

Isochronous control is not practical in a large isolated microgrid with more than one generator participating in the frequency control, because each generator will oppose the other, trying to compensate any changes in the power mismatch alone[2]. Hence, in such a system, frequency controllers are designed to allow the steady-state frequency to drop as the load increases, as shown in Figure 2.4. The slope of the curve in this figure is a unique characteristic of each controller and is referred to as "speed regulation" or "droop" (R). Typically, a generator has a speed droop of 5 to 6 percent, which is calculated as follows:

$$R\% = \frac{\omega_{NL} - \omega_{FL}}{\Delta P} \times 100 \tag{2.2}$$

where ω_{NL} is the no-load steady-state speed, ω_{FL} is the full-load steady-state speed, and ω_0 is rated speed.

Droop control allows for smooth load sharing between the generators in the system with no intercommunication required; the system frequency deviation is used as the local

[2]In special situations, multiple adjacent generators can operate under the isochronous paradigm.

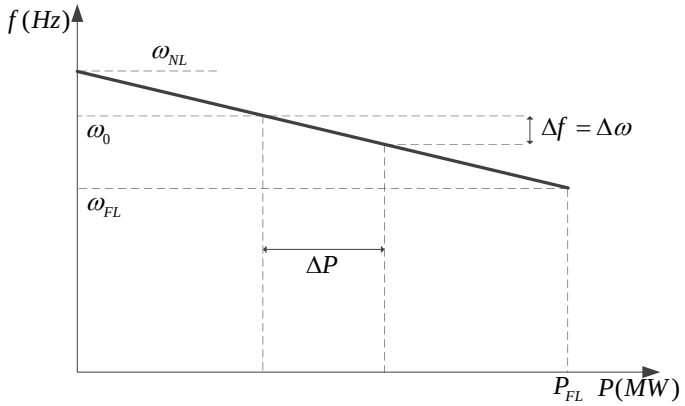

Figure 2.4: Governor droop characteristics.

feedback. Thus, suppose that two generators, generating P_1 and P_2 respectively, are operating at the initial frequency f_0. A load perturbation of ΔP_L then occurs in the system, resulting in a drop in the system frequency, to which the droop-based controls react by increasing the generation output until the system reaches the new equilibrium frequency $f^{'}$. The amount of load picked up by each generator is in reverse relation to its droop R, as shown in Figure 2.5. Hence:

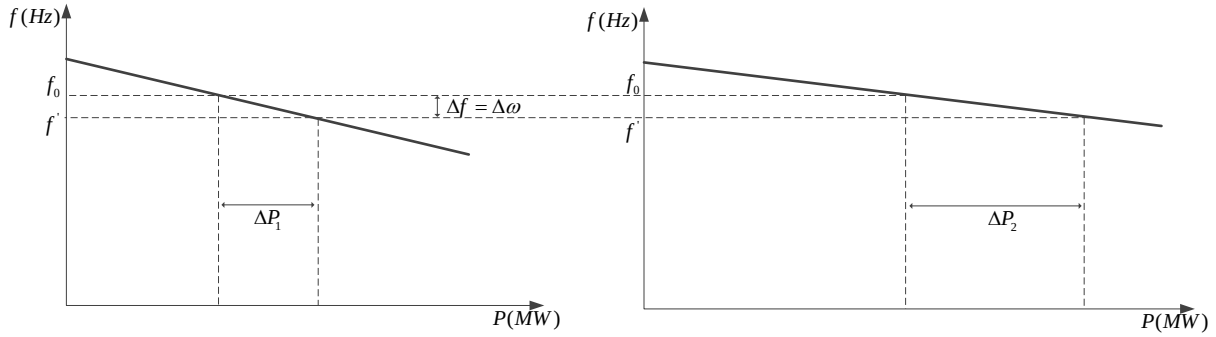

Figure 2.5: Load sharing by drooping governors.

$$\frac{\Delta P_1}{\Delta P_2} = \frac{R_2}{R_1} \tag{2.3}$$

According to this equation, the generator with higher R participates less in compensating for load perturbations in the system.

Isochronous Load Sharing

Under the Isochronous Load Sharing (ILS) control paradigm, each unit operates based on the isochronous control principle described previously; however, the units communicate their loading level to each other through load sharing communication lines to guarantee that each unit is operating at the same percentage of its full-load rating. Hence, the steady-state frequency of the isolated microgrid is maintained at its nominal point. The changes in the generation units' outputs can be mathematically modelled as follows [65]:

$$\frac{\Delta P_i}{\bar{P}_i} = \frac{\Delta P_j}{\bar{P}_j} \tag{2.4}$$

where ΔP_i and $\bar{P}_i$ are the change in the power output and the rated power of DG unit i, respectively. It is crucial for the generation units participating in ILS control to establish and maintain reliable communication among themselves, otherwise the units would oppose each other when regulating frequency. Thus, to ensure reliable operation, the units should be physically close to one another.

2.3.2 Frequency Control in Synchronous Machines [77]

In a synchronous machine, the angle between the position of the rotor axis and the resultant magnetic field axis is known as the "power or load angle" δ. When the system is subject to a disturbance, an oscillatory motion occurs in which the rotor accelerates or decelerates with respect to the rotating air gap mmf; if the system remains stable, the rotor will return to synchronism. The equation which describes this oscillatory behaviour is known as the "swing equation" and is of paramount importance in power system stability analysis:

$$\frac{2H}{\omega_s}\frac{d^2\delta}{dt^2} = P_{m(pu)} - P_{e(pu)} \tag{2.5}$$

where ω_s is the electrical angular velocity, P_m is the driving mechanical power, P_e is the developed electrical power by the generator, and H is "per unit inertia constant", which can be defined as follows:

$$H = \frac{Kinetic\,Energy}{Machine\,Rating} \tag{2.6}$$

During small-perturbations, (2.5) can be re-written as:

$$\frac{2H}{\omega_s}\frac{d\Delta\frac{\omega}{\omega_s}}{dt} = \Delta P_{m(pu)} - \Delta P_{e(pu)} \tag{2.7}$$

The Laplace transform of (2.7) yields:

$$\Delta\omega(s) = \frac{1}{2Hs}[\Delta P_m(s) - \Delta P_e(s)] \tag{2.8}$$

which shows how a synchronous generator reacts to changes in the mechanical and electrical powers, and can be depicted as shown in Figure 2.6:

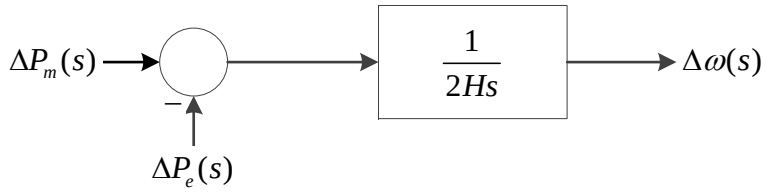

Figure 2.6: Block diagram of generator model (2.8).

Load Model

Generally, loads may or may not be sensitive to frequency. For example, for pure resistive loads, the electrical power is entirely a function of the operating voltage and is not sensitive to frequency. On the other hand, loads such as induction motors are sensitive to changes in frequency. Hence, a general model of any electrical load can be represented as follows:

$$\Delta P_e = \Delta P_L + D\Delta\omega \tag{2.9}$$

where ΔP_L is the portion of the load that is not sensitive to changes in frequency, and $D\Delta\omega$ is the frequency-sensitive part of the load. D is a constant that indicates the percentage of the change in the load over the percentage of the change in the system frequency. Hence, the block diagram of a generator in Figure 2.6 can be integrated with (2.9), resulting in the block diagram illustrated in Figure 2.7.

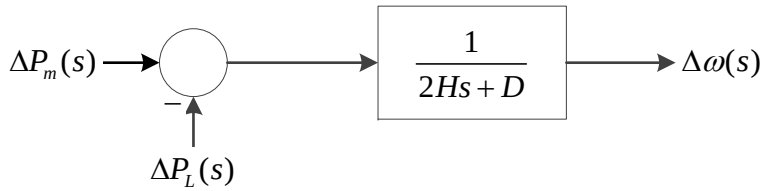

Figure 2.7: Block diagram of a generator-load model.

Turbine

The purpose of a turbine (e.g., hydraulic, steam, and gas) is to provide mechanical power to the rotating generator shaft. Turbines have many different models with a variety of mechanical and dynamic characteristics; however, they all work based on the same principle, i.e. the kinetic energy of a flowing fluid (e.g., steam, water, and hot gas) is used to rotate the turbine shaft, where the output power of the turbine is a function of its mechanical valve position that defines the flow of the fluid into the turbine. In Figure 2.8, the block diagram of a simple non-reheat steam turbine is presented, where ΔP_V shows the changes in the valve position, and τ_T is a time constant that models the mechanical delay in the turbine response to changes in the valve position.

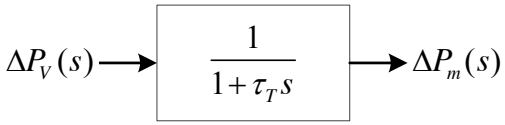

Figure 2.8: Block diagram of a non-reheat steam turbine.

Governor Model

The objective of a governor in the system is to re-adjust the turbine valve position, and consequently the mechanical input power of the generator (output power of the turbine) according to changes in the system frequency. Changing the mechanical input power of the generator will change its output electrical power, which directly affects the system frequency.

From the governor speed characteristics, the following equation can be derived:

$$\Delta P_g = \Delta P_{ref} - \frac{1}{R}\Delta\omega \tag{2.10}$$

The Laplace transform of (2.10) yields:

$$\Delta P_g(s) = \Delta P_{ref}(s) - \frac{1}{R}\Delta\omega(s) \tag{2.11}$$

The governor then changes the turbine valve position ΔP_V with a specific time delay τ_g, resulting in the block diagram of Figure 2.9 for the speed governor system.

From the block diagrams of the governor, turbine, and generator-load system, it is possible to derive the block diagram of a full synchronous machine frequency control system,

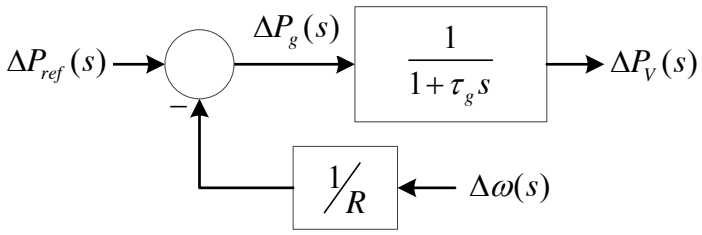

Figure 2.9: Block diagram of a speed governing system.

shown in Figure 2.10. To better understand the behaviour of the this system subject to a load perturbation of $-\Delta P_L(s)$, Figure 2.10 can be redrawn with $-\Delta P_L(s)$ as the input and frequency deviation $\Delta\omega(s)$ as the output as shown in Figure 2.11.

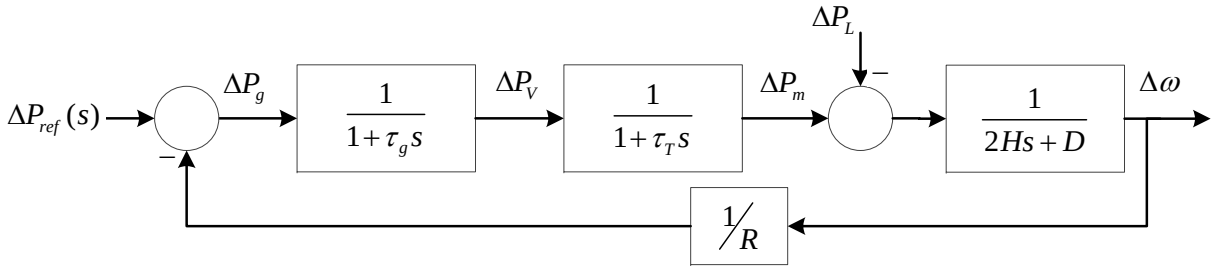

Figure 2.10: Block diagram of synchronous machine frequency control system.

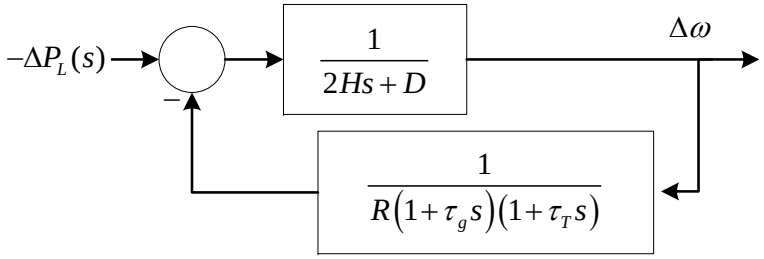

Figure 2.11: Block diagram of synchronous machine frequency control system with ΔP_L as input.

Utilizing the Laplace final value theorem, and assuming the load change is a step input, i.e. $\Delta P_L(s) = \frac{\Delta P_L}{s}$, the steady-state deviation in frequency can be derived as follows:

$$\Delta\omega_{ss} = (-\Delta P_L)\frac{1}{D + 1/R_1 + 1/R_2 + \cdots + 1/R_n} = \frac{-\Delta P_L}{\beta} \tag{2.12}$$

Observe in (2.12) that a steady-state deviation of the frequency is dominantly defined by

the governor droops in the system, where $\beta = D + {}^1/_{R_1} + {}^1/_{R_2} + \cdots + {}^1/_{R_n}$ is the system frequency response characteristic.

2.3.3 Voltage Control in Synchronous Machines [77]

The primary voltage controller of a synchronous generator is referred to as Automatic Voltage Regulator (AVR). An AVR manipulates the generator excitation level in order to keep the output terminal voltage within specific limits. A typical AVR consists of an amplifier, excitation controller, and a sensor. To better understand the operating principles of a typical AVR, simple models of its different components along with the generator model are presented.

Generator Model

A simple model of a synchronous generator can be provided by a linear relationship between the generator terminal voltage and its field voltage, with a gain K_G and a time constant τ_G, which can be represented with the following transfer function:

$$\frac{V_t(s)}{V_F(s)} = \frac{K_G}{1 + \tau_G s} \tag{2.13}$$

where K_G is around 1 and τ_G is in order of a few seconds.

Sensor Model

A sensor will measure the terminal voltage via a transformer and send the measured signal to the AVR through an amplifier. The sensor can be modelled by a simple first order transfer function as follows:

$$\frac{V_S(s)}{V_t(s)} = \frac{K_R}{1 + \tau_R s} \tag{2.14}$$

where τ_R has a very small value, in the range of a few milliseconds. The amplifier can also be modelled in a similar way as follows:

$$\frac{V_R(s)}{V_e(s)} = \frac{K_A}{1 + \tau_A s} \tag{2.15}$$

where K_A is in the range of hundreds, while τ_A can be in the order of tens of milliseconds.

Exciter Model

There are several different excitation system model types for a synchronous generator [78]. Modelling a realistic excitation system in detail is a complicated task and requires various aspects, such as the magnetic circuit saturation, to be taken into consideration [79]. However, the following adequate linear model of the excitation system presented by a first order transfer function can be used for small generators of the kind found in isolated microgrids:

$$\frac{V_F(s)}{V_R(s)} = \frac{K_E}{1 + \tau_E s} \tag{2.16}$$

Modern exciters have a very low τ_E, typically in the range of hundreds of milliseconds.

AVR Model

Considering the models provided for various components of the system, it is possible to obtain the simplified block diagram of an AVR shown in Figure 2.12. From the figure, it is possible to calculate the closed-loop transfer function of the terminal voltage $V_t(s)$ to the reference voltage $V_{ref}(s)$, as follows:

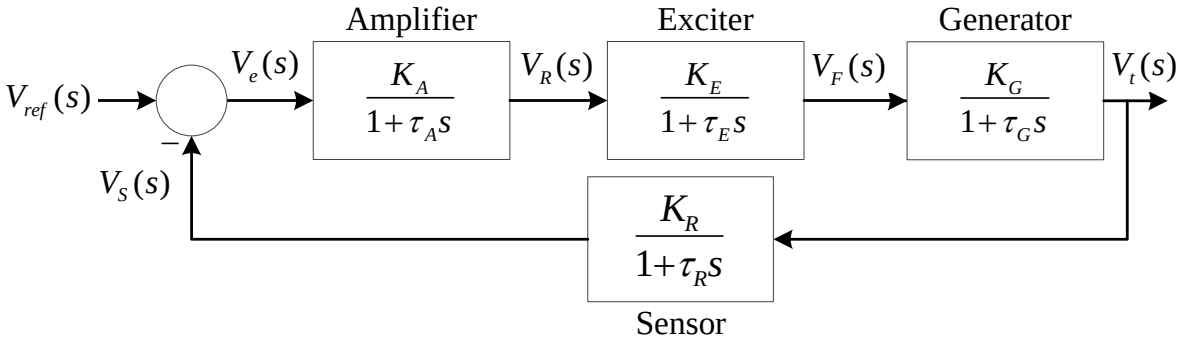

Figure 2.12: Block diagram of an AVR.

$$\frac{V_t(s)}{V_{ref}(s)} = \frac{K_A K_E K_G K_R (1 + \tau_R s)}{(1 + \tau_A s)(1 + \tau_E s)(1 + \tau_G s)(1 + \tau_R s) + K_A K_E K_G K_R} \tag{2.17}$$

This equation can be used to model the response of the AVR with respect to a reference voltage such as the steady-state terminal voltage.

2.3.4 Frequency and Voltage Controls in Inverters

DC/AC inverters such as the ones used in PV, FC, and ESS are able to mimic the behaviour of the governor and exciter systems of a synchronous machine through voltage and current controls. These controllers are based on feedback signals transformed into the d-q reference frame [27], yielding the typical converter controls shown in Figure 2.13, where it is shown that an inverter can be operated in Current Control Mode (CCM) or Voltage Control Mode (VCM) based on the microgrid control mechanism. Generally, inverters can be controlled under three different paradigms: grid forming, grid supporting, and grid feeding [80].

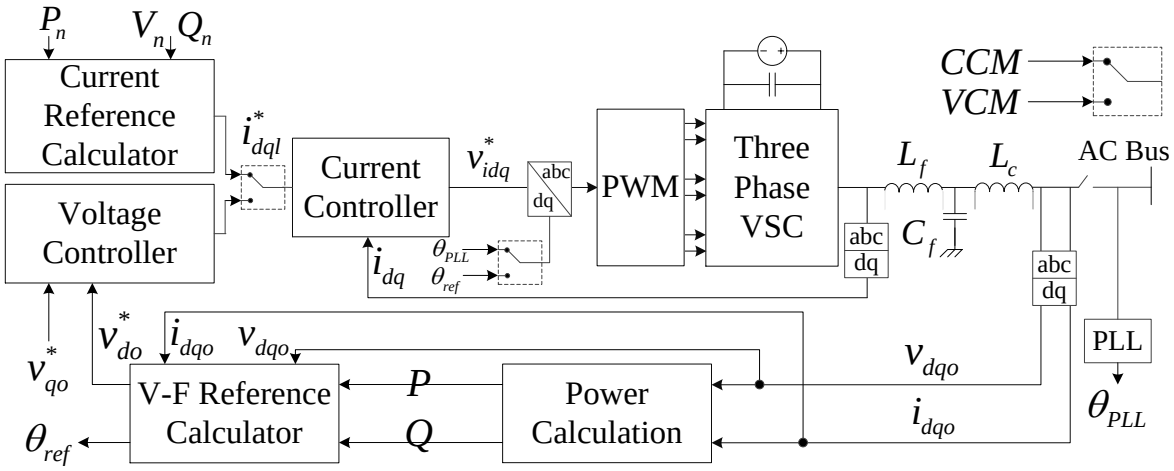

Figure 2.13: Typical inverter control scheme.

Grid forming inverters are in charge of controlling the voltage amplitude and frequency in the system; hence, they are controlled in the VCM mode of operation [81], which can be represented as an ideal AC voltage source with a low-output impedance. Grid forming inverters are usually used in inverter-based microgrids when there is no dominant synchronous machine in the system. Because of the low-output impedance, grid forming inverters require an accurate synchronization system to be able to operate in parallel with other grid forming inverters in the system, which makes grid forming inverters prone to system instabilities.

Grid supporting inverters can be operated both in VCM or CCM modes, and participate in the voltage and frequency regulation by controlling its active and reactive power exchange with the grid [82]. Droop-based regulation techniques are used in grid supporting inverters to regulate the injection/absorption of active/reactive power based on the changes

in the system frequency/voltage [83]; hence, the inverter emulates the self-regulation behaviour of a synchronous machine.

Finally, grid feeding inverters are controlled in CCM mode and are designed to inject the active and reactive power defined by the control reference set-point; they do not participate in voltage and frequency regulation in the system. Grid feeding inverters are the most common type of inverters used in RES, such as PV or wind [84]. Usually the active and reactive power set-points are calculated using a Maximum Power Point Tracking (MPPT) algorithm to maximize the energy yield [85].

Droop-based Grid Supporting Inverter in VCM Mode

Droop-based grid supporting inverters in VCM mode consist of controllers that include all parts necessary for other types of inverter controls, i.e. a droop-based reference calculator block, a voltage control block, and a current control block. As shown in Figure 2.13, the inverter is connected to the rest of the system via an LC filter along with a coupling inductor L_c. The purpose of a droop-based grid supporting inverter is to provide the voltage magnitude and phase set-points based on a droop strategy, mimicing the behaviour of a synchronous machine. The back-to-back voltage and current control loops are designed to provide the control signal for the PWM module of the VSC, and to ensure that the output voltage follows the reference set-points provided by the power controller block. At the same time, these two control loops provide enough damping for the LC filter and the L_c.

The calculations in the Power Calculation block are performed according to Park's dq–axes theory as follows, and depicted in Figure 2.14, based on the notation in Figure 2.13:

$$\begin{aligned} p &= v_{do} i_{do} - v_{qo} i_{qo} \\ q &= v_{do} i_{qo} - v_{qo} i_{do} \end{aligned} \tag{2.18}$$

where v_o and i_o are voltage and current of the line after the low pas filter, as shown in Figure 2.13. These instantaneous powers are then passed through low-pass filters to obtain the fundamental frequency real and reactive powers P and Q as follows:

$$\begin{aligned} P &= \frac{\omega_c}{s + \omega_c} p \\ Q &= \frac{\omega_c}{s + \omega_c} q \end{aligned} \tag{2.19}$$

where ω_c is the cut-off frequency of the low-pass filters.

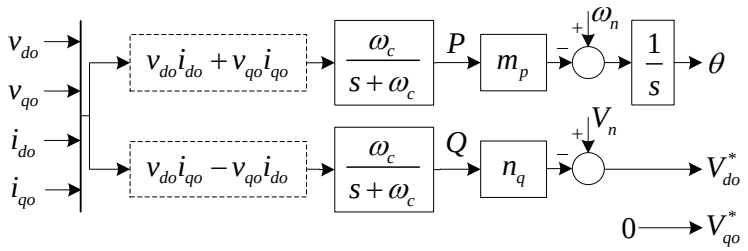

Figure 2.14: Droop-based reference set-points.

Artificial droops are introduced to allow for the frequency and voltage magnitude to decrease as active and reactive power injections increase, respectively; thus, a behaviour similar to that of a synchronous machine is synthesized to allow for proper power sharing between different generation units. The following calculations are then performed:

$$\omega_o = \omega_n - m_p P \tag{2.20}$$

$$V_{do}^* = V_n - n_q Q \qquad V_{qo}^* = 0 \tag{2.21}$$

where V_n and ω_n are the nominal voltage magnitude and frequency. The output voltage magnitude reference is aligned with the d- axis of the reference frame, while the q- axis reference is set to zero. In addition, m_p and n_q are the frequency and voltage droop gains respectively, and determine the proper power sharing amongst the DERs to maintain the active and reactive power balance in the system. These droop coefficients are obtained as follows:

$$m_p = \frac{\omega_{\max} - \omega_{\min}}{P_{\max}} \tag{2.22}$$

$$n_q = \frac{V_{do_{\max}} - V_{do_{\min}}}{Q_{\max}} \tag{2.23}$$

Voltage and Current Control Blocks

The d- and q-axis voltage references obtained in the power calculation block are passed through the voltage controller to obtain the d- and q-axis current references, as shown in Figure 2.15(a). Observe that the voltage controller block consists of two identical PI controllers and feed-forward terms to decouple the two axes.

From Figure 2.15, the following voltage controller equations can be obtained:

$$\frac{d\Phi_d}{dt} = V_{do}^* - V_{do} \quad \frac{d\Phi_q}{dt} = V_{qo}^* - V_{qo} \tag{2.24}$$

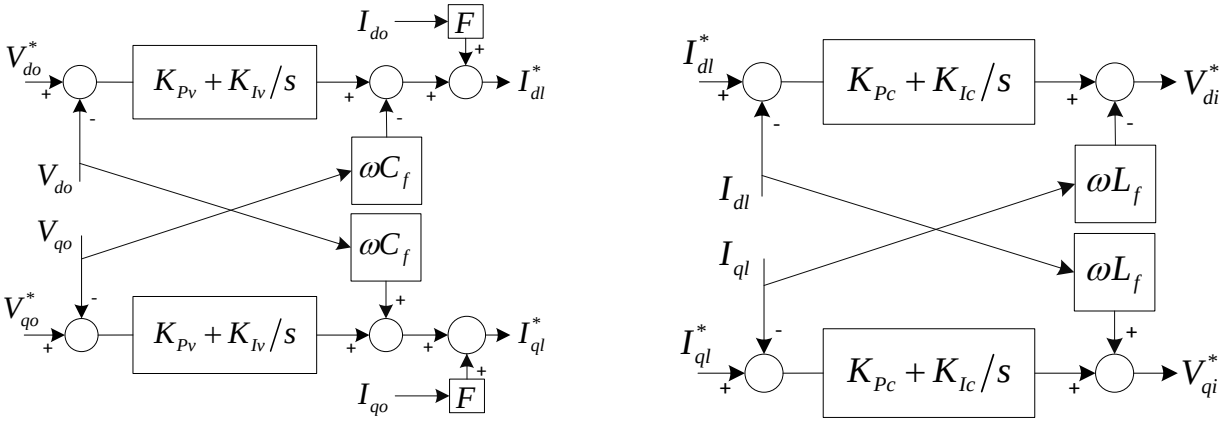

(a) Voltage Controller. (b) Current Controller.

Figure 2.15: Inverter control blocks.

$$I^*_{dl} = FI_{do} - \omega_n C_f V_{qo} + K_{Pv}\left(V^*_{do} - V_{do}\right) + K_{Iv}\Phi_d \tag{2.25}$$

$$I^*_{ql} = FI_{qo} + \omega_n C_f V_{do} + K_{Pv}\left(V^*_{qo} - V_{qo}\right) + K_{Iv}\Phi_q \tag{2.26}$$

where K_{Pv} and K_{Iv} are the proportional and integral gains of the voltage PI controller, C_f is the output filter capacitor, and I^*_{dl} and I^*_{ql} are the current references that are passed through the current controller block. These current references are then passed through the current controller to obtain the final PWM reference signals in d- and q- axis, as shown in Figure 2.15(b), resulting in the following equations:

$$\frac{d\gamma_d}{dt} = I^*_{dl} - I_{dl} \quad \frac{d\gamma_q}{dt} = I^*_{ql} - I_{ql} \tag{2.27}$$

$$V^*_{di} = -\omega_n L_f I_{ql} + K_{Pc}\left(I^*_{dl} - I_{dl}\right) + K_{Ic}\gamma_d \tag{2.28}$$

$$V^*_{qi} = \omega_n L_f I_{dl} + K_{Pc}\left(I^*_{ql} - I_{ql}\right) + K_{Ic}\gamma_q \tag{2.29}$$

where K_{Pc} and K_{Ic} are the proportional and integral gains of the current PI controller, L_f is the output filter inductor, and V^*_{di} and V^*_{qi} are the voltage references, which are transformed back to abc-reference frame to obtain the sinusoidal control signals for the PWM scheme of the VSC.

2.4 Unit Commitment

Generally, UC and EMS for isolated microgrids can be categorized into two main structures: centralized and decentralized [14]. The focus here is on centralized UC techniques, with the general architecture shown in Figure 2.16 [57]. Observe that the UC problem is solved based on inputs that include forecasted power output of the non-dispatchable generators for a pre-defined look-ahead window, forecasted local load for a pre-defined look-ahead window, State-of-charge (SoC) of the ESSs, operational limits of dispatchable generators and ESSs, and security and reliability constraints of the microgrid. The outputs are the commitment decision variables and the DERs output power reference set-points, which are sent via a proper communication infrustructure.

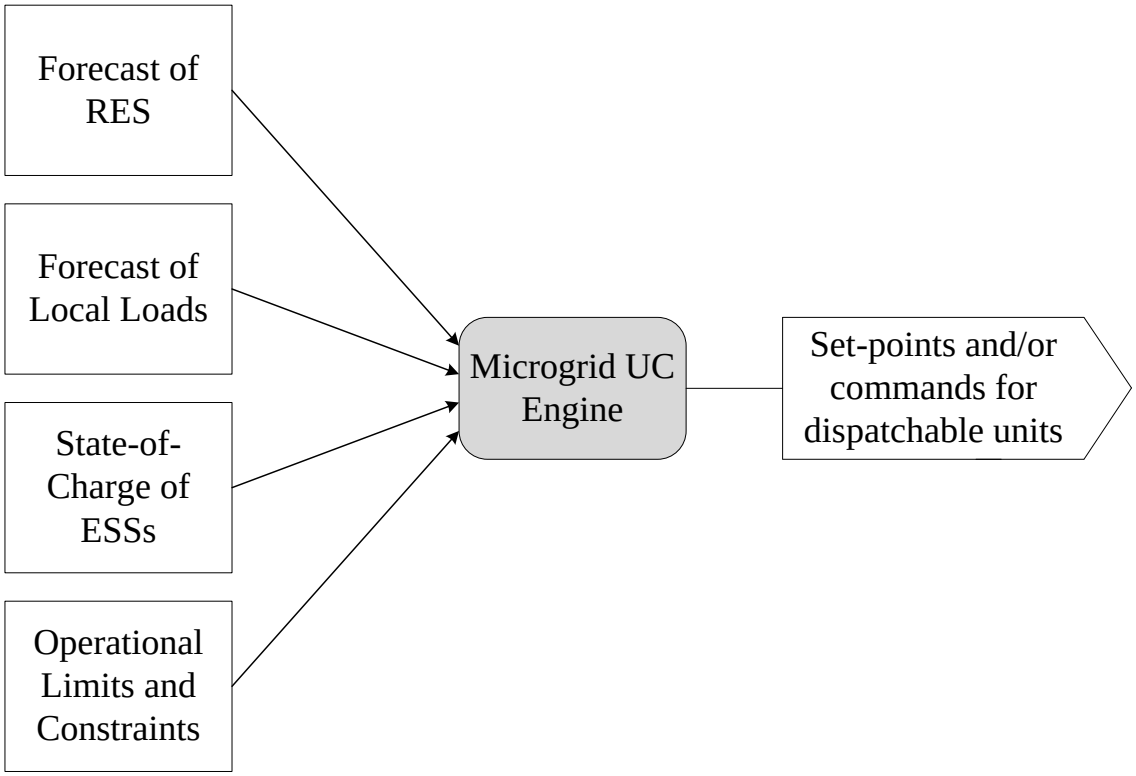

Figure 2.16: Centralized UC for isolated microgrids.

The UC model can be formulated as a mixed-integer optimization problem for a pre-defined time horizon, as follows [57]:

$$\begin{aligned} \min \quad & \sum_{t=1}^{T} J_{UC}(x_t, u_t, p_t) + G(\omega_t) \\ s.t. \quad & g(x_t, u_t, \omega_t, p_t) = 0 \quad \forall t \\ & h(x_t, u_t, \omega_t, p_t) \leq 0 \quad \forall t \end{aligned} \tag{2.30}$$

where p_t is the vector representing the system parameters, demand, and operational constraints such minimum up/down times and ramping limits; u_t is the vector representing the continuous control variables such as optimal dispatch; x_t is the vector of state variables; and finally $\omega \in \{0, 1\}$ represents the binary decision variables associated with the generators commitment status. The objective function to be minimized consists of two parts: $J_{UC}(.)$, which represents the generators fuel cost, and $G(.)$, which represents the costs associated with the units start-up/shut-down operation and the fixed operational costs of a committed generator[3]. The function $g(.)$ represents the set of equality constraints, including the power-balance of the system, and the logic constraints associated with the binary variables; $h(.)$ represents the inequality constraints including the generation limits, ramping limits, minimum up/down times, etc.

In isolated microgrids, the system size is usually small with short feeders compared to conventional power systems; hence, the UC can yield an optimal dispatch, since it is feasible to approximate the classical power flow constraints with the the active power demand-supply balance equations. Thus, under such an assumption, the UC model would form a MILP problem that can be solved using highly efficient commercial grade software packages, such as CPLEX [87]. There are numerous solution techniques that are explored and reported in literature to solve the UC within a reasonable computation time [88–91].

2.5 Summary

This chapter provided a basic background review of microgrids and associated stability issues, and voltage and frequency control in isolated microgrids, as well as the formulation of UC in microgrids. Thus, the definition of microgrids and basic related concepts of voltage and frequency stability were first introduced and discussed. Then, voltage and frequency control techniques were described in the context of isolated microgrids, including models of different components such as generator, governor, exciter, and inverters. Finally, a general formulation of UC models in microgrids were provided, discussing the objective function, equality and inequality constraints, and solution techniques.

[3] In some works, $J_{UC}(.)$ is a dual function of generators fuel cost and emission [86].

Chapter 3

Hybrid Droop-based Frequency Control in Inverter-based Isolated Microgrids

This section compares the performance of different droop-based control techniques in an islanded microgrid that operates solely on electronically interfaced DERs. Specifically, the following techniques are compared: the conventional droop-based control including a full SPWM-based VSC with power, voltage and current controls explained in Section 2.3.4 [27]; transient decentralized droop controls that are built upon conventional droop controls with extra feedback loops [37]; angle droop controls that operate based on drooping the power angle instead of the frequency [92]; and herein a proposed hybrid controller that merges the advantages of both the transient decentralized droop controller and the angle droop controller. A simple test system is used for these comparisons, demonstrating the advantages and disadvantages of the various droop controls studied, particularly of the proposed hybrid controller.

3.1 Transient Decentralized Droop Control

Transient droops are proposed in [37] to address the problem of poor transient response of droop controllers, providing transient active damping of the low frequency power sharing modes of the system. Thus, additional derivative terms are incorporated into the droop

equations (2.20) and (2.21), as follows:

$$\omega_o = \omega_n - m_p P - \hat{m}_p \frac{dP}{dt} \tag{3.1}$$

$$V_{do}^* = V_n - n_q Q - \hat{n}_q \frac{dQ}{dt} \tag{3.2}$$

where $\hat{m}_p$ and $\hat{n}_q$ are the transient droop gains. The rest of the control mechanism, including the voltage and current controllers remains the same as described in Section 2.3.4. This configuration enables the controllers to obtain the voltage and frequency regulation via original droop gains, whereas the transient gains can be tuned to damp the oscillatory behaviour of the output active and reactive power. Small-signal analysis is carried out in [37] to demonstrate that the desired dynamic performance can be achieved by varying $\hat{m}_p$ and $\hat{n}_q$, without affecting the steady-state performance set by m_p and n_q. In addition, the damping of the active and reactive power sharing controls can be adjusted by means of ole placement technique.

3.2 Angle Droop Control

To alleviate large variations of the frequency for normal load changes, angle droop is proposed as an alternative to frequency droop, fascilitating power sharing by controlling the output voltage angle of each VSC [92]. Under such a control paradigm, the frequency droop equation in Figure 2.14 is changed from frequency to voltage angle, as follows:

$$\delta_o = \delta_n - m_\delta P \tag{3.3}$$

where δ_n is the rated voltage angle when it is supplying the load at its rated power, and m_δ is the angle droop coefficient. This droop coefficient is determined so that, when the DER output power P is nominal, the operating voltage angle δ_o is zero; thus, $\delta_n = m_\delta P_{rated}$. This approach is utilizing a DC load flow analysis of a system with two DERs in [92], where it is shown that the DER output active powers are in inverse proportion to their angle droop coefficients, as follows:

$$\frac{P1}{P2} \approx \frac{m_{\delta 2}}{m_{\delta 1}} \tag{3.4}$$

The rest of the control strategy, including the voltage versus reactive power droop, and the voltage and current control loops remains the same as described in Section 2.3.4.

3.3 Hybrid Droop Control

To simultaneously address the problem of poor transient and frequency response, a new hybrid controller is proposed in this section that provides transient active damping of the low frequency modes of the system, and achieves the proper power sharing by controlling the output voltage angle of each VSC. The active power droop block diagram of the new hybrid controller is shown in Figure 3.1, where the droop equations are modified as follows:

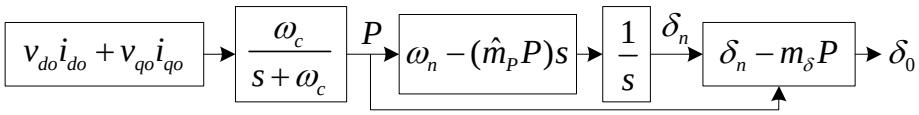

Figure 3.1: Active power droop structure of the hybrid controller.

$$\omega_o = \omega_n - \hat{m}_p \frac{dP}{dt} \tag{3.5}$$

$$\delta_n = \int_0^{2\pi} \omega_o \, dt \tag{3.6}$$

$$\delta_o = \delta_n - m_\delta P \tag{3.7}$$

$$V_{od}^* = V_n - n_q Q - \hat{n}_q \frac{dQ}{dt} \tag{3.8}$$

Here, ω_n is the nominal angular frequency, $\hat{m}_P$ and $\hat{n}_q$ are the transient droops, V_n is the nominal voltage, and m_δ is the angle droop coefficient.

Under the hybrid droop control paradigm, the transient droop gains are tuned to ensure an enhanced transient response, while the angle droop coefficient is tuned to achieve the proper power sharing among the converters, based on (3.4), where the DERs output active power is in inverse proportion to their angle droop coefficients.

3.4 Results and Comparison

The test system shown in Figure 3.2 is used to evaluate and compare the performances of the aforementioned control techniques, modeling it in detail in PSCAD/EMTDC [93] as a three-phase system with two DERs represented as ideal DC sources. The DERs are interfaced via PWM-based VSCs with power, voltage, and current controllers, as discussed in the previous chapter. The test system is based on the systems used in [27], [37], and [92].

Table 3.1 summarizes the systems parameters and the parameters corresponding to each control strategy, with all the parameters that the three control strategies have in common being the same. The *LC* filter parameters are chosen from [37]; note that these parameters may not be realistic due to inverter loss and voltage drop. However, from a theoretical perspective, the droop control techniques performances discussed in this chapter does not depend on the filter parameters; thus, it is expected that these control techniques would demonstrate similar performance in more realistic test systems. The controllers are tuned based on trial-and-error to achieve an acceptable transient response and load sharing. The droop gains are adjusted so that the active and reactive power outputs of DER2 are double of those for DER1.

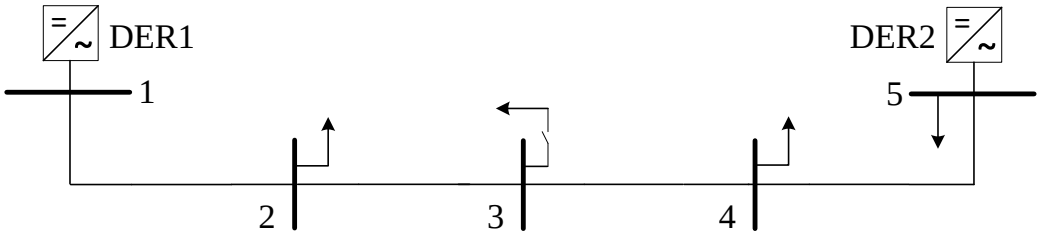

Figure 3.2: Test System.

3.4.1 Existing Controllers

The controls are tested by connecting an additional 30 kW load at Bus 3 at $t = 0.5$s. Figures 3.3(a)-3.3(c) show the active and reactive power output for all three existing controllers; note that all three different strategies are able to achieve an acceptable power sharing among the parallel DERs. However, the transient performance of the system with the transient droop strategy is considerably improved compared to the other two strategies, as the system has a smoother active and reactive power output. Observe that the angle droop shows similar transient response as the conventional droop control.

Figure 3.4 shows the plot of system frequency before and after connection of the additional load. Observe that angle droop control improves the system frequency response, with near-to-zero steady state deviation from the nominal set-point. The transient droop control has a slightly slower response compared to the conventional droop-based control technique, and has the same steady state deviation as the conventional control, and neither is suitable for situations where frequency recovery to its nominal value is required.

Table 3.1: DERs power Rating and Network Parameters

DERs Nominal Ratings (kVA)	
DER1	40
DER2	80
Network Parameters	
Nominal frequency	60 Hz
Three phase RMS L-L Voltage	208 V
Total Load at nominal voltage	80 kVA
Feeder1-2	$0.05+0.1j$ Ω
Feeder2-3	$0.03+0.1j$ Ω
Feeder3-4	$0.01+0.02j$ Ω
Feeder4-5	$0.02+0.1j$ Ω

DER1 Parameters					
L_f	R_f	C_f	m_p	n_q	$\hat{m}_p$
1.5 mH	0.15 Ω	50 μF	$8e^{-5}$	$3e^{-3}$	$4e^{-6}$
m_δ	K_{Pv}	K_{Iv}	K_{Pc}	K_{Ic}	$\hat{n}_q$
0.001	0.045	200	10	20000	$15e^{-5}$

DER2 Parameters					
L_f	R_f	C_f	m_p	n_q	$\hat{m}_p$
1.5 mH	0.15 Ω	50 μF	$4e^{-5}$	$15e^{-4}$	$2e^{-6}$
m_δ	K_{Pv}	K_{Iv}	K_{Pc}	K_{Ic}	$\hat{n}_q$
0.0005	0.045	200	10	20000	$75e^{-6}$

3.4.2 Hybrid Droop Technique

The DERs active and reactive powers for the hybrid droop controller are shown in Figure 3.5, while the frequency response of the system is compared with the one for the angle droop controller in Figure 3.6. Note that under the hybrid droop control paradigm, the power is properly shared between the DERs. In addition, the system transient response

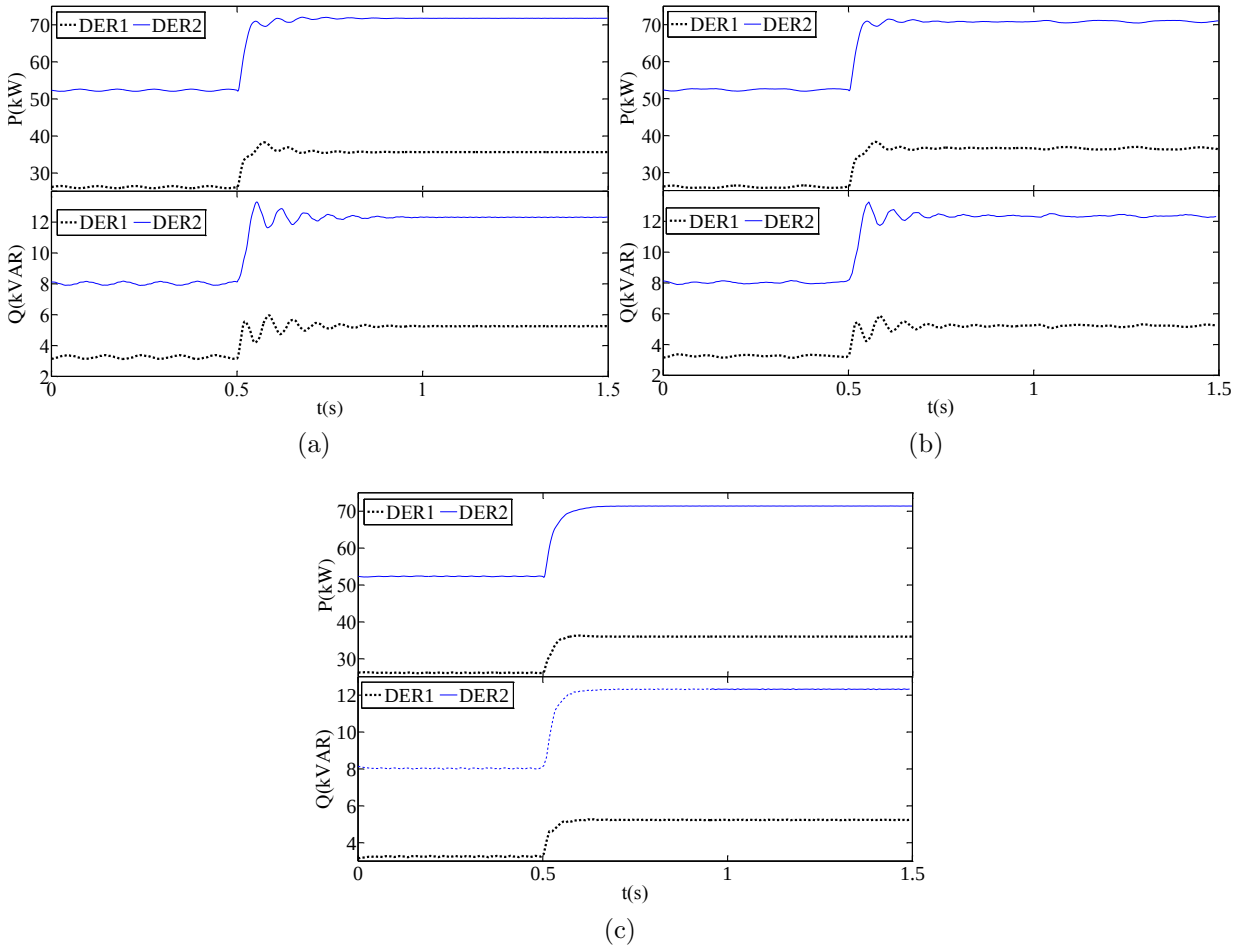

Figure 3.3: Active and reactive power output of DERs with three control techniques: (a) frequency droop, (b) angle droop, and (c) transient droop.

is enhanced, and is the same as the transient response of the transient droop mechanism. Moreover, the frequency response of the system has zero steady-state error and is almost the same as the frequency response under the the angle droop control paradigm.

3.4.3 Comparison

Both transient and angle droop controls suffer from drawbacks that should be taken into consideration in practice. The first increases the complexity of the system in terms of tuning

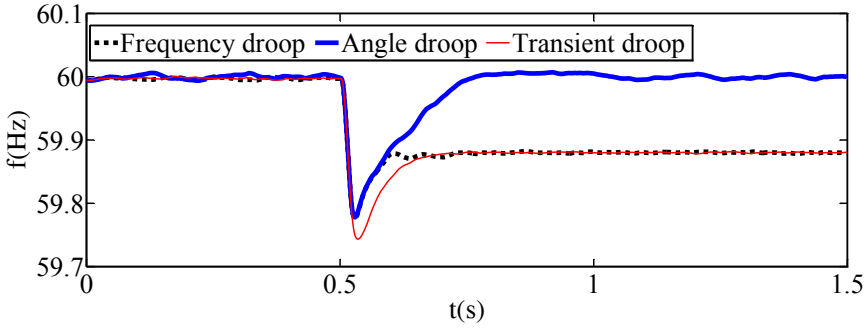

Figure 3.4: Frequency response of the system with the three control techniques.

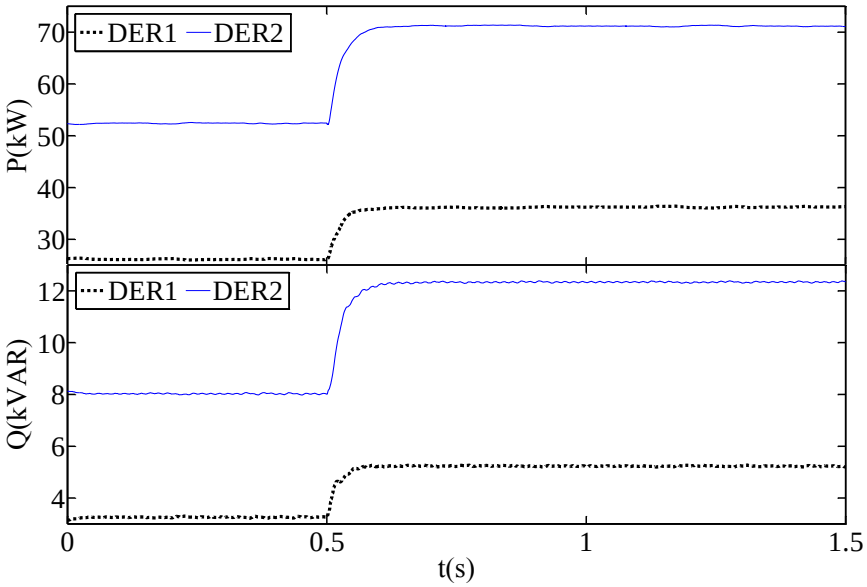

Figure 3.5: Active and reactive power output of DERs with the proposed hybrid controller.

and implementation, since obtaining droop gains that are based on the derivate of the output power can be problematic in practice. The latter control needs Phasor Measurement Units (PMUs) to ensure proper angle referencing in the system, thus undermining the advantage of decentralized, communication independent, droop controls. A brief summary of the advantages and disadvantages of each control technique is presented in Table 3.2.

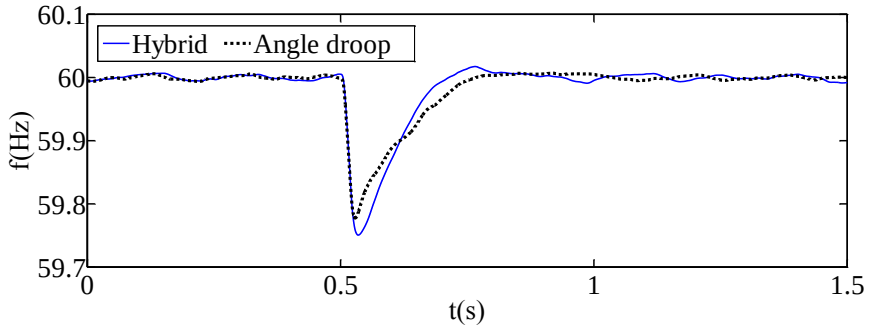

Figure 3.6: Frequency response with the angle droop and the proposed hybrid control techniques.

Table 3.2: Advantages and Disadvantages of Control Techniques

Technique	**Advantages**	**Disadvantages**
Frequency droop	Simpler tuning and implementation	Poor transient response and steady-state deviation
Angle droop	Improved frequency response	Need for PMUs and poor transient response
Transient transient droop	Improved transient response and small-perturbation stability	Complicated implementation and tuning
Hybrid droop	Improved transient and frequency response	Increased implementation and tuning complexity and the need for PMUs

3.5 Summary

In this chapter, conventional, transient, and angle droop controls were discussed. The performance of each control technique was evaluated through time domain simulations on a simple test system, and it was shown through simulation results that the transient droop control demonstrated better transient response, while angle droop control exhibited no steady-state deviation in the frequency response of the system. Following that, a new hybrid droop control was proposed based on the transient and angle droop control, showing that it has better transient and improved frequency response. In spite of the increased complexity in the tuning and implementation of the proposed controller, it demonstrates an overall superior performance that would justify its adoption instead of the other discussed controls. The main content of this chapter is published in [94].

Chapter 4

Voltage-based Frequency Controller

This chapter presents a frequency control mechanism for an isolated/islanded microgrid through voltage regulation. The proposed scheme makes use of the voltage sensitivity of loads in isolated microgrids. The performance of the proposed controller is evaluated and validated through various simulation studies in the PSCAD/EMTDC software environment based on a realistic microgrid test system, using small-perturbation stability analysis to demonstrate the positive effect of the proposed controller in system damping.

4.1 Load Voltage Dependency

Loads in power systems, particularly microgrids, can be typically modelled by the following equation [16]:

$$P_L = P_{L0}\left(\frac{V_L}{V_{L0}}\right)^{n_P} \tag{4.1}$$

which is equivalent to a ZIP load model:

$$P_L = P_{L0}\left[Z_p\left(\frac{V_L}{V_{L0}}\right)^2 + I_p\left(\frac{V_L}{V_{L0}}\right) + P_p\right] \tag{4.2}$$

$$n_P \approx \frac{2\times Z_p + 1\times I_p + 0\times P_p}{Z_P + I_p + P_p} \tag{4.3}$$

Similarly:

$$Q_L = Q_{L0}\left(\frac{V_L}{V_{L0}}\right)^{n_Q} \tag{4.4}$$

$$Q_L = Q_{L0}\left[Z_q\left(\frac{V_L}{V_{L0}}\right)^2 + I_q\left(\frac{V_L}{V_{L0}}\right) + P_q\right] \tag{4.5}$$

$$n_Q \approx \frac{2\times Z_q + 1\times I_q + 0\times P_q}{Z_q + I_q + P_q} \tag{4.6}$$

where P_L is the active power demand; Q_L is the reactive power demand; P_{L0} is the rated active power, and Q_{L0} is the rated reactive power at nominal operating voltage V_{L0}; and n_P and n_Q are voltage indexes for the active power and reactive power, respectively; Z_p, I_p, and P_p, and Z_q, I_q, and P_q are the constant impedance, constant current, and constant power coefficients for active and reactive power respectively. As it can be seen from (4.1), the active power demand sensitivity to the operating voltage ($\partial P/\partial V$) is determined by n_P; thus as n_P increases, the sensitivity of power consumption with respect to operating voltage also increases. In [95], a comprehensive study is carried out to model residential loads that shows an average n_P for existing residential load models in the range of 1.1 to 1.7, which are the values expected in isolated microgrids, where the majority of the power is consumed by households for heating and lightning purposes (resistive loads).

Throughout this thesis, two different values of n_P are assumed, $n_P = 1.5$ ($Z_p = 0.6$, $I_p = 0.3$, $P_p = 0.1$) and $n_P = 1.2$ ($Z_p = 0.3$, $I_p = 0.6$, $P_p = 0.1$), which are in accordance with practical measurements in [51]. For a system with $n_P = 1.5$, a change in the operating load voltage ΔV, will result in an active power demand change ΔP_L, as follows:

$$\Delta P_L = \left((V_L + \Delta V_L)^{1.5} - V_L^{1.5}\right)\frac{P_{L0}}{V_{L0}^{1.5}} \tag{4.7}$$

Assuming that V_L and V_{L0} are both 1 pu, i.e. the loads were operating at their nominal operating voltage prior to change, (4.7) can be re-written as follows:

$$\Delta P_L = \left((1 + \Delta V_L)^{1.5} - 1\right)P_{L0} \tag{4.8}$$

From this equation, in a system with $n_P = 1.5$, a 5% decrease in the operating voltage will reduce the active power demand by around 7.4%. In other words, a relatively slight drop in the operating voltage results in a comparable demand reduction. Furthermore, if during a change in voltage, and subsequently demand, the input mechanical power remains fixed,

i.e. $\Delta P_M = 0$ (2.8), the latter can be written as:

$$\Delta\omega(s) = \frac{0.076 P_{L0}}{2Hs} \tag{4.9}$$

where H is typically in the range of 1 to 10 seconds. Thus, if $H = 1$ s, then for a 0.05 per unit change in the voltage, the frequency deviation of the system would be:

$$\Delta\omega(s) = \frac{0.076 P_{L0}}{2\ s} \tag{4.10}$$

Hence, using the final value theorem, the steady-state deviation of the frequency with respect to changes in the load voltage would be:

$$\Delta\omega(s)_{ss} = \lim_{s\to 0} S\left(\frac{0.076 P_{L0}}{2\ s}\right) = 0.038\ P_{L_0} \tag{4.11}$$

Observe that this leads to a 3.8% change in system frequency for a 1 pu nominal load. Therefore, it is possible to adequately manipulate the system frequency by modifying the operating load voltage.

Even though the presented analysis is somewhat simple, and the roles of other microgrid components involved in the process are neglected, it gives a reasonable idea of the impact of load voltage variations on system frequency. Hence, this strategy is utilized in this chapter to provide a virtual reserve capacity for the system, which is provisioned from the proposed VFC. It would have an instantaneous effect on the system demand and thus alleviate the need for investing in ESS. In the coming sections, the VFC is discussed in detail and time-domain simulation results are presented, to demonstrate the potential of using load voltages for system frequency control.

4.2 Proposed Voltage-Based Frequency Controller

Figure 4.1 shows the proposed VFC for an isolated microgrid. The input signal to the controller is the system frequency deviation from the nominal set-point Δf. The frequency error is passed through a Proportional-Integral (PI) controller to ensure that the steady-state error is zero, and the gain K_{VFC} determines the damping factor provided by the VFC. The signal is passed through a lead-lag block to compensate for the phase difference between the voltage regulator input and output; to obtain the best response, more than one lead-lag block may be used in practice. The limits VFC_{max} and VFC_{min} constrain

the output signal to ensure that the voltage remains within a desired range. The output signal of the VFC is then added to the reference set-point signal of the voltage regulator V_{ref}. In a diesel-based system, the voltage regulator is the synchronous machine excitation system, as shown in Figure 4.2; in an inverter-based system, the voltage regulator would be the voltage control block, hence the VFC would be integrated in the inverter control system as shown in Figure 4.3.

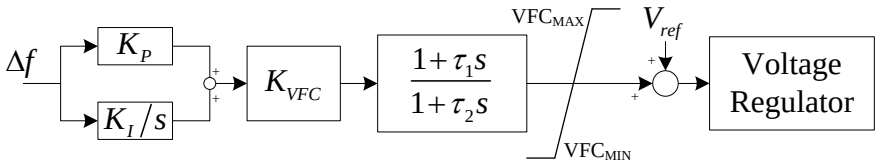

Figure 4.1: The proposed VFC for a system voltage regulator, such as the one for a synchronous machine.

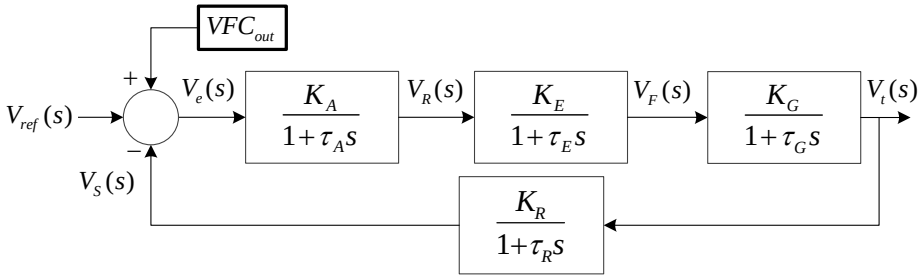

Figure 4.2: Block diagram of the proposed VFC and its integration with a synchronous machine.

It can be observed in Figure 4.1 that the VFC control structure is similar to that of a Power System Stabilizer (PSS). However, there are fundamental differences in the application domain and performance of VFC and PSS. First, PSS acts on the derivative of rotor speed of a synchronous machine, and is designed to damp the low frequency electromechanical oscillations in power systems in the range of 1-2 Hz, such as inter-area oscillations. Such phenomena may occur in traditional power systems with large transmission networks. However, low frequency electromechanical oscillations are not a major concern in isolated microgrids due to relatively short feeders. Second, PSS is not designed to address large frequency deviations and/or eliminate steady-state frequency error. On the other hand, since VFC reacts to large frequency changes, it provides virtual reserves for the system that compensates for the active power mismatch and can potentially prevent frequency instabilities in isolated microgrids.

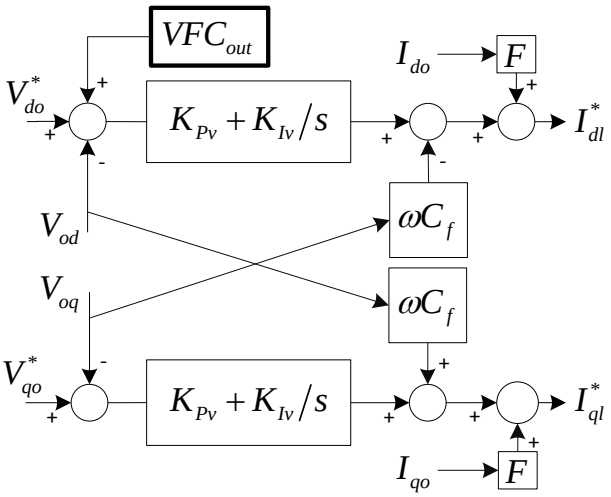

Figure 4.3: Block diagram of the proposed VFC and its integration with a VSC.

The general transfer function of the VFC is given as follows:

$$G_{VFC}(s) = K_{VFC}\frac{1+\alpha s+\beta s^2}{\tau_i s+\gamma s^2} \tag{4.12}$$

$$\alpha = (K_P+1)\tau_i+\tau_2 \qquad \beta = K_P\,\tau_i\,\tau_2+\tau_i\,\tau_1 \qquad \gamma = \tau_i\,\tau_2 \tag{4.13}$$

and $\tau_i = \frac{1}{K_I}$, τ_1, and τ_2 are the integrator and lead-lag block time constants, respectively an K_P is the proportional gain. Care should be taken to tune the controller so as to ensure the overall system stability. In addition, the controller gain K_{VFC} should properly address the relation between the system operating frequency and the voltage.

In general, the VFC parameters would be very much dependent on the system characteristics. In a diesel-based isolated microgrid, the relation between changes in the operating voltage and hence frequency can be derived from (2.8) as follows:

$$\Delta f' = -f_0 P_{L0}\frac{((V_L+\Delta V_L)^{n_P}-V_L^{n_P})}{2HV_{L0}^{n_P}} \tag{4.14}$$

Assuming that $V_{L0} = 1$ pu and the system is operating at its nominal voltage prior to any change, (4.14) can be re-written as:

$$\Delta V_L = (\Delta f'\mu+1)^{1/n_P}-1 \tag{4.15}$$

where $\mu = \frac{-2H}{f_0 P_{L0}}$ reflects the system characteristics, since the inertia constant H, nominal frequency f_0, load power P_{L0}, and voltage index n_P determine the voltage frequency dependency. For an inverter-based system, the relation between the changes in the operating voltage and hence frequency can be derived from (4.15) as follows:

$$\Delta f = f_n - m_p P_{L0} \frac{((V_L + \Delta V_L)^{n_P} - V_L^{n_P})}{V_{L0}^{n_P}} \tag{4.16}$$

Assuming that $V_0 = 1$ pu and the system is operating at its nominal voltage prior to any change, (4.16) can be re-written as:

$$\Delta V_L = \left(\frac{f_n - \Delta f}{m_p P_{L0}} + 1 \right)^{1/n_P} - 1 \tag{4.17}$$

4.3 Impact of VFC on Small-Perturbation Stability

Small-perturbation analysis is carried out using eigenvalue studies with the system linearized around a nominal operating point [16]. However, this approach is useful for systems in balanced conditions, which is not the case in general for microgrids given the system model complexities [96]. Hence, in this thesis a modal estimation approach is utilized, in particular the Prony technique, to estimate the system eigenvalues [97]. Thus, the generator speed signal $\omega(t)$ is extracted in continuous form and sampled in discrete form $\omega(k)$, and is represented as a sum of n damped complex sinusoids, as follows:

$$\omega(t) = \sum_{i=1}^{n} \bar{R}_i e^{\lambda_i t} = \sum_{i=1}^{n/2} A_i e^{\alpha_i t} \cos(\beta_i t + \Phi_i) \tag{4.18}$$

$$\omega(k) = \sum_{i=1}^{n} \bar{R}_i Z_i = \sum_{i=1}^{n} \bar{R}_i e^{\lambda_i T_s} \tag{4.19}$$

where $\bar{R}_i$ is an output residue corresponding to the mode $\lambda_i = \alpha_i + j\beta_i$, T_s is the sampling time, $A_i = 2|\bar{R}_i|$, and k is the discrete time. According to the Prony method, λ_i and $|\bar{R}_i|$ can be calculated considering that (4.19) is the solution to a difference equation with order n as follows:

$$\omega(k) = -a_1\omega(k-1) - a_2\omega(k-2) - \cdots - a_n\omega(k-n) \tag{4.20}$$

This model is often referred to as an auto-regressive model [98], where the output is dependent on the past outputs.

Re-writing (4.20) in a matrix form results in the following:

$$\Omega = D\theta \tag{4.21}$$

$$\Omega = [\omega_{k+n}\ \omega_{k+n+1}\ \omega_{k+n+2}\ \dots\ \omega_{k+N}]^T_{N-n+1} \tag{4.22}$$

$$\theta = [-a_1\ -a_2\ \dots\ -a_n]^T \tag{4.23}$$

$$D = \begin{bmatrix} \omega_{k+n-1} & \omega_{k+n-2} & \dots & \omega_k \\ \omega_{k+n} & \omega_{k+n-1} & \dots & \omega_{K+1} \\ \vdots & & & \\ \omega_{k+N-1} & \omega_{k+N-2} & \dots & \omega_{k+N-n} \end{bmatrix} \tag{4.24}$$

where N is the number of samples. A least square method can be utilized to compute θ, and the system characteristic equation can be formed using the vector θ as follows:

$$Z^n + a_1 Z^{n-1} + a_2 Z^{n-2} + \dots + a_n = 0 \tag{4.25}$$

The eigenvalues of the system are the roots of (4.25). In this Chapter, the number of complex sinusoids, i.e. the number of the complex poles of the system is considered to be 8; This number was chosen by trial and error, with 8 modes giving the closest estimation of the input signal. The calculations are carried out using the MATLAB built-in Prony function, as discussed next.

4.4 Results for Diesel-based Test System

To demonstrate the effectiveness of the proposed VFC, a test system, based on the CIGRE benchmark for medium voltage distribution network [13], is implemented in PSCAD/EMTDC [93], with two diesel-based synchronous machines along with three DERs. The general schematic of the test system is shown in Figure 4.4, and the corresponding data is provided in the Appendix. The total load of the system is about 7 MVA, distributed among the buses so as to have an unbalanced load. Feeders are modelled as coupled π sections. Observe that the CIGRE benchmark test system used in this thesis has a loop configuration that adds to the complexity of controls. The results obtained from the test scenarios presented in this chapter are expected to be similar for a radial configuration of the CIGRE benchmark test system, since the performance of the VFC dominantly depends on the load voltage sensitivity and voltage regulators' time constant.

The DERs are connected through bi-directional VSCs that are fully modelled as shown

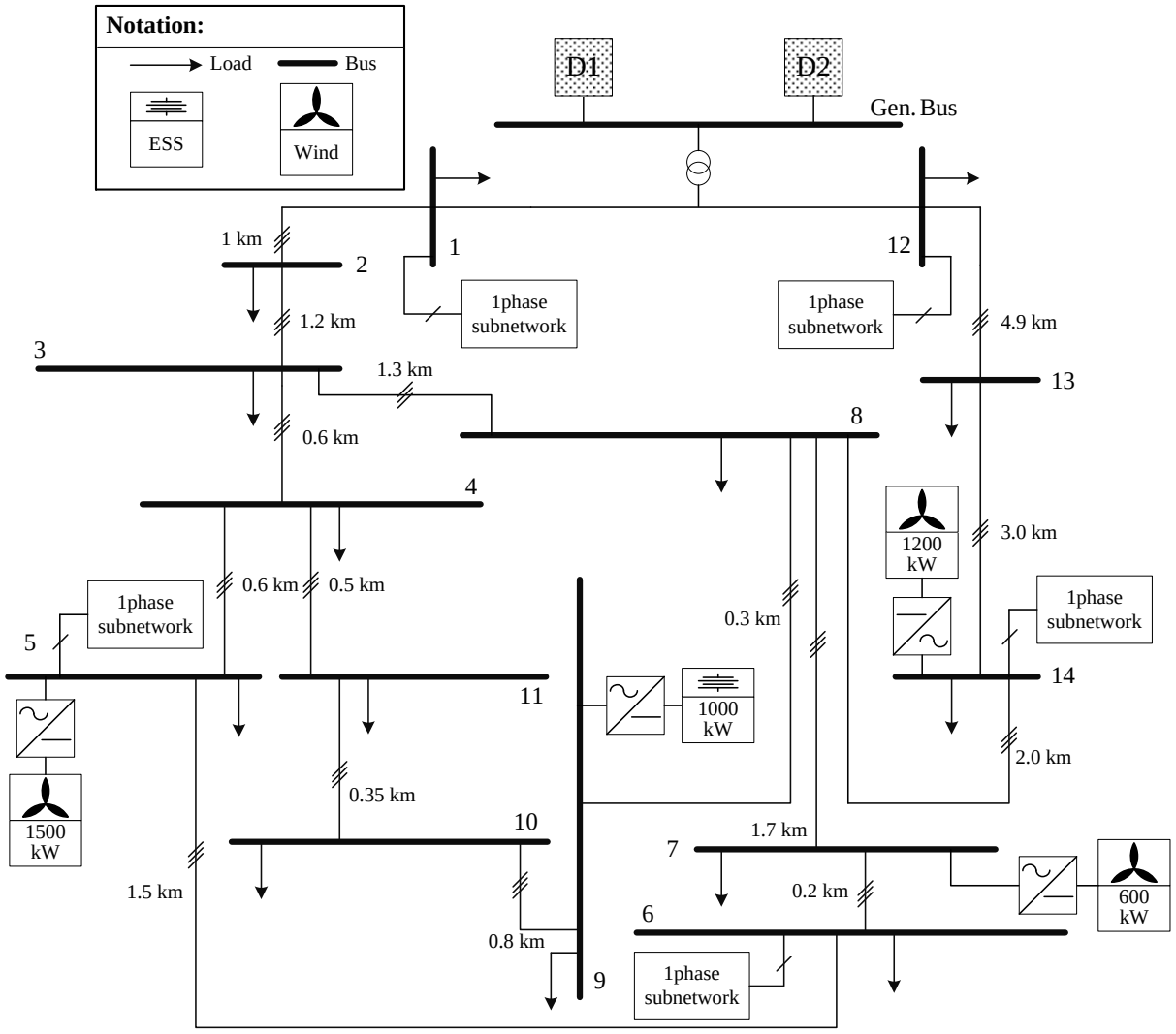

Figure 4.4: Test microgrid based on a medium voltage distribution network benchmark.

in Figure 2.13, including PWM, $abd \leftrightarrow dq$ transformations, PLLs, and control blocks. These are modelled as ideal dc sources, and their active power output is modelled using actual measurements from an actual low-voltage 300 kW wind turbine, measured over 185s with a resolution of 0.1s, as shown in Figure 4.5. For the purpose of this study, DER#1 comprises five sub-units, DER#2 two sub-units, and DER#3 four sub-units, with each sub-unit output being the same as the power depicted in Figure 4.5; hence, the nominal ratings of the DERs are 1.5 MW, 600 kW and 1.2 MW, respectively.

The synchronous machines nominal rating is a combined 5.4 MVA. In most of the cases discussed here, the two synchronous machines are in charge of regulating the voltage, and the DERs are operating under the CCM, paradigm with unity power factor and no contribution to voltage regulation. Since in isolated microgrids, the voltage is dominantly controlled by the synchronous machine voltage regulation systems, the VFC is implanted on the exciters of these machines; The standard IEEE AC1A excitation systems are used in this work [99]. Thus, the synchronous machines correspond to master controls regulating the voltage and frequency, and the DERs are the slave controls supplying active power to the system. The parameters of the VFC are given in Table 4.1 and are obtained using the Ziegler-Nichols Tuning technique [100]. It should be mentioned that two lead-lag filters have been used to obtain the best performance of the controller; hence, in Table 4.1, τ_1 and τ_2 are the parameters of the first filter and τ_1' and τ_2' are the parameters of the second filter.

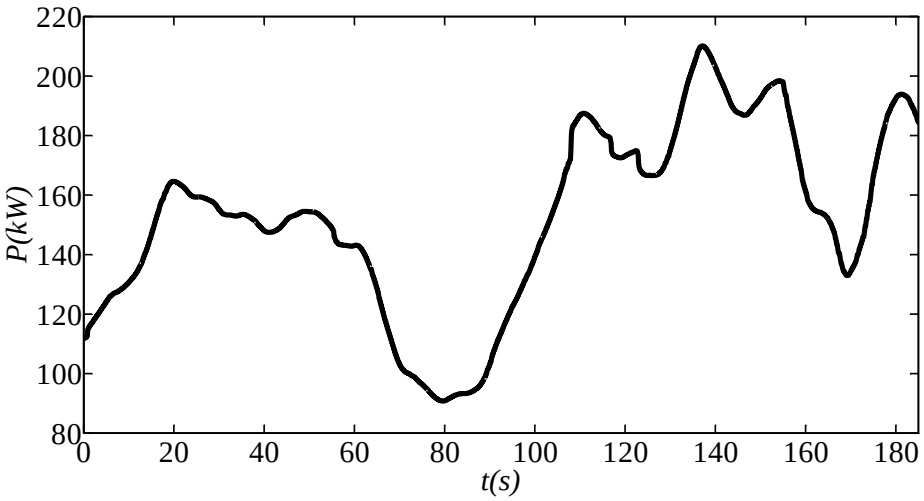

Figure 4.5: Low-voltage 300 kW wind turbine measured output power.

Table 4.1: VFC Parameters

Parameter	**Value**	**Parameter**	**Value**	**Parameter**	**Value**
K_P	0.2	τ_i(s)	2.65	τ_1(s)	0.01
τ_2(s)	0.9	τ_1'(s)	0.01	τ_2'(s)	0.25

4.4.1 Critical Eigenvalues vs. K_{VFC}

Critical eigenvalues are monitored to evaluate the impact of the VFC on the system small-perturbation stability. Figure 4.6 shows the trajectory of the most critical eigenvalue with respect to changes in K_{VFC}, from 0 (VFC not in effect) to 3.5; this eigenvalue corresponds to the low-frequency dominant mode of the system, and is largely sensitive to the controlling parameters. Observe that as K_{VFC} increases, the damping increases untill reaching a point where for further increase of the gain the system overall damping deteriorates. Table 4.2 summarizes the critical eigenvalue damping with respect to changes in K_{VFC}. Note that $K_{VFC} = 1$ yields the best result, and hence is adopted here as the VFC gain for the test microgrid.

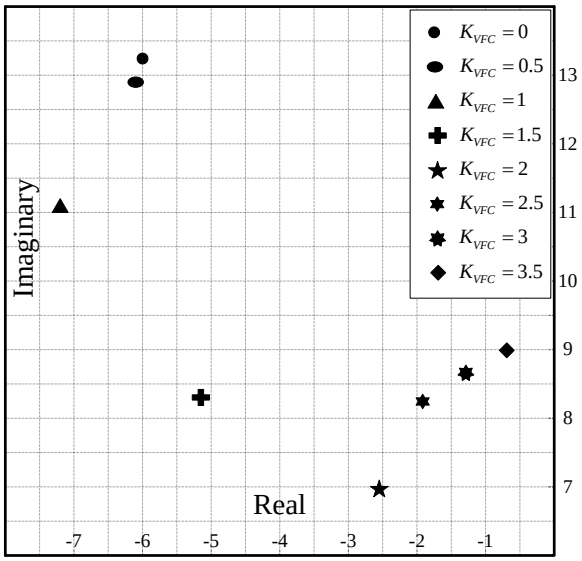

Figure 4.6: Dominant eigenvalue for different values of K_{VFC}.

Table 4.2: Critical Eigenvalue Damping

K_{VFC}	ζ	K_{VFC}	ζ
0	0.422	0.5	0.432
1	0.539	1.5	0.532
2	0.307	2.5	0.229
3	0.148	3.5	0.076

4.4.2 Scenario 1: VFC vs. Fast-Acting ESS

The effectiveness of the VFC during wind fluctuations is demonstrated by comparing the response of the system with and without the VFC. The initial wind generation power penetration level of the system is around 20%, and increases up to 40% following the profile in Figure 4.5.

Figure 4.7 presents the frequency response of the base system without (solid line) and with the proposed VFC (dotted line), and the RMS three-phase line-to-line voltages for the generator bus and Bus 8. The active and reactive power generation of diesel Unit 1 is shown in Figure 4.8, with diesel Unit 2 exhibiting the same power injections. Note that the VFC is capable of providing a smooth frequency response as wind output fluctuates, even for a significant penetration of up to 40% of the total power in the system. This is especially significant, since the system with the VFC has no storage. Observe that the voltage variations are kept within the operating voltage range of 0.88-1.1 pu, which is acceptable in isolated microgrids [101]. Also, observe that the active power output of the diesel generators with the VFC has no significant change since the VFC compensates for the wind variations.

To better evaluate the effectiveness of the VFC, the frequency response of the system with a fast-acting ESS and no VFC is also shown in Figure 4.7. The fast-acting ESS control strategy is similar to the one discussed in [10], and its battery is modelled based on the battery model proposed in [102]. This ESS is connected to Bus 9, and operates at unity power factor under the CCM paradigm; it is charged or discharged according to the power imbalance in the system and has a regulating capacity of 30 MW/Hz, which is a high power-frequency droop, considering that normal ESS droops are in the range of 1 MW/Hz. Such a high droop is chosen for the ESS to achieve a frequency response similar to that of the VFC. Observe from the plot of the output active power of the ESS in Figure 4.9, that the ESS absorbs up to 1 MW of active power and about 20 kWh of energy is exchanged with the microgrid. Assuming that the initial SoC of the battery is 20%, the minimum capacity of storage required for this scenario over the course of 180 seconds is almost 25 kWh, and if the wind fluctuations follows the same pattern for an hour, the ESS should be as large as 0.5 MWh. Hence, since valve regulated lead-acid (VRLA) batteries are among the most common batteries used in isolated microgrids, such an ESS would be quite expensive, since the procurement price for the VRLA ranges from $5 million to up to $12 million per MWh [103], without considering the price of operation and maintenance. Thus, the implementation of the proposed VFC can bring significant savings by reducing the need for ESS.

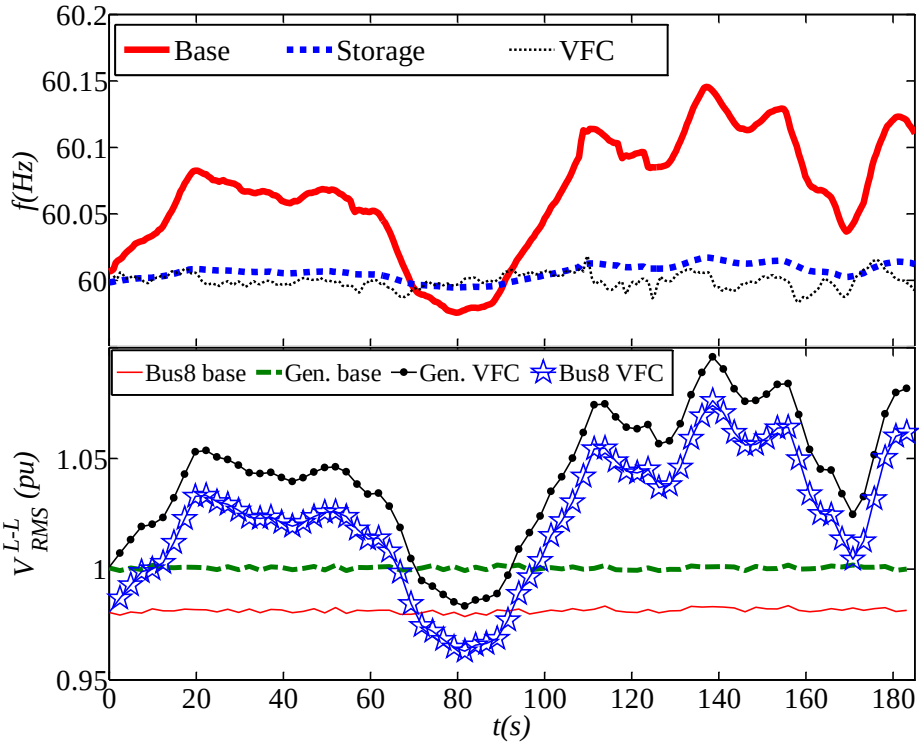

Figure 4.7: Voltage and frequency response of the system due to wind fluctuations for Scenario 1.

4.4.3 Scenario 2: Disconnection of DER Units

To demonstrate the effectiveness of the proposed VFC during large disturbances, all the DERs are disconnected at $t = 1$s. Prior to disconnection, the microgrid is assumed to be in steady-state, and the instantaneous wind power penetration is about 30%, i.e. the DERs are generating more than 2 MW of active power.

Figure 4.10 demonstrates the frequency response and the RMS three-phase line-to-line voltage of the generator bus for the base system (solid line) and for the proposed VFC (dashed line). Also, the active and reactive power injection of diesel Unit 1 is illustrated in Figure 4.11, with diesel Unit 2 exhibiting the same power injection. Observe that for the base system, the frequency drops below 59.8 Hz after the disturbance, which is considered as the minimum acceptable operating frequency of microgrids by some utilities [101]; therefore, the base system would require load shedding for secure operation. On the other hand, the frequency response of the system with the VFC is significantly improved with a steady-state frequency around 59.9 Hz, while the voltage remains within acceptable

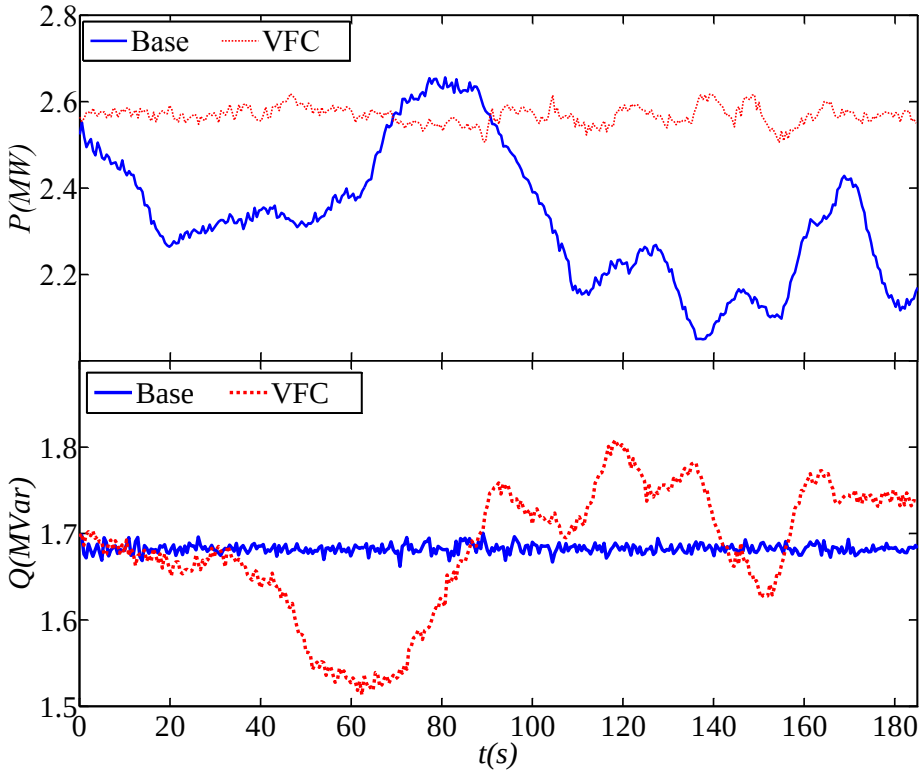

Figure 4.8: Active and reactive power injection of diesel Unit 1 with and without the VFC for Scenario 1.

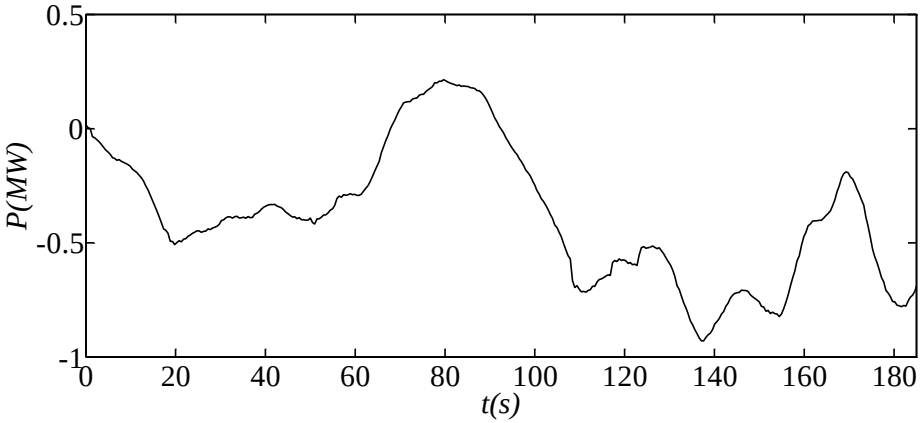

Figure 4.9: Active power output of the ESS due to wind fluctuations (Scenario 1).

limits according to [101]; hence, the system does not require load curtailment in this case.

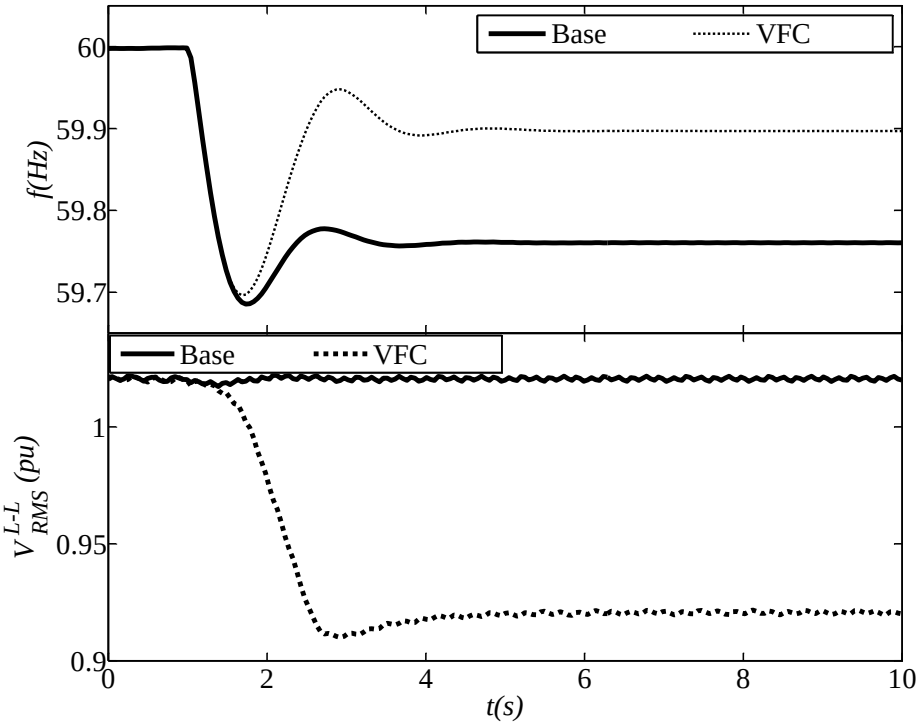

Figure 4.10: Voltage and frequency response of the system before, during, and after the disconnection of DER units for Scenario 2.

Note that the lower voltage limit for the VFC operation is set to 0.92 pu, which is 0.04 pu higher than the minimum permitted operating voltage, so that the voltage drops through the feeders as the distance increases from the generator bus do not exceed the maximum allowed values in steady-state. For a typical-size isolated microgrid, voltage drops through the feeders would be around 1-2 percent, as shown by the voltages at Bus 5, Bus 8, Bus 7, and Bus 14 depicted in Figure 4.12; observe that all these voltages remain within the acceptable range of operation, with a voltage drop of no more than 0.02 pu with respect to the Gen. Bus.

4.4.4 Scenario 3: Effect of Operating Voltage Limit

In all previous cases, the voltage limit is considered to be in the range of 0.92-1.1 pu at the generation bus. To examine the impact of these limits on the VFC performance, new voltage limits of 0.95-1.05 pu are used here.

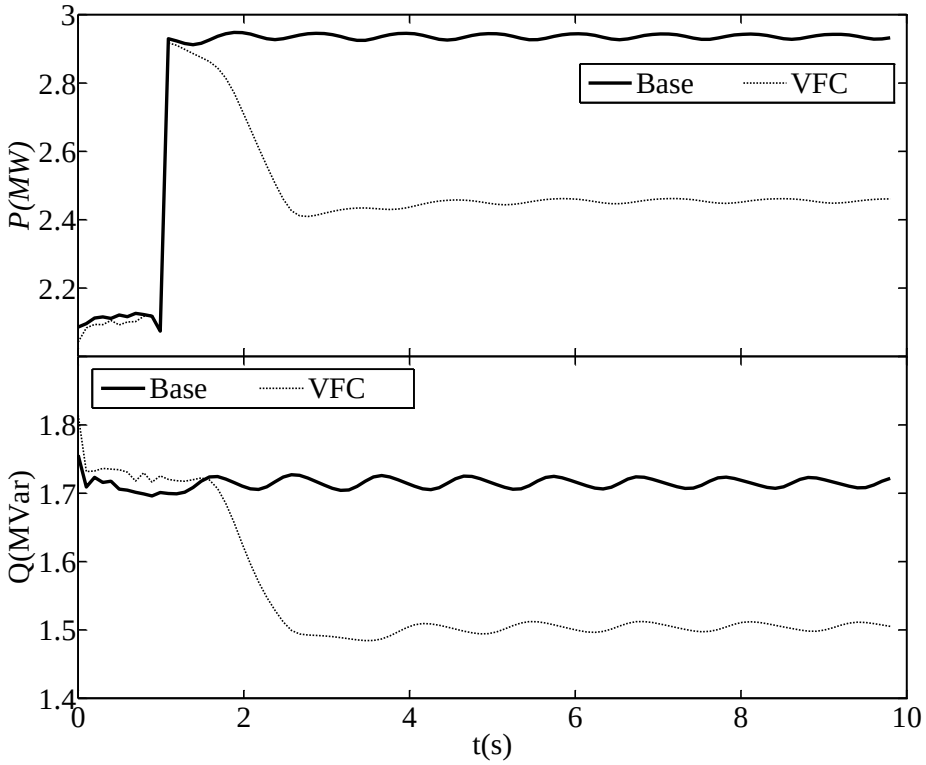

Figure 4.11: Active and reactive power injection of diesel Unit 1 with and without the VFC for Scenario 2.

Figure 4.13 shows a comparison of the frequency responses and the RMS line-to-line voltage of the generation bus for the different voltage limits. Note that the frequency response is the same when the voltage is within ±0.05 pu of the nominal voltage, i.e. before $t = 110$ s. However, once the voltage reaches a 1.05 pu limit, the VFC is not capable of regulating the frequency anymore, since decreasing the operating voltage limit decreases the virtual reserve that the VFC can provide to the system, thus reducing its frequency regulation capability.

4.4.5 Scenario 4: Effect of Load Modelling

As discussed in Section 4.1, the performance of the VFC directly depends on n_P; thus, to examine its impact on the proposed VFC mechanism, n_P is set to 1.2 here. Figure 4.14 shows a comparison of the frequency responses for both values of n_P. Observe that as the voltage-dependency of the loads decreases, i.e. as n_P decreases, the voltage variations

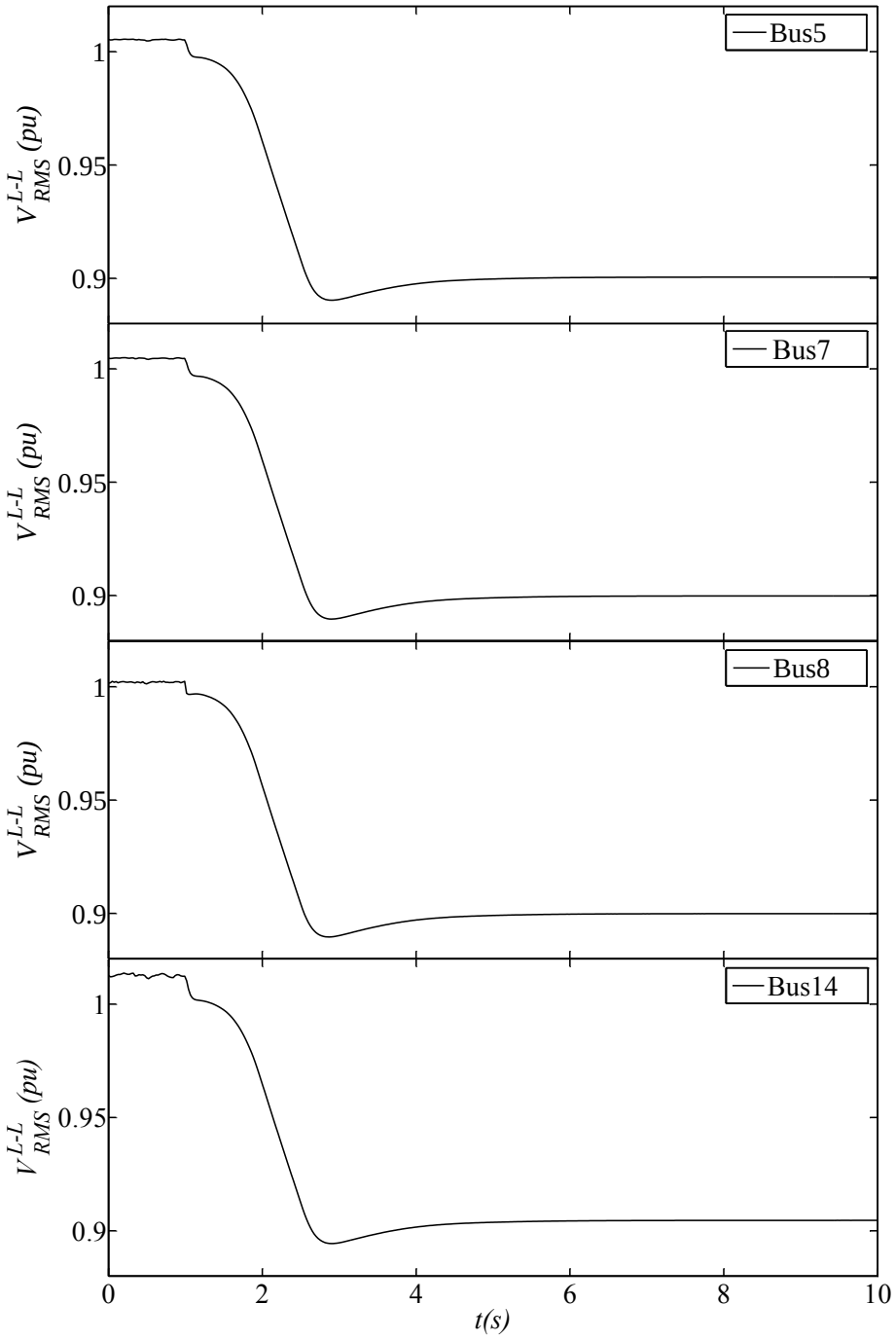

Figure 4.12: Voltages at different buses of the system for Scenario 2.

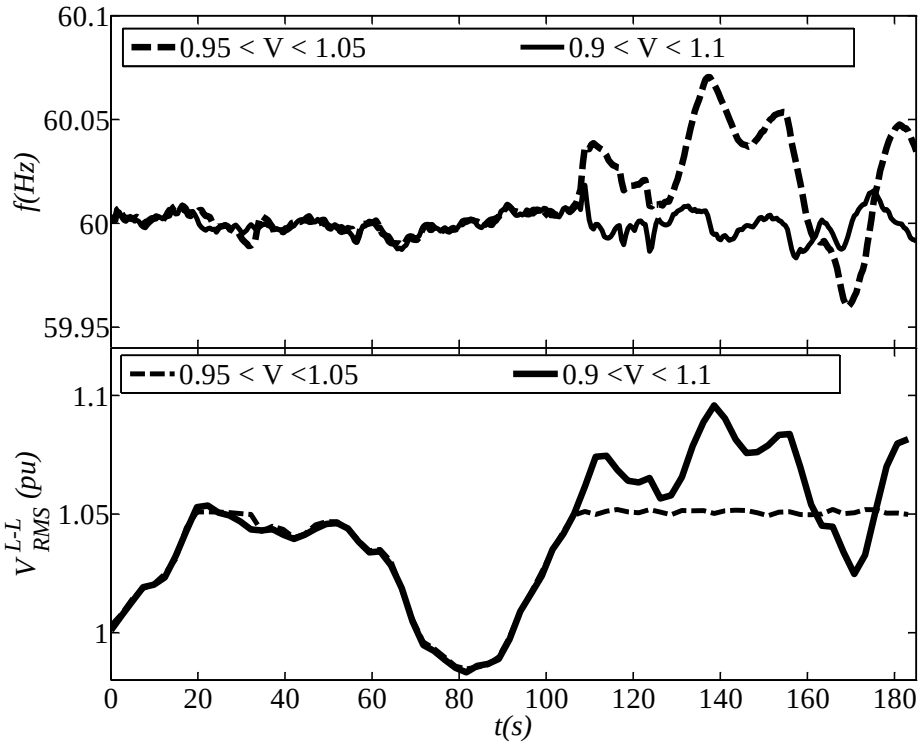

Figure 4.13: Voltage and frequency response of the system with different voltage limits for Scenario 3.

increase and reach a limit between $t = 120$ s to $t = 160$ s, as expected. However, the VFC still manages to properly regulate the effect of the wind fluctuations on the system frequency.

4.4.6 Scenario 5: Diesel Units at Different Buses

In all previous cases, both diesel generators are connected at the Gen. Bus. Hence, in the test scenario here, the diesel Unit 2 is connected at Bus 5, while the diesel Unit 1 remains connected at the Gen. Bus; both generator ratings and parameters are the same as before. The same test scenario as the one in Section 4.4.2 is then carried out, where the effectiveness of the VFC during wind fluctuations is demonstrated by comparing the response of the system with and without the VFC.

Figure 4.15 demonstrates the frequency response of the system with and without the VFC. Voltages at the Gen. Bus and Bus 8 are shown in Figure 4.16; the active power output

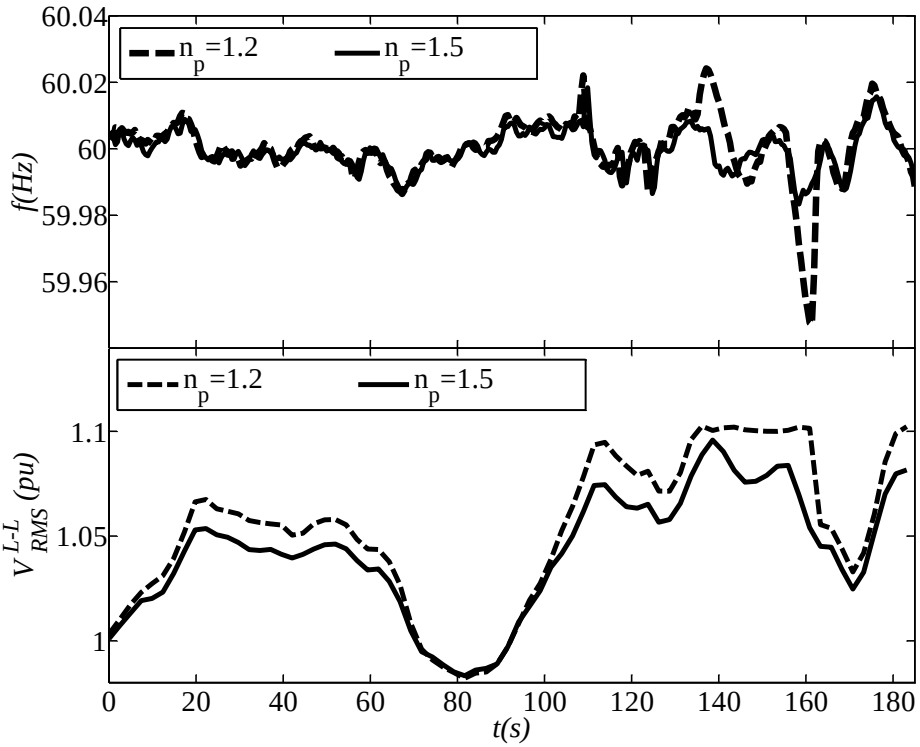

Figure 4.14: Voltage and frequency response of the system with different n_P for Scenario 4.

of Unit 1 is shown in Figure 4.17 with Unit 2 exhibiting the same active power response. The reactive output of both units are shown in Figure 4.18 and Figure 4.19, respectively. Observe in Figures 4.15-4.19 that the system shows similar satisfactory performance as in the previous cases, with the frequency close to 60 Hz and the voltages within acceptable operating limits.

4.5 Results for Inverter-based Test System

A DER-based version of the CIGRE benchmark for medium voltage distribution networks as shown in Figure 4.20 is used in this section. The total unbalanced load in the system is 7.14 MVA, which is modelled in detail for each bus and consists of 60% constant impedance, 30% constant current, and 10% constant power loads, i.e. $n_P = 1.5$.

The DERs ratings are 3.5 MVA for DER 1 and DER 2, and 1.3 MVA for DER 2. The DERs are modelled as ideal DC sources, and are controlled based on the VSC principles

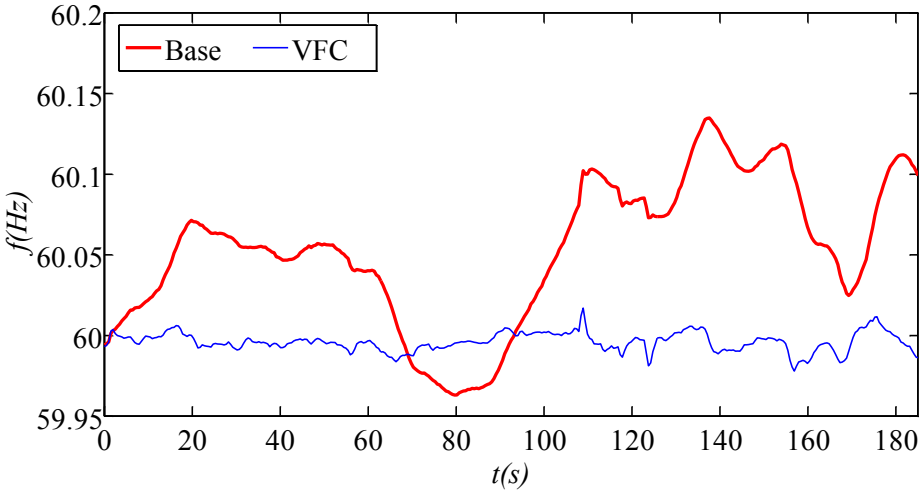

Figure 4.15: Frequency response of the system with and without the VFC for scenario 5.

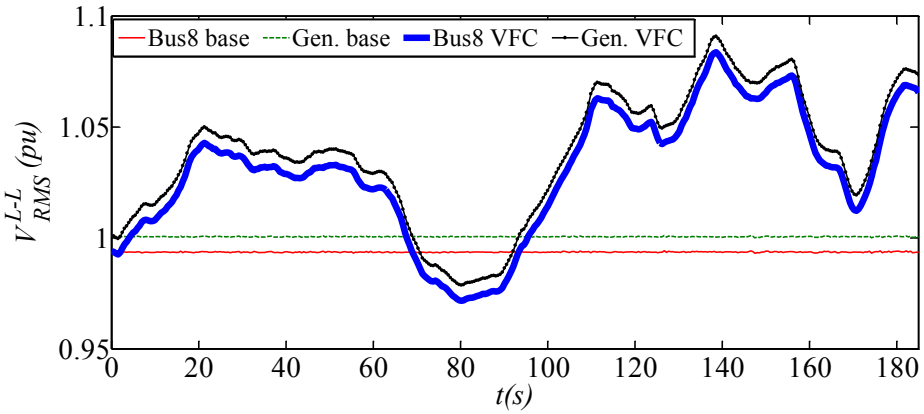

Figure 4.16: Voltage response of the system with with and without the VFC for scenario 5.

explained in Chapter 2; the DERs parameters are given in Table 4.3. Similar to the previous section, the VFC parameters are tuned based on a Ziegler-Nichols method to obtain an acceptable performance; these parameters are given in Table 4.4. Two lead-lag filters are used to obtain the best performance of the controller; hence, in Table 4.4, τ_1 and τ_2 are the parameters of the first filter, and τ_1' and τ_2' are the parameters of the second filter.

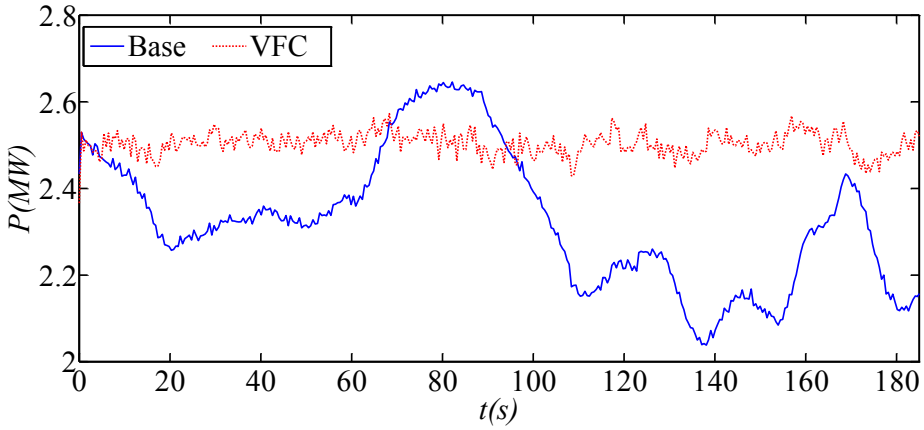

Figure 4.17: Active power injection of diesel Unit 1 with and without the VFC for scenario 5.

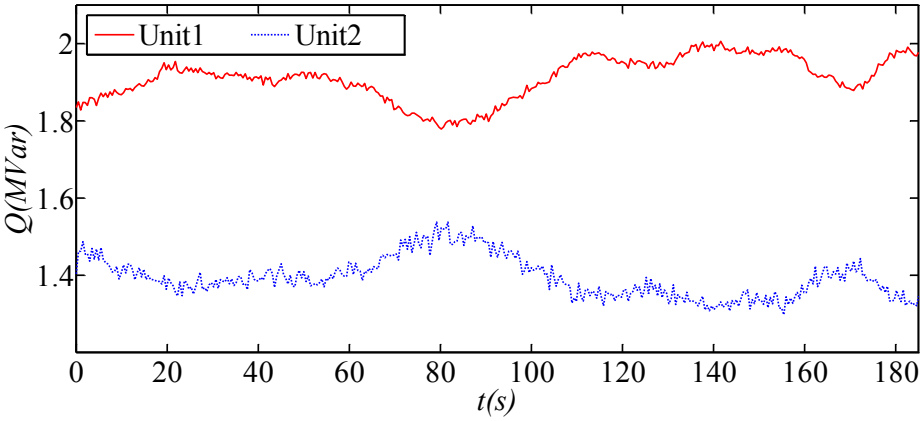

Figure 4.18: Reactive power injection of diesel Unit 1 and Unit 2 without the VFC for scenario 5.

4.5.1 Scenario 6: Disconnection of DER 2

In this case, DER 1 and DER 2 are operating in the VCM mode and participate in the frequency droop control, and DER 3 is operating in the CCM mode. The performance of the system with and without the VFC is compared when DER 3 is suddenly disconnected. The VFC is integrated with DER 1 and DER 2, and is tuned to keep the voltage within the operating voltage range of 0.91 - 1.1 pu, which is acceptable in low and medium voltage islanded microgrids [101]. Prior to the disconnection of DER 3, the network is in steady state, with DER 3 being disconnected at $t = 0.5$s.

The performance of the system without the VFC is shown in Figure 4.21, and with

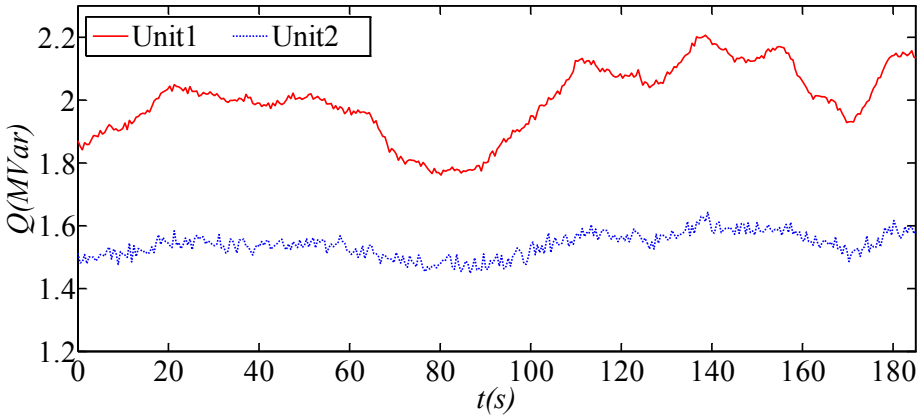

Figure 4.19: Reactive power injection of diesel Unit 1 and Unit 2 with the VFC for scenario 5.

Table 4.3: DER Parameters.

Parameters	**DER 3**	**DER 1 & DER 2**
Switching frequency	5 kHz	5 kHz
L_f	38 μH	0.16 mH
R_f	1.2 mΩ	4.2 mΩ
C_f	2.2 mF	0.62 mF
ω_c	30 rad/s	30 rad/s
m	5.4 (rad/s)/MW	2.7 (rad/s)/MW
n	0.057 kV/MVAr	0.027 kV/MVAr
K_{pv}	0.1	0.1
K_{iv}	200	200
K_{pc}	0.1	0.1
K_{ic}	200	200

Table 4.4: VFC Parameters

Par.	**Value**	**Par.**	**Value**	**Par.**	**Value**	**Par.**	**Value**
K_P	0.2	τ_i(s)	2.65	τ_1(s)	0.01	τ_2(s)	0.9
τ_1'(s)	0.01	τ_2'(s)	0.25	K_{VFC}	2.5		

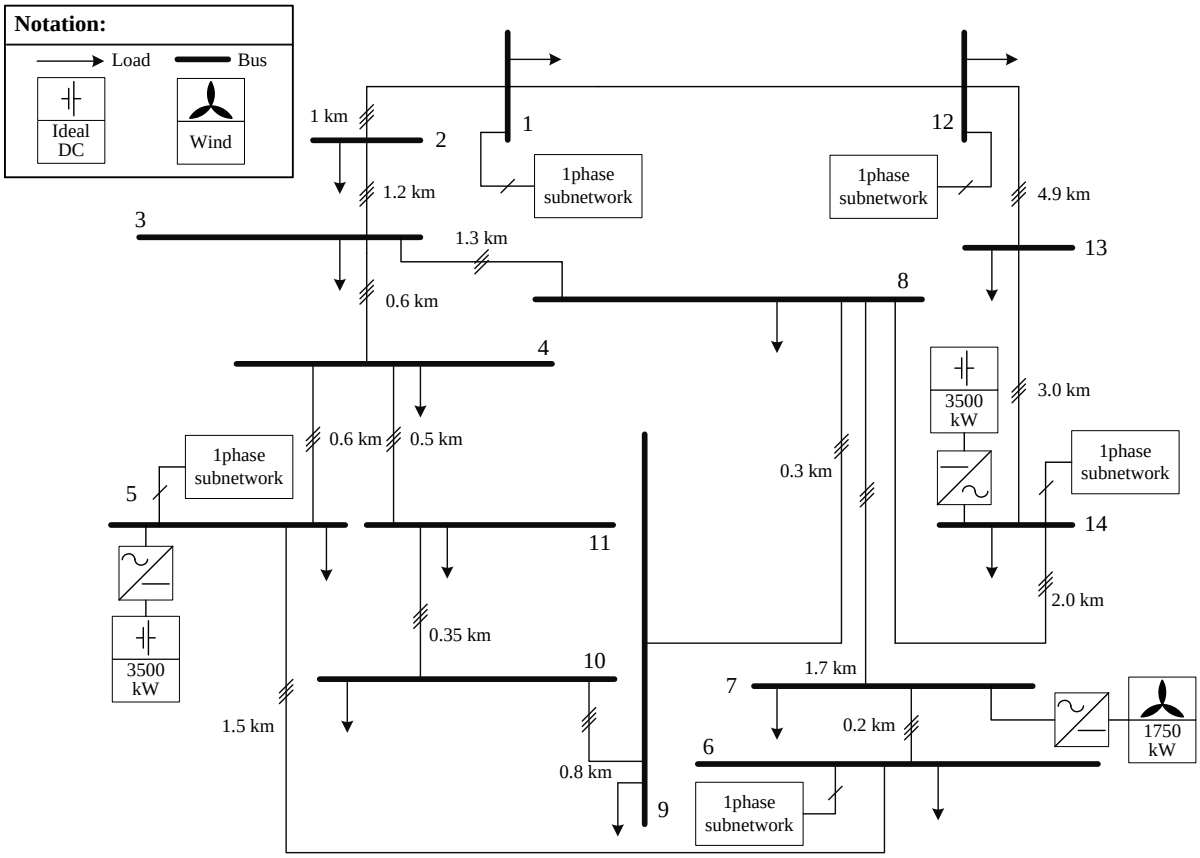

Figure 4.20: DERs-based Test microgrid based on a medium voltage distribution system benchmark.

the VFC in Figure 4.22. Before the disturbance, DER 1 and DER 2 are injecting around 2.5 MW, while DER 3 is injecting 1.25 MW. After the disturbance, the frequency of the system without VFC drops to 59.7 Hz, which is not acceptable [101]. Hence, to recover from such a disturbance, the system needs ESS to compensate for the sudden loss of generation. However, for the system with the VFC, the frequency is stabilized at around 59.9 Hz, allowing the system to continue operating. Observe that the voltages are within the acceptable range of operation; however, since the disturbance is relatively large, minimum voltage limits are reached, which is the reason why frequency does not return to its nominal value.

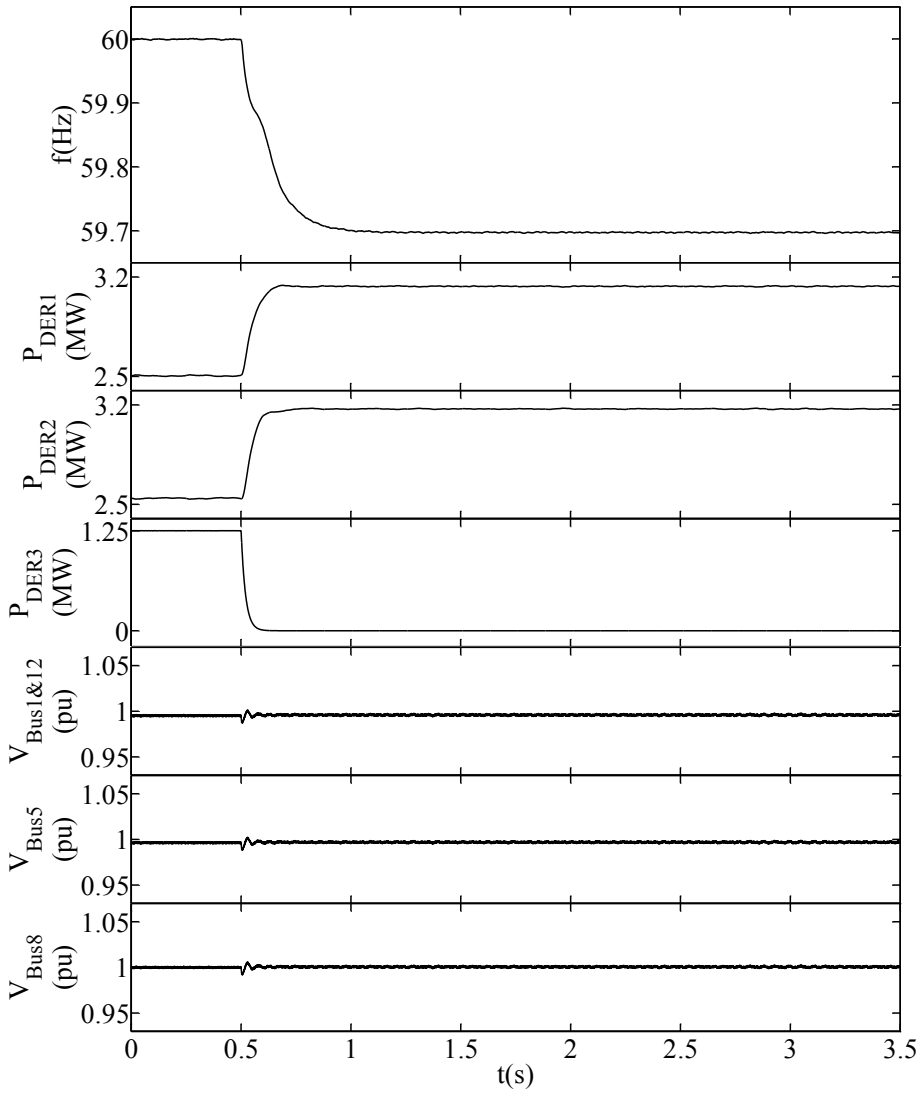

Figure 4.21: Response of the system without VFC for scenario 6.

4.5.2 Scenario 7: Fast Active Power Output Variation

In this case, DER 1 and DER 2 are operating in the VCM mode and participate in the frequency droop mechanism, while DER 3 is operating in the CCM mode with constant power factor to simulate a wind power generator. The performance of the system with and without the VFC is compared during a fast active power output variation for DER 3; these variations correspond to the wind profile in Figure 4.5. The VFC is integrated into

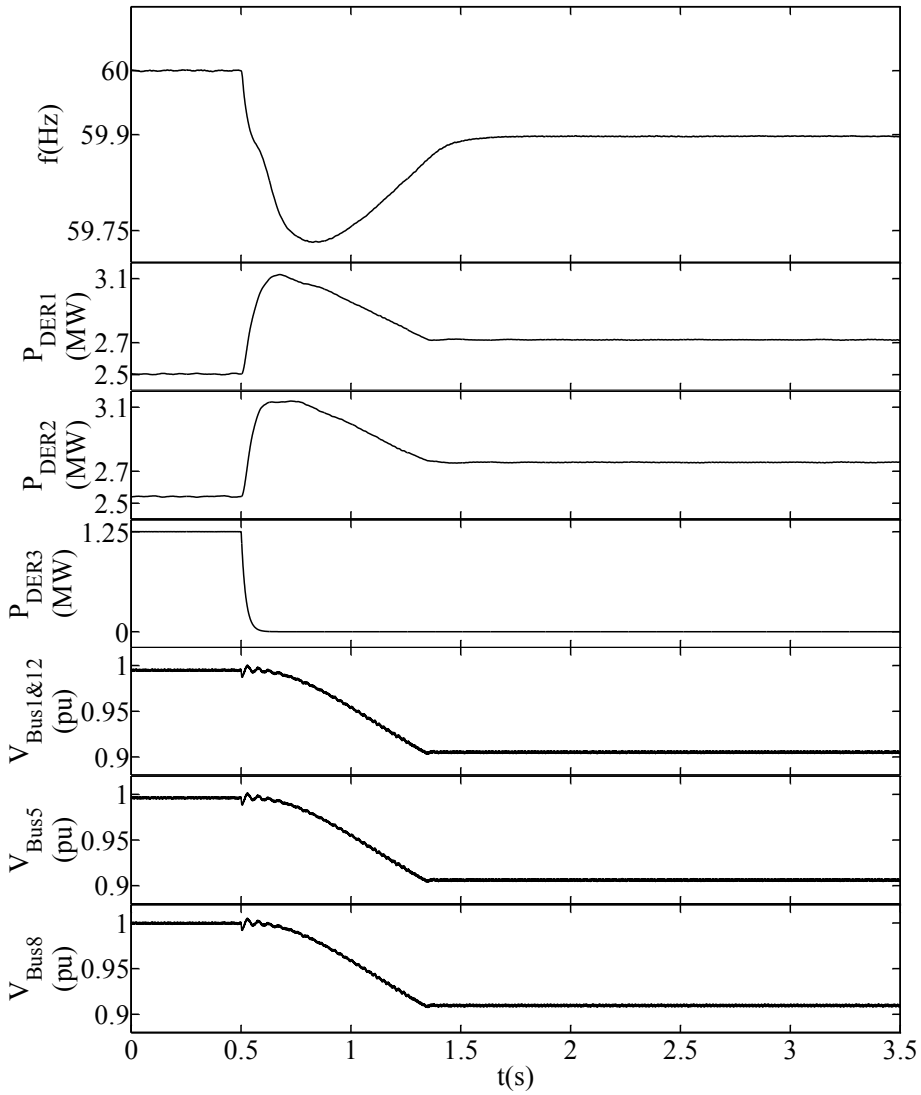

Figure 4.22: Response of the system with VFC for scenario 6.

DER 1 and DER 2.

The performance of the system without the VFC is shown in Figure 4.23, and the performance of the system with the VFC is shown in Figsure 4.24. Observe that for the system without the VFC, the frequency variation is between 60 Hz to 59.83 Hz, while for the system with VFC, the frequency variation is negligible. Note also that the active power injection of DER 1 and DER 2 has no significant variation for the system with VFC, since

this controller compensates for the DER 3 output fluctuations. Finally, observe that the bus voltages are within the acceptable range of operation.

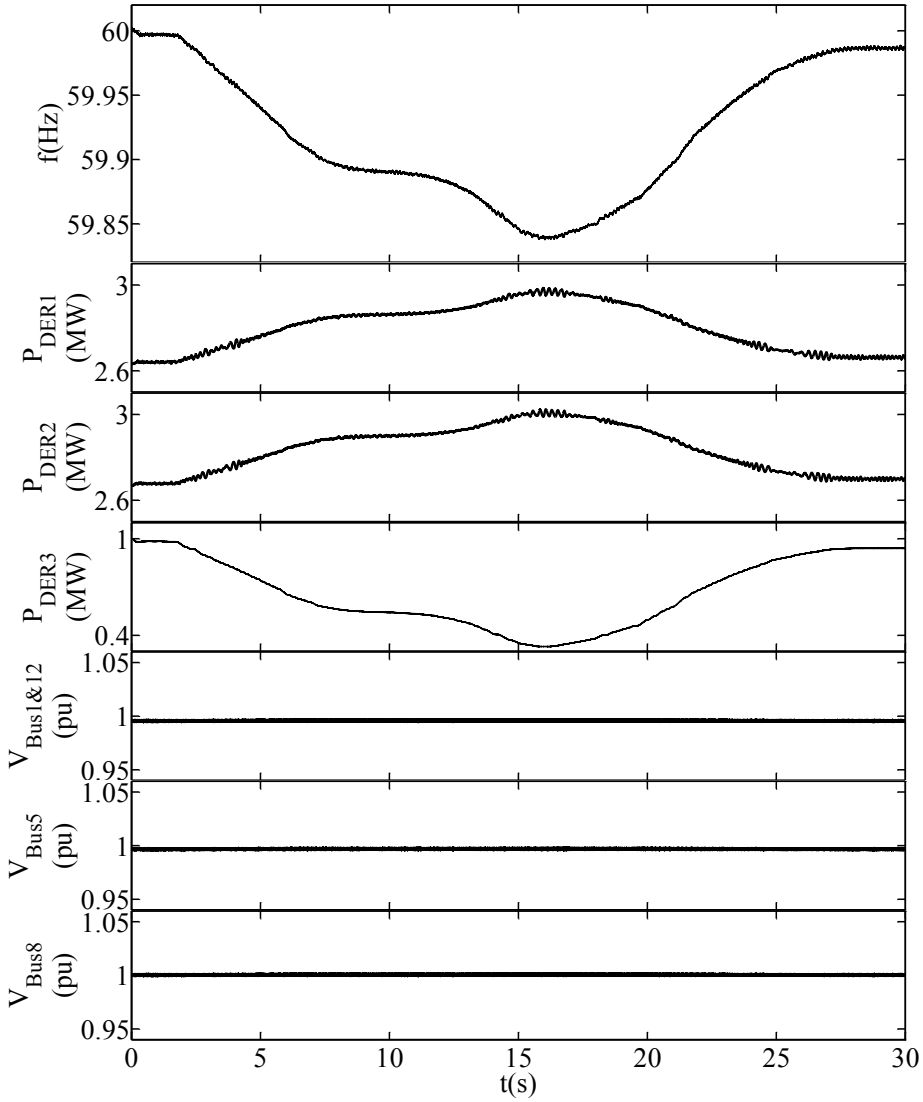

Figure 4.23: Response of the system without the VFC for scenario 7.

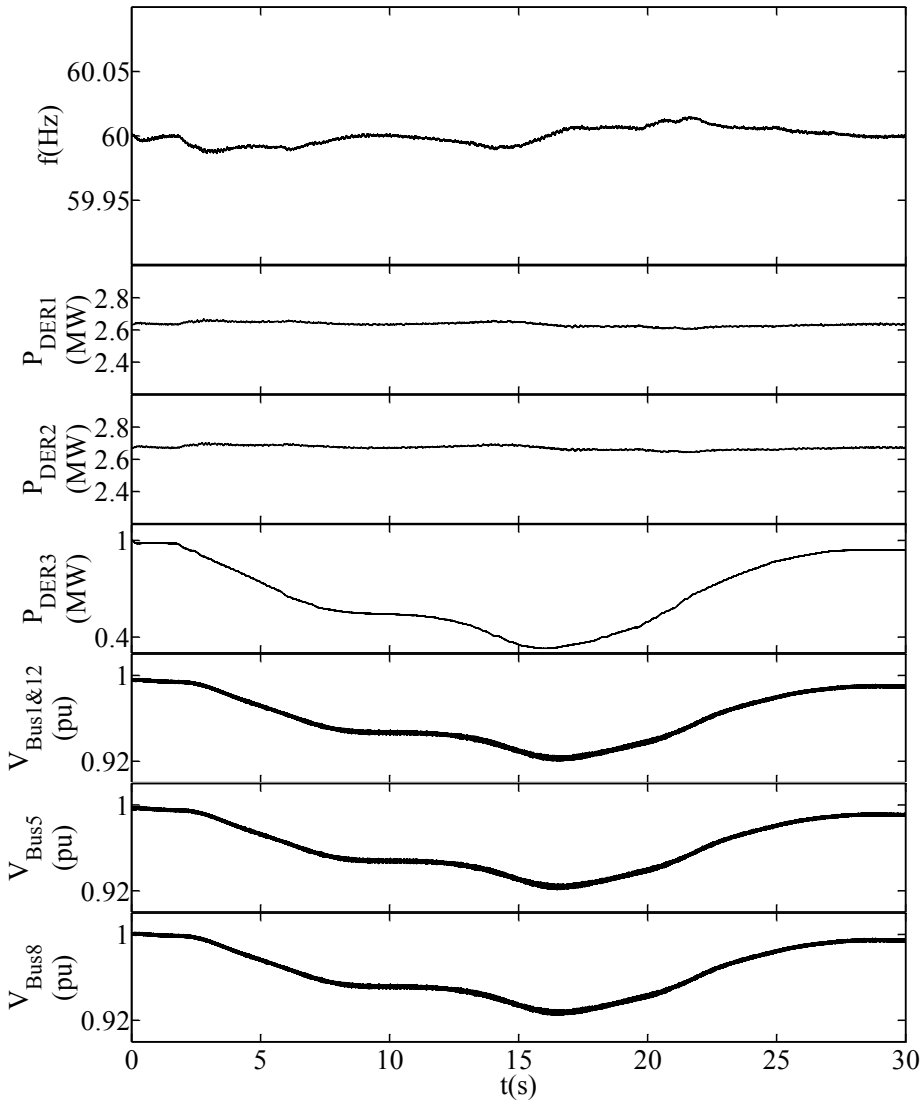

Figure 4.24: Response of the system with the VFC for scenario 7.

4.6 Discussion

There are some aspects of the VFC that should be carefully taken into consideration. First, as shown in (4.16), the performance of the VFC depends on the system load composition, as demonstarted in Sections 4.4.2 and 4.4.5. Hence, in systems with very low voltage index n_P, the VFC would not be able to regulate the frequency. However, the focus of this work

is on isolated microgrids, such as those that exist in remote communities, where loads are dominantly residential, with n_P often higher than 1.1% [104–107]. For these types of microgrids, experimental results are provided in [51] where the viability of frequency regulation through load voltage control is discussed, showing that for the archipelago of Guadeloupe in France, a 2.4% change in the voltage results in 3.5% change in the actual power consumption. According to (4.8), this implies that the voltage index for such a system would be $n_P = 1.47$, which is in the range used in this work. The authors also show that a 5% change in the voltage reference set-point of the generators will significantly improve the system transient frequency response for an 8% generation loss disturbance.

Second, the grid size will affect the VFC performance as well. Thus, for very large systems, changing the generators output voltage will not necessarily decrease remote bus voltages. Additionally, for systems with long inductive feeders, the voltage drop for end-feeders may be significant, thus limiting the operating range of the VFC. However, both scenarios are unlikely to be an issue for isolated microgrids, where the size of the grid is typically in the order of a few km. Observe that the test system used in this chapter is relatively large, with feeders as long as 5 km and buses as far as 10 km from the Gen. Bus. However, the results show that the VFC is capable of regulating the frequency, while all the voltages in the system remain within acceptable operating ranges.

Third, the VFC response time is determined by the time constant of the voltage regulators in the system. In diesel-based isolated microgrids, the time constant corresponding to the field excitation of synchronous machines determines the VFC speed; this value is typically around 500 ms for typical sized synchronous machines used in isolated microgrids, and is sufficient to address the variations of RES output, which are in the range of 1 second, as shown in Figure 4.7. For inverter-based isolated microgrids, the VFC response time is much faster and depends on the voltage control block of the inverter, which makes it comparable to the response time of fast ESS.

4.7 Summary

A fast voltage-based frequency controller was proposed in this chapter for isolated/islanded microgrids, acting as an additional control to conventional frequency controllers to improve frequency response of the system. Based on the realistic analysis and results presented in this chapter, the proposed controller is simple, has a straightforward implementation, and is easily applicable to a variety of different systems and voltage regulation devices (e.g., synchronous machines, DERs with voltage regulation capacity).

The proposed controller offers several advantages, reducing the dependency of a microgrid with high renewable energy sources penetration on ESS, which makes these types of microgrids more viable. Hence, the VFC can play the role of a virtual storage, with capacity depending on the operating voltage levels and type of loads. In addition, the controller can be very effective in minimizing the impact of large disturbances on the system such as loss of a generation, enhancing small-perturbation stability by providing more damping for the system. The controller also provides zero steady-state error with respect to existing frequency control techniques, and requires no additional investment or communication infrastructure. Finally, its response is almost instantaneous, and since the voltage can be kept within acceptable limits, it has no significant impact on customer quality of service; however, its performance is dependent on the load mix and overall voltage ranges.

The main content of this chapter was published in [108], [109], and [110].

Chapter 5

Unit Commitment in Isolated Microgrids Considering Frequency Control

This chapter proposes a mathematical model of frequency control impact on generator output in isolated microgrids, for integration into the UC problem. The proposed approach considers changes in the generation output due to frequecny control using a linear model, and based on that, a novel UC is developed to yield a more realistic solution for isolated microgrids. The proposed UC is formulated based on a day-ahead with MPC approach. To test, validate, and demonstrate the advantages of the proposed UC, a modified version of a CIGRE benchmark test system is used.

5.1 UC Model

5.1.1 Objective Function

Generally in UC problems, the objective function is formulated based on the cost of providing a certain amount of energy between two dispatch time intervals; this energy is determined by the net demand of the system D, which is defined as follows:

$$D_k = P_{L,k} - \sum_{i \in \mathcal{R}} P^r_{i,k} \tag{5.1}$$

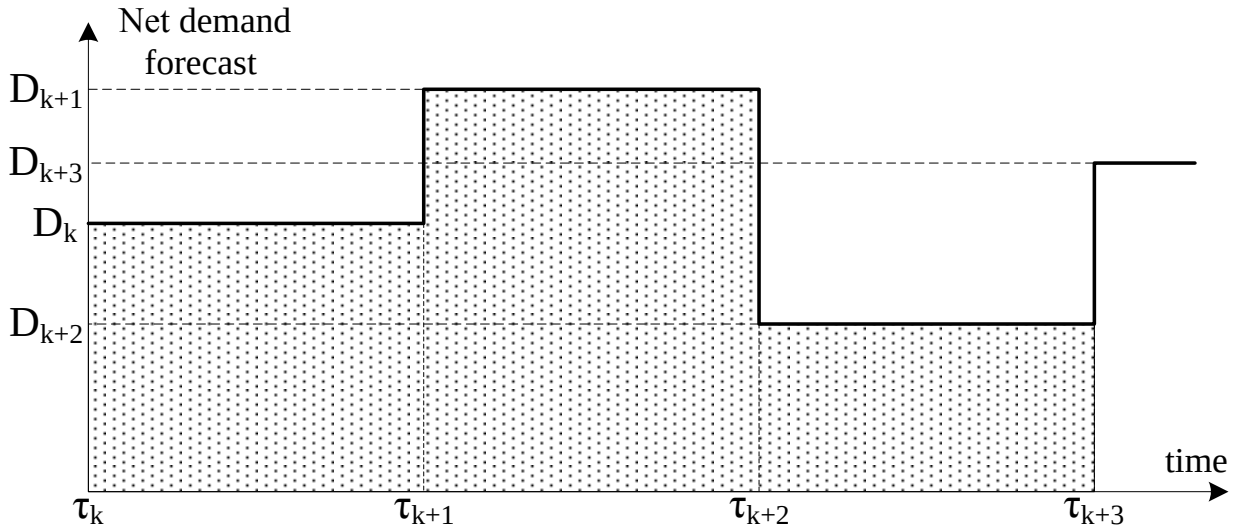

Figure 5.1: Energy provision in the conventional UC.

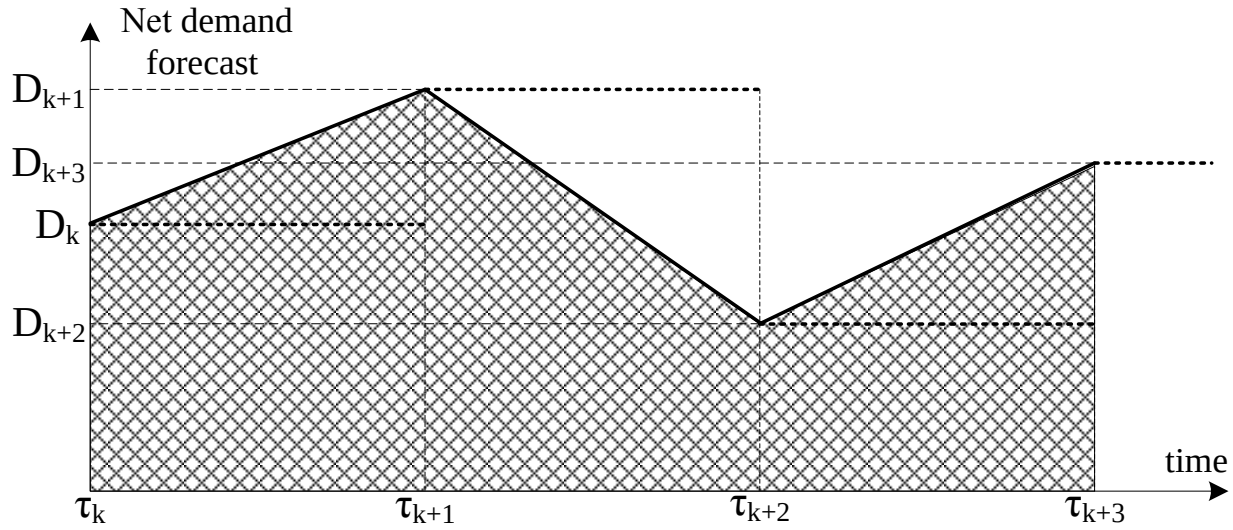

Figure 5.2: Energy provision in the proposed UC.

where $P_{L,k}$ is the loading level at dispatch time k, and $P^r_{i,k}$ is the renewable unit i active power output at dispatch time k. In conventional UC, the basic assumption is that output power levels are fixed over a dispatch interval and jump to another value at the next interval, forming a staircase profile, as seen in Figure 5.1. Hence, the amount of energy provided by the generation units during each interval, is calculated as follows:

$$E_k = D_k \, \Delta\tau \tag{5.2}$$

However, in practice, the net demand does not jump from one value to another every dispatch interval, but it gradually changes until it reaches another value. Given that dispatch intervals are short, these changes can be modelled linearly, as shown in Figure 5.2; this assumption is shown in Section 5.2.1 to be valid based on realistic measurements. In Figure 5.2, the forecasted net demand for each dispatch time is the same as in Figure 5.1; however, in this case, the power output levels are not fixed during the each dispatch time interval, yielding a different energy profile. Thus, the energy required during each dispatch time interval can be calculated as follows:

$$E_k = \frac{D_k + D_{k+1}}{2} \, \Delta\tau \tag{5.3}$$

which is a generalized form of (5.2), and is equal to it only when D_k is equal to D_{k+1}, i.e. when the net demand does not change for two consecutive dispatch times.

Generation units react to changes in the net demand D according to the frequency control mechanism used. Those units that do not participate in frequency control have a constant power output during each dispatch time interval. However, assuming that changes in D are linear, the output of units participating in frequency control would change linearly depending on their droop coefficient R in droop mode, or their nominal rating P^g_{rated} in ILS mode. For droop-based frequency regulation, the following equations can be used to determine the output of a generation unit:

$$\sum_{i \in \mathcal{F}} \Delta P^g_{i,k} = D_{k+1} - D_k \tag{5.4}$$

$$\frac{\Delta P^g_{i,k}}{ID_i} = \Delta f_k \, \omega_{i,k} \quad \forall i \in \mathcal{F} \tag{5.5}$$

where $\Delta P^g_{i,k}$ is the difference between the active power output of DG unit i at the beginning and the end of dispatch time interval k[1]; ID_i is the inverse of droop of dispatchable unit i; $\omega_{i,k}$ is the commitment binary variable for DG unit i; Δf_k is the frequency change during the dispatch time interval k, and $\mathcal{F}$ is the set of units that participate in frequency control.

Equation (5.5) is nonlinear; hence, to keep the problem within the UC linear framework,

[1]Note that due to the frequency regulation, the output of the generators at the end of dispatch time interval k is equal to the net demand at the beginning of dispatch time interval $k+1$.

this equation can be decomposed into four linear constraints, as follows [111]:

$$\frac{\Delta P^g_{i,k}}{ID_i} - (1-\omega_{i,k})\,\frac{(D_k - D_{k+1})^2}{ID_i} \leq \Delta f_k \quad \forall i \in \mathcal{F} \tag{5.6}$$

$$\frac{\Delta P^g_{i,k}}{ID_i} + (1-\omega_{i,k})\,\frac{(D_k - D_{k+1})^2}{ID_i} \geq \Delta f_k \quad \forall i \in \mathcal{F} \tag{5.7}$$

$$\omega_{i,k}\,\frac{-(D_k - D_{k+1})^2}{ID_i} \leq \Delta P^g_{i,k} \quad \forall i \in \mathcal{F} \tag{5.8}$$

$$\omega_{i,k}\,\frac{(D_k - D_{k+1})^2}{ID_i} \geq \Delta P^g_{i,k} \quad \forall i \in \mathcal{F} \tag{5.9}$$

Observe in (5.6)-(5.9) that depending on whether $\omega_{i,k}$ is 0 or 1, $\frac{\Delta P^g_{i,k}}{ID_i}$ would be equal to 0 or Δf_k, as per (5.5); therefore, under the proposed UC paradigm, each dispatchable generation unit is dispatched at a certain level $P^g_{i,k}$ at dispatch time k. However, the outputs of units that participate in frequency control are expected to change by $\Delta P^g_{i,k}$ at the end of dispatch time interval k; hence, the power output of each dispatchable unit during the dispatch time interval k can be modelled as follows:

$$P^g_i(t) = P^g_{i,k} + \frac{\Delta P^g_{i,k}}{\Delta\tau}\,t \quad \forall i \in \mathcal{F} \wedge \tau_k \leq t < \tau_{k+1} \tag{5.10}$$

The operating cost of dispatchable generation unit i is usually given by the quadratic cost function as follows:

$$C^g_i = a_i\,(P^g_i)^2 + b_i\,P^g_i + c_i \tag{5.11}$$

In conventional UC, where P^g_i is assumed fixed over the dispatch time interval, (5.11) can be multiplied by the duration of the time interval to calculate to total cost of energy delivery by unit i; however, in the proposed UC, $P^g_i(t)$ is a function of time, as per (5.10).

Hence, cost of delivering energy can be derived as follows:

$$\begin{aligned} C\tau_{i,k}^{g} &= \int_{0}^{\Delta\tau} \left(a_i P_i^g(t)^2 + b_i P_i^g(t) + c_i\right) dt \\ &= \left[a_i \left((P_{i,k}^g)^2 + \frac{(\Delta P_{i,k}^g)^2}{3} + P_{i,k}^g \Delta P_{i,k}^g\right)\right. \\ &\left. + b_i \left(P_{i,k}^g + \frac{\Delta P_{i,k}^g}{2}\right) + c_i\right] \Delta\tau \\ &\qquad\qquad \forall i \in \mathcal{F} \wedge \tau_k \leq t < \tau_{k+1} \end{aligned} \tag{5.12}$$

Defining $Pa_{i,k}^g = P_{i,k}^g + \Delta P_{i,k}^g/2$, (5.12) can be re-written as follows:

$$\begin{aligned} C\tau_{i,k}^{g} = &\left[a_i \left((Pa_{i,k}^g)^2 + \frac{(\Delta P_{i,k}^g)^2}{12}\right) + \right. \\ &\left. b_i Pa_{i,k}^g + c_i\right] \Delta\tau \quad \forall i \in \mathcal{F} \end{aligned} \tag{5.13}$$

Therefore, considering the generation units start-up and shut-down costs, the final cost function for generation units that participate in frequency control can be stated as follows:

$$OC_{i,k}^{g} = C\tau_{i,k}^{g} + Cst_i^g.u_{i,k}^g + Csh_i^g.v_{i,k}^g \quad \forall i \in \mathcal{F} \tag{5.14}$$

where Cst_i^g and $u_{i,k}^g$ are the cost parameter of binary variable representing start-up operation; similarly, Csh_i^g and $v_{i,k}^g$ represent the shut-down operation.

The cost function for units that are not participating in frequency control can be derived by multiplying (5.11) by $\Delta\tau$, as follows:

$$C\tau_{j,k}^{g} = \left(a_j (P_{j,k}^g)^2 + b_j P_{j,k}^g + c_j\right) \Delta\tau \quad \forall j \in \mathcal{P} \tag{5.15}$$

where $\mathcal{P}$ is the set of units that does not participate in frequency control. Thus, similar to (5.14), the final cost function for these units is:

$$OC_{j,k}^{g} = C\tau_{j,k}^{g} + Cst_j^g.u_{j,k}^g + Csh_j^g.v_{j,k}^g \quad \forall j \in \mathcal{P} \tag{5.16}$$

Therefore, the final objective function to be minimized can be defined as follows:

$$Z = \sum_{k \in \mathcal{T}} \left(\sum_{i \in \mathcal{F}} OC^{g}_{i,k} + \sum_{j \in \mathcal{P}} OC^{g}_{j,k} \right) \tag{5.17}$$

Note that (5.17) guarantees that the generation units dispatch level $P^{g}_{i,k}$ $\forall i$ are optimized based on the more realistic energy requirement (5.3) rather than (5.2). It is important to consider that (5.3) is not an actual constraint included in the UC problem; instead, the conventional power balance constraint is sufficient, since it is the frequency control responsibility to satisfy the power balance during the rest of the time interval, thus ensuring that the energy required is supplied by the generation units. Since the changes in the generation unit output due to frequency control is properly modelled in (5.17), the overall UC is guaranteed to consider and optimize for these changes.

The procedure used here to obtain the final objective function can be applied to any other linear or nonlinear heat-rate function. Furthermore, even though (5.6) is developed based on droop-based control, it can be modified to account for either single-unit or ILS controls. For the former, the set $\mathcal{F}$ only contains a single generation unit index, and there is no need for (5.5)-(5.9); for the latter, to model the ILS control mode, ID_i should be replaced by $P^{g}_{rated,i}$ in (5.5)-(5.9).

5.1.2 Operating Constraints

Power Balance

Similar to conventional UC, the proposed UC requires that the generated power and demand be equal at each dispatch time, yielding the following constraints:

$$\sum_{i \in \mathcal{G}} P^{g}_{i,k} + \sum_{i \in \mathcal{R}} P^{r}_{i,k} + \sum_{i \in \mathcal{S}} \left(P^{s,dch}_{i,k} - P^{s,chg}_{i,k} \right) - P_{L,k} = 0 \qquad \forall k \in \mathcal{T} \tag{5.18}$$

where $P^{s,dch}_{i,k}$ and $P^{s,chg}_{i,k}$ are the discharging and charging power of the ESS in the system; $\mathcal{G}$, $\mathcal{R}$, and $\mathcal{S}$ are the set of diesel generation units, renewable generation units, and ESS units, respectively.

Dispatchable Units

The following constraints are required to model all relevant generator limits:

$$\underline{P}_i^g \omega_{i,k} \leq P_{i,k}^g \leq \bar{P}_i^g \omega_{i,k} \quad \forall i \in \mathcal{G} \wedge k \in \mathcal{T} \tag{5.19}$$

$$P_{i,k+1}^g - P_{i,k}^g \leq \bar{R}_i^g \Delta\tau + u_{i,k}^g \underline{P}_i^g \quad \forall i \in \mathcal{P} \wedge k \in \mathcal{T} \tag{5.20}$$

$$P_{i,k}^g - P_{i,k+1}^g \leq \underline{R}_i^g \Delta\tau + v_{i,k}^g \underline{P}_i^g \quad \forall i \in \mathcal{P} \wedge k \in \mathcal{T} \tag{5.21}$$

$$u_{i,k}^g - u_{i,k-1}^g - u_{i,t}^g \leq 0 \quad \forall i \in \mathcal{G} \wedge k \in \mathcal{T}^* \wedge t \in \mathcal{T}_1 \tag{5.22}$$

$$u_{i,k-1}^g - u_{i,k}^g + u_{i,t}^g \leq 1 \quad \forall i \in \mathcal{G} \wedge k \in \mathcal{T}^* \wedge t \in \mathcal{T}_2 \tag{5.23}$$

$$u_{i,k}^g - v_{i,k}^g = \omega_{i,k}^g - \omega_{i,k-1}^g \quad \forall i \in \mathcal{G} \wedge k \in \mathcal{T} \tag{5.24}$$

$$u_{i,k}^g + v_{i,k}^g \leq 1 \quad \forall i \in \mathcal{G} \wedge k \in \mathcal{T} \tag{5.25}$$

and,

$$\begin{aligned} \mathcal{T}_1 &= \{t+1, \ldots, min\{t + MU_i^g - 1, length(\tau)\}\} \\ \mathcal{T}_2 &= \{t+1, \ldots, min\{t + MD_i^g - 1, length(\tau)\}\} \end{aligned} \tag{5.26}$$

where $\underline{P}_i^g$ and $\bar{P}_i^g$ are the minimum and maximum output power generation of unit i, respectively; $\underline{R}_i^g$ and $\bar{R}_i^g$ are the minimum and maximum ramp-rate of dispatchable unit i respectively; $u_{i,k}^g$ and $v_{i,k}^g$ are the start-up and shut-down decision binary variables for diesel engine i at time step k.

For ILS control, another constraint is included to ensure that each unit is operating at the same percentage of its full-load rating, as follows [65]:

$$P_{j,k}^g \sum_{i \in \mathcal{F}} \omega_{i,k}^g \bar{P}_i^g - \bar{P}_j^g \omega_{j,k}^g \sum_{i \in \mathcal{F}} P_{i,k}^g = 0 \quad \forall j \in \mathcal{F} \tag{5.27}$$

Since this constraint is nonlinear, it has been decomposed into its linear equivalent constraints; hence, a new auxiliary variable $\alpha_{i,j,k}^g = \omega_{i,k}^g P_{j,k}^g$ is defined, resulting in the following set of constraints:

$$\sum_{i \in \mathcal{F}} \alpha_{i,j,k}^g \bar{P}_i^g - \bar{P}_j^g \sum_{i \in \mathcal{F}} \alpha_{j,i,k}^g = 0 \quad \forall j \in \mathcal{F} \tag{5.28}$$

$$0 \leq \alpha_{i,j,k}^g \leq \omega_{i,k}^g \bar{P}_{j,k}^g \quad \forall i, j \in \mathcal{F} \tag{5.29}$$

$$P^g_{j,k} - \left(1 - \omega^g_{i,k}\right) \bar{P}^g_j \leq \alpha^g_{i,j,k} \leq P^g_{j,k} + \left(1 - \omega^g_{i,k}\right) \bar{P}^g_j \quad \forall i, j \in \mathcal{F} \tag{5.30}$$

ESS

The following set of constraints are included to properly model the ESS behaviour:

$$\underline{SoC}_i \leq SoC_{i,k} \leq \overline{SoC}_i \quad \forall i \in \mathcal{S} \wedge k \in \mathcal{T} \tag{5.31}$$

$$SoC_{i,k+1} - SoC_{i,k} = \left(P^{s,chg}_{i,k} \eta_i - \frac{P^{s,dch}_{i,k}}{\eta_i} \right) \Delta\tau \quad \forall i \in \mathcal{S} \wedge k \in \mathcal{T} \tag{5.32}$$

$$0 \leq P^{s,chg}_{i,k} \leq \bar{P}^s_i \left(1 - d^s_{i,k}\right) \quad \forall i \in \mathcal{P} \wedge k \in \mathcal{T} \tag{5.33}$$

$$0 \leq P^{s,dch}_{i,k} \leq \bar{P}^s_i d^s_{i,k} \quad \forall i \in \mathcal{P} \wedge k \in \mathcal{T} \tag{5.34}$$

where $\underline{SoC}_i$ and $\overline{SoC}_i$ are the minimum and maximum SoC of ESS unit i, respectively; $SoC_{i,k}$ is the the SoC of ESS unit i at time step k; $P^{s,chg}_{i,k}$ and $P^{s,dch}_{i,k}$ are the charging and discharging powers of ESS unit i at time step k; η_i is the charging/discharging efficiency of ESS unit i, and $d^s_{i,k}$ is the binary variable for ESS unit i representing the discharging/charging status at time step k. Note that the charging and discharging efficiencies are considered the same here, for the sake of simplicity, but in practice they may be slightly different.

The SoC maximum and minimum limit constraints and the SoC evolution model over time are modelled in (5.31) and (5.32). Also, (5.33) and (5.34) make sure that the ESS charge and discharge powers are within a certain range and would not take place simultaneously.

5.1.3 Reserve Constraints

Spinning reserves play a key role in frequency control, and hence it should be carefully modelled in the UC problem. Traditional UC models consider these constraints without considering the intra-interval generation changes. However, in the control of isolated microgrids, this approach is not adequate for either droop control or ILS control, because multiple generators participate in regulating the system frequency and the reserve constraint

should be applied to all participants as an aggregate. Therefore, the reserve constraint is represented here as follows:

$$\sum_{i \in \mathcal{F}} \left(\omega_{i,k}^{g} \bar{P}_{i}^{g} - P_{i,k}^{g} \right) \geq RES_{k} \quad \forall k \in \mathcal{T} \tag{5.35}$$

where RES_k is the amount of reserve required and is considered to be 10% of $P_{L,k}$ in this thesis. Furthermore, at least one of the units that participate in frequency control should be committed at every dispatch time step, which can be enforced as follows:

$$\sum_{i \in \mathcal{F}} \omega_{i,k}^{g} \geq 1 \quad \forall k \in \tau \tag{5.36}$$

Finally, it should be ensured that the output of dispatchable units that participate in frequency control will remain within acceptable generation limits during the dispatch time interval; this can be enforced as follows:

$$\underline{P}_{i}^{g} \leq PE_{i,k}^{g} \leq \bar{P}_{i}^{g} \quad \forall i \in \mathcal{F} \wedge k \in \mathcal{T} \tag{5.37}$$

where $PE_{i,k}^{g}$ can be obtained from (5.10) as follows: $PE_{i,k}^{g} = P_{i}^{g}(\tau_{k+1})$. Note that (5.37) is different from the conventional UC constraint that requires the dispatch values to be within an acceptable range, only at the beginning of the dispatch interval.

5.2 Results and Discussions

To test and validate the efficiency of the proposed UC for isolated microgrids, a modified version of the CIGRE benchmark system for medium voltage networks is used [13], as shown in Figure 5.3. The test system has a total installed capacity of 27 MW, with 5 diesel engines, ESS, and wind and PV based renewable energy resources. The peak load in the system is around 15 MW. Nominal ratings of the diesel engines are given in Table 5.1; the nominal rating of the wind turbine is 8000 kW and of the PV unit is 1000 kW. Units D1, D3, and D4 participate in frequency control. Typical values are assumed for parameters and heat-rates corresponding to the diesel engines [58]. For the ESS, ESS1 has a maximum power rating of 1500 kW, a maximum energy rating of 5000 kWh, and a minimum allowable SoC of 300 kWh; and ESS2 has a maximum power rating of 500 kW, a maximum energy rating of 1000 kWh, and a minimum allowable SoC of 150 kWh. In all test cases, the wind, PV, and load profiles are based on high resolution (1 s) realistic measurements from an actual isolated/remote microgrid.

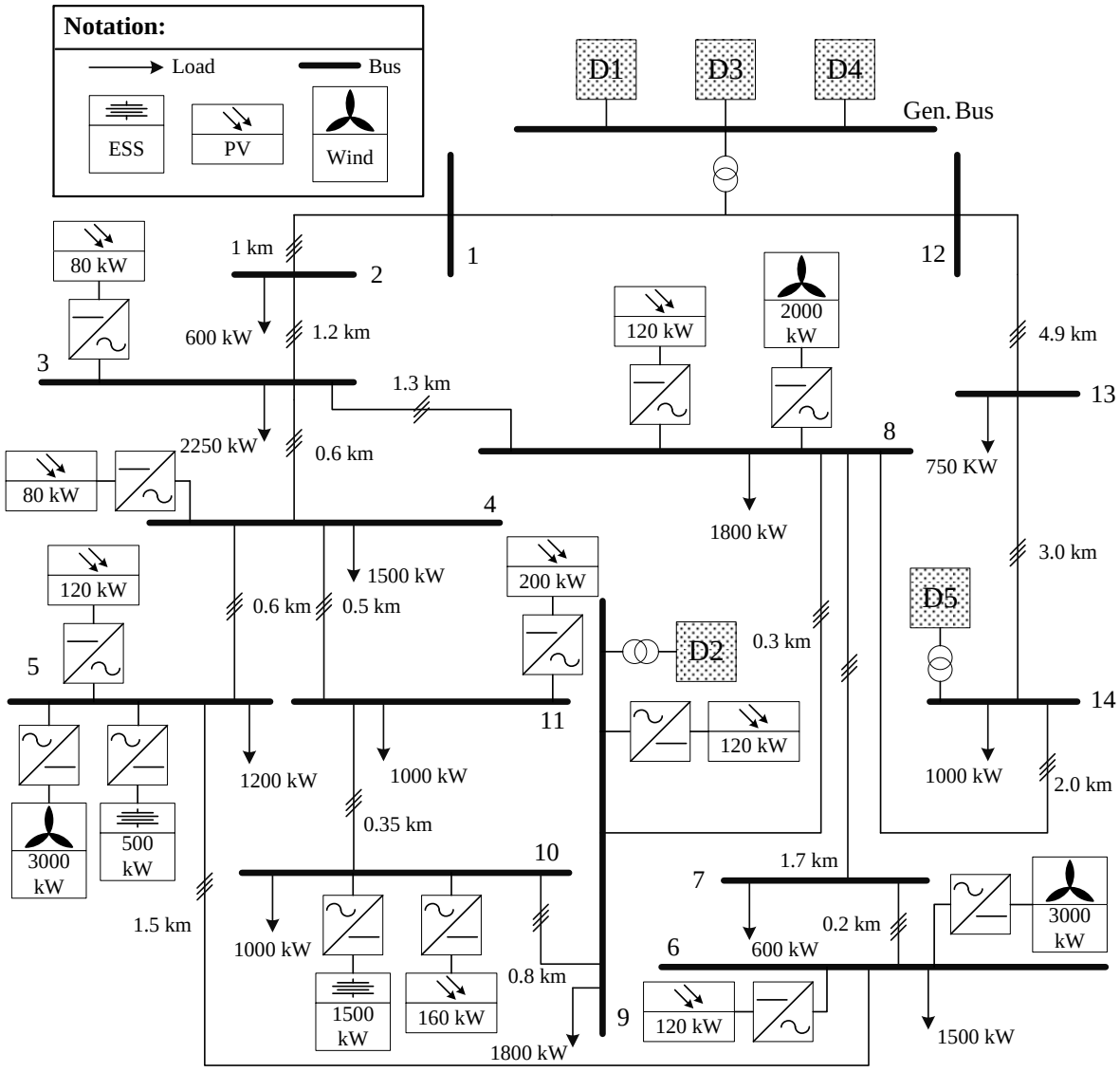

Figure 5.3: Cigre benchmark system for medium voltage netwrok.

The performance of the proposed UC is tested over 24 h of operation, and a dispatch time interval of 5 min. The Mixed Integer Quadratic Programming (MIQP) model is coded in GAMS [112], and is solved using the CPLEX solver [87]. The benefits of the proposed UC are demonstrated through several test case studies described next.

Table 5.1: Diesel Generators Parameters

	D1	D2	D3	D4	D5
a_i (\$/kWh^2)	0.00015	0.00025	0.00015	0.00010	0.0005
b_i (\$/kWh)	0.2881	0.2876	0.2571	0.224	0.3476
c_i (\$/h)	7.5	0	25.5	45.5	0
Cst_i^g (\$)	15	7.35	45	95	10
Csh_i^g (\$)	5.3	1.44	8.3	15.3	0
ID_i (kW/Hz)	4000	-	2000	5000	-
$\bar{P}_i^g$ (kW)	5000	1500	4000	6000	1000
$\underline{P}_i^g$ (kW)	180	100	150	200	100

5.2.1 Scenario 1: Proof of Concept

This scenario is specifically conducted to demonstrate the basics of the proposed algorithm, and how it results in a more efficient dispatch solution. In the test system, only units D1, D3, and D4 are included as dispatchable, since the focus here is on frequency control impact, and these are the units that participate in frequency control, and wind is considered as the only renewable source with an average penetration of 46%; the rest of the DERs in Figure 5.3 are not included in this scenario. It is assumed that the diesel generators are operating in droop control mode. The performance of the proposed UC is compared with the conventional UC only for one dispatch time interval, i.e. $\mathcal{T} = \{1, 2\}$, of 5 min duration.

The solid line in Figure 5.4 illustrates scaled actual measurements of the net demand D during a dispatch time interval in a real remote microgrid [113]; the net demand at $t = 0$ and $t = 300$ is 8865 kW and 4256 kW, respectively. Assuming perfect forecast, the dotted area in Figure 5.4 illustrates the energy to be supplied by the proposed UC, which is 547 kWh; in a conventional UC, the required energy to be supplied would be 737 kWh.

The dispatch values, costs, and computation time of the proposed UC and the conventional UC are shown in Table 5.2. Observe that the objective function value of the conventional UC is considerably higher than the objective function value of the proposed UC, indicating that the conventional UC overestimates the required energy during the dispatch time interval, dispatching 737 kWh compared to 547 kWh in the proposed UC. To calculate the actual operation cost, the output of the diesel generators for the 300 s interval, resulting from the measured-based data shown in Figure 5.4, was used. As noted

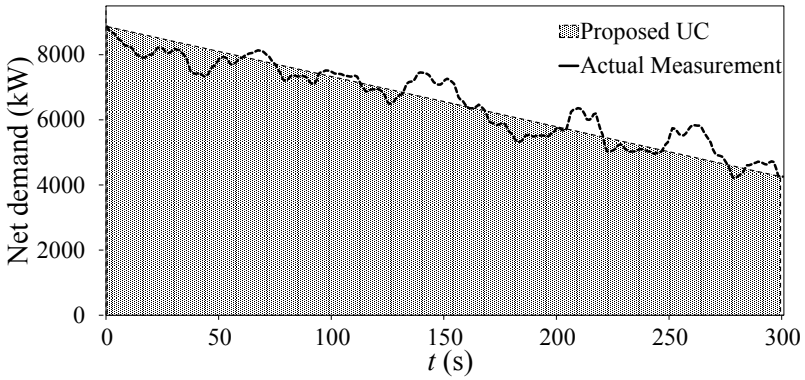

Figure 5.4: Data used in Scenario 1 from scaled measurements of net demand in an actual remote microgrid.

from Table 5.2, compared to the conventional UC, the proposed UC yields around 1% cost savings. Note that the simulated cost is very close to the solution obtained by the proposed UC, since the proposed UC obtained the solution by optimizing an amount of energy close to the actual required energy during the 300 s interval. Observe also that the computation time for both UC approaches are similar in an Intel(R) Xeon(R) CPU L7555 1.87GHz (4 processors) server.

Table 5.2: Proposed UC vs. Conventional UC for Scenario 1

UC	P_1^g (kW)	P_3^g (kW)	P_4^g (kW)	Objective Function ($)	Simulated Cost ($)	CPU Time (s)
Conv.	2777	1857	4231	471	299	1.45
Prop.	2591	2276	3998	303	296	1.45

5.2.2 Scenario 2: ILS Control, Deterministic Forecast

This scenario considers the full test system, with all diesel and renewable generation units. To validate the advantage of the proposed UC compared to the conventional UC, a perfect forecast is assumed for the load and renewable outputs; the wind, PV, and demand forecasted values used are shown in Figure 5.5. Also, an extra constraint is added to ensure that the SoC of the batteries are equal at the beginning and end of the day to avoid ESS depletion. The test is conducted for 24 h of operation, with dispatch interval of 5 min.

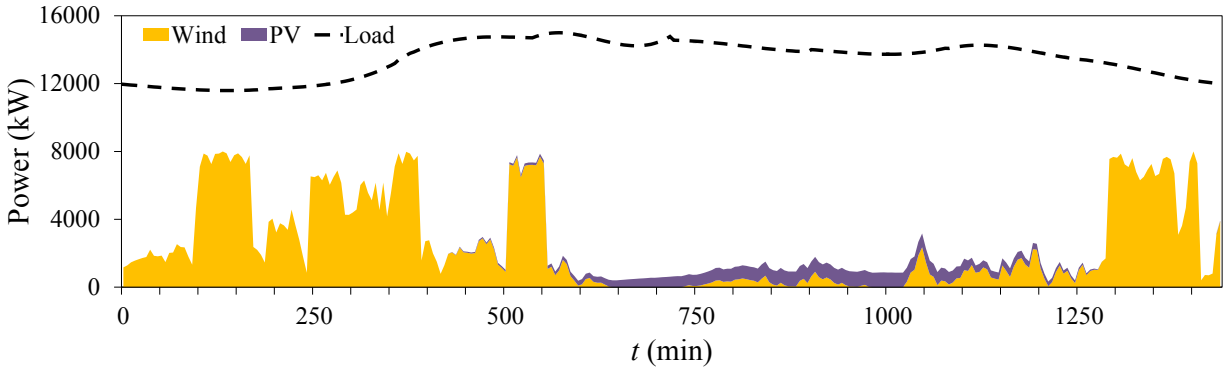

Figure 5.5: Wind, PV, and load forecasted values based on scaled measurements in an actual remote microgrid for Scenarios 2, 3, and 4.

Figure 5.6 shows the dispatch results obtained with the proposed and the conventional UC. Observe the differences in the UC and charging/discharging patterns of the ESS, which are magnified for two different dispatch windows; in addition, the dispatch difference of the diesel engines are shown in Figure 5.7. Note that these differences are significant when the net demand fluctuation is high, and low when the net demand fluctuation is also low.

The computation time and operation costs are reported in Table 5.3; the actual cost is calculated using the same method described in Scenario 1. Observe in Table 5.3 that the simulated cost of operating the system for 24 h in 5 min dispatch intervals for the proposed UC is \$168,148, whereas it is \$172,410 for the conventional UC; hence, under perfect forecast assumption and given that the system is operating in ILS control mode, dispatching the units using the proposed UC will reduce the operation cost by 2.47%, yielding a saving of \$4261 for the day. Also, note that the total computation time for the simulated 24 h of the proposed UC is similar to the conventional one.

Table 5.3: Proposed UC vs. Conventional UC for Scenario 2

UC	Obj. Function (\$)	Simulated Cost (\$)	Time (s)
Conv.	172,445	172,410	21
Prop.	168,148	168,148	65

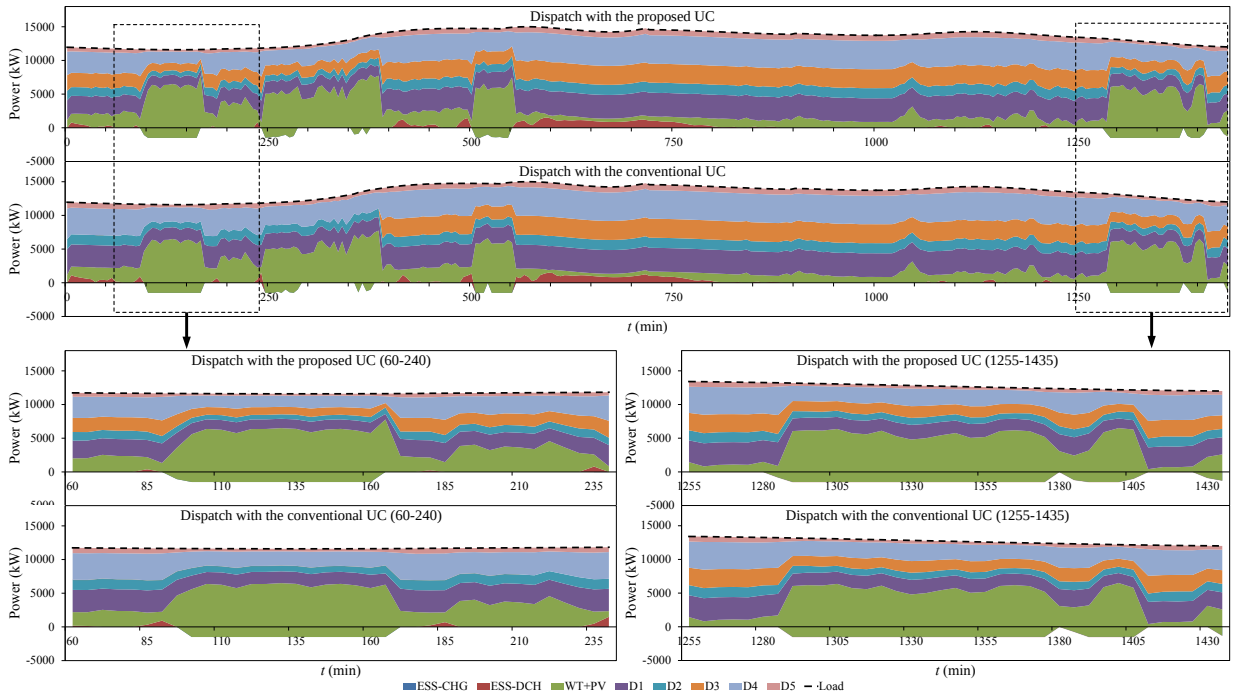

Figure 5.6: Dispatch results with the proposed and conventional UC for scenario 2.

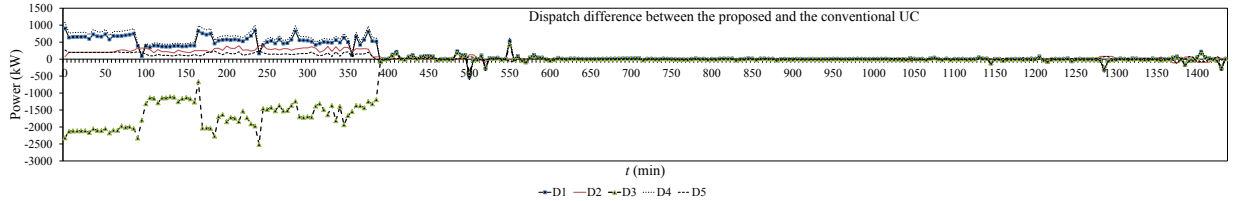

Figure 5.7: Dispatch differences with the proposed and the conventional UC for scenario 2.

5.2.3 Scenario 3: ILS Control with MPC

In this scenario, the same model as in Scenario 2 is used, but considering errors in the forecasted values of renewable energy and demand; these errors are computed assuming a cumulative density function (CDF) with a standard deviation obtained from a linear approximation of the difference between the current time step and the forecasted time step, as per [61]. To mitigate the impact of forecast inaccuracy, the optimal dispatch solutions obtained in each time step is only applied to the next time interval, and the problem is re-solved for the next time step with the updated forecast, repeating the process until the end of the 24 h, with a shrinking time horizon. This solution methodology is referred to

as a receding horizon approach [58].

The dispatch results obtained are shown in Figure 5.8, and the dispatch differences are shown in Figure 5.9. The solution and actual costs, and the computation times are reported in Table 5.4. Observe that using the proposed UC, the actual costs for operating the system would decrease by 0.6%, saving around $1000 for the day. Note also that the total computation time for the simulated 24h of the proposed method is reduced by around 50% compared to the conventional method.

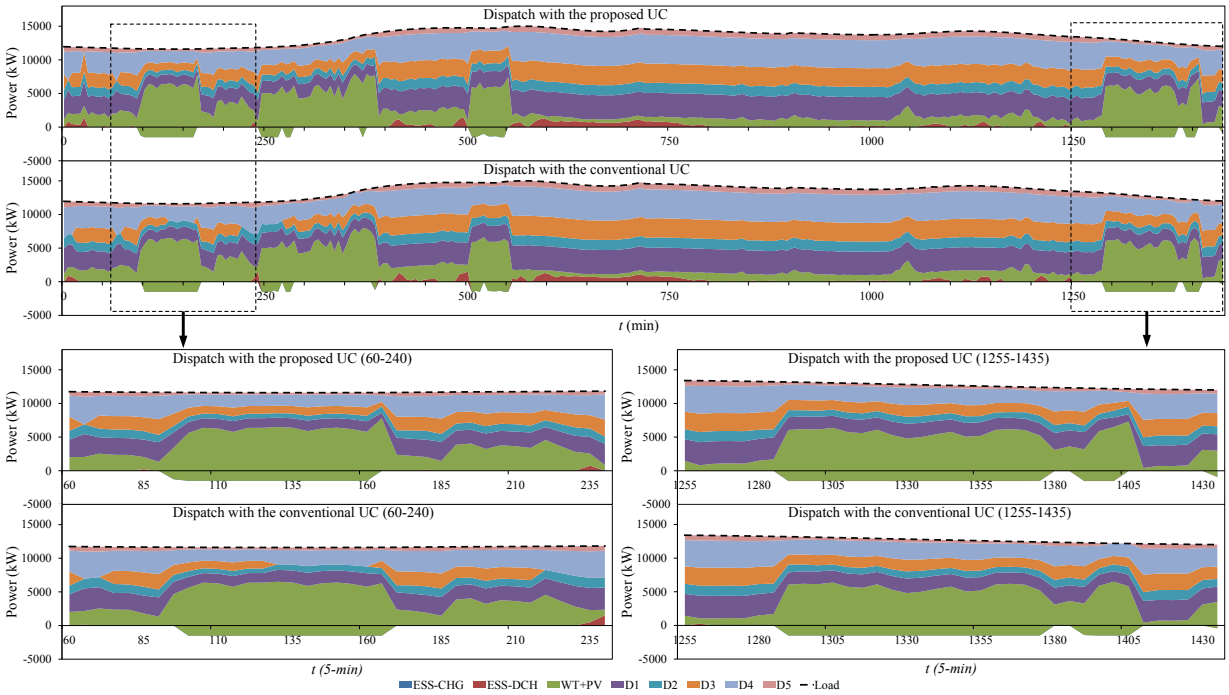

Figure 5.8: Dispatch results with the proposed and conventional UC for Scenario 3.

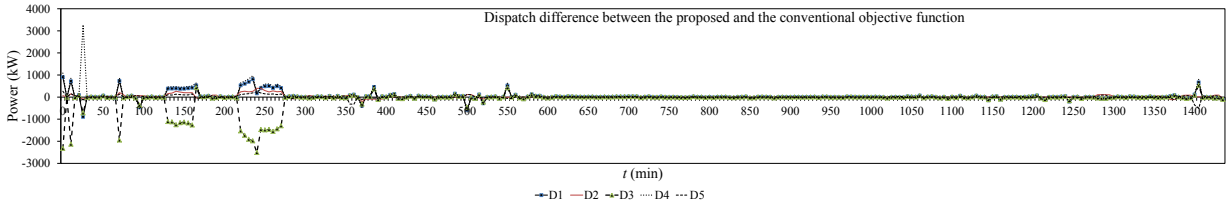

Figure 5.9: Dispatch differences with the proposed and the conventional UC for Scenario 3.

Table 5.4: Proposed UC vs. Conventional UC for Scenario 1

UC	Obj. Function ($)	Simulated Cost ($)	Time (s)
Conv.	169,852	169,843	5951
Prop.	168,855	168,855	2781

5.2.4 Scenario 4: Droop Control with MPC

In this Scenario, the same model as in Scenarios 2 and 3 is used, except that the diesel units are assumed to operate in droop control mode. Note that the errors for the forecasted values of renewable energy and demand are computed using the same CDF as in Scenario 3, yielding different error values compared to the previous case.

The dispatch results obtained are shown in Figure 5.10, and the dispatch differences are shown in Figure 5.11. The solution and actual costs and the computation times are reported in Table 5.5. Observe that using the proposed UC, the actual costs of operating the system would decrease by 1.15%, saving $1941 for the day. However, in this case the total computation time for the simulated 24 h is higher for the proposed UC, but still within online dispatch requirements.

Table 5.5: Proposed UC vs. Conventional UC for Scneario 4

UC	Obj. Function ($)	Simulated Cost ($)	Time (s)
Conv.	169,149	169,134	656
Prop.	167,193	167,193	1001

5.3 Discussions

5.3.1 Performance of Droop Control and ILS Control

From the results presented in Scenarios 3 and 4, in Section 5.2, it may seem that the UC formulation with droop control outperforms the UC formulation with ILS control, since the UC in the former case yields a smaller objective function and takes less computational time. However, this cannot be generalized, as the performance of the UC in droop control mode and ILS control mode depends on several factors such as the droop coefficients, the

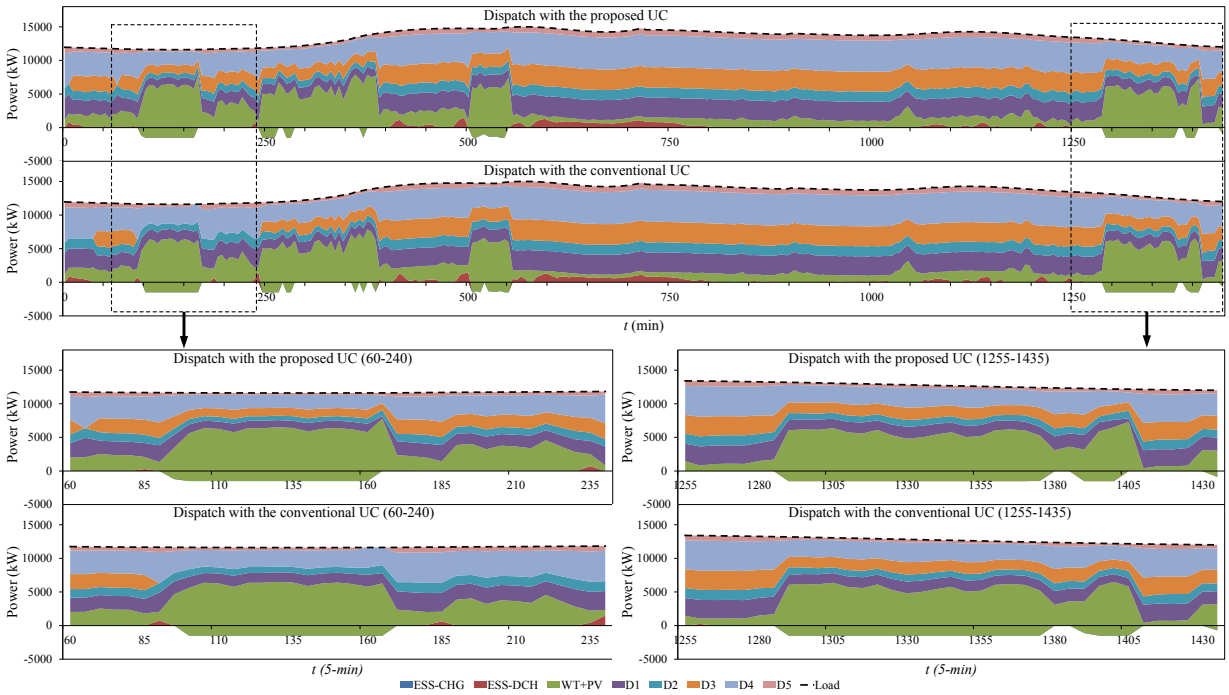

Figure 5.10: Dispatch results with the proposed and conventional UC for Scenario 4.

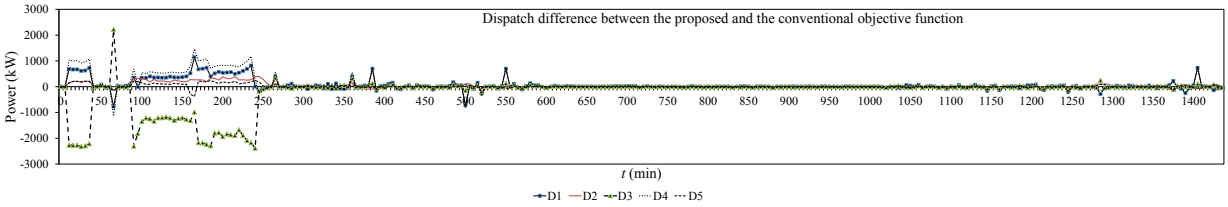

Figure 5.11: Dispatch differences with the proposed and the conventional UC for Scenario 4.

generators nominal rating, the forecasted values of renewable energy and demand, and other parameters.

5.3.2 Control Hierarchies

It is important to properly classify the proposed UC in the hierarchy of active power control. The active power control in isolated microgrids usually consists of two control levels [14]. The first level, or primary control, consists of local turbine governors and inverter controls that respond immediately to changes in the system, bringing the rate

of change of frequency to zero in a few seconds. Thus, primary controls are in charge of maintaining the system frequency stability.

In bulk power systems, Automatic General Control (AGC), or secondary control, takes care of frequency deviation, considering the power exchange among control areas. In isolated/islanded microgrids, AGC is not necessary in ILS mode, since the primary control does not cause frequency deviations in steady state. For droop control, the dispatch of units is used to recover the steady-state frequency; hence, the UC plays the role of AGC or secondary control in isolated/islanded microgrids, as discussed in [14].

5.3.3 Primary Control Performance of Droop vs. ILS

As mentioned in Section 5.1.1, primary control regulates the frequency, ensuring frequency stability in real-time. The proposed UC mathematically models and considers the impact of primary frequency control, so that it more accurately optimizes each DER output. From the primary control perspective, ILS control, in principle, exhibits a superior performance compared to droop control, since there is no steady state frequency deviation; however, in this case, DERs need to communicate their power output, which imposes additional communication requirements not needed in droop control. Note that in droop control operation, if the droop coefficients are chosen in reverse proportion to the generation units nominal rating, the load sharing would be exactly the same as in the ILS control mode; hence, there would be little difference in the immediate response of the two techniques.

5.4 Summary

In this chapter, a mathematical model that represented changes in the dispatchable unit outputs was proposed for isolated microgrids, for various frequency control techniques. The developed mathematical model was integrated into a UC model considering various operational constraints for a system with multiple DERs. In addition, typical reserve constraints were modified to ensure the feasibility of frequency regulation in the system. The mathematical model was kept linear to allow its integration into current utility EMS.

It was shown through several case studies in a complex isolated test microgrid that the conventional UC either over-estimated or under-estimated the energy required during each time interval, yielding dispatch levels that were not necessarily optimized for the actual required energy. By properly modelling the changes in the dispatchable unit outputs

considering their frequency regulation characteristics, it was demonstrated that the proposed method results in dispatch settings that were better optimized, yielding savings in operational costs. Finally, it was shown that adopting the proposed UC had no significant impact on computation times with respect to current utility practices.

The main content of this chapter has been published in [114].

Chapter 6

Conclusions, Contributions and Future Work

6.1 Summary

This thesis concentrated on the problem of frequency control in isolated microgrids. Specifically, the problem was investigated for two different system time-frames: transient dynamic time scale of 100 ms to a few seconds, and static dispatch time frame of 5 minutes. A comprehensive investigation of the effects of various frequency control techniques on transient and frequency stability of isolated microgrids under balanced and unbalanced conditions has been presented in this paper; based on these investigation, a practical voltage-based frequency controller has been proposed that offers several advantages and is easy to implement. In addition, the impact of frequency control techniques on the optimal dispatch of isolated microgrids had been investigated, and the problem of UC in these systems has been reformulated to account for the impact of frequency control.

In Chapter 2, a basic background review of microgrids and associated stability issues was provided; voltage and frequency control in isolated microgrids, as well as the formulation of UC in microgrids were also discussed. Thus, the definition of microgrids and basic related concepts of voltage and frequency stability were first introduced and discussed. Then, voltage and frequency control techniques were described in the context of isolated microgrids, including models of different components such as generator, governor, exciter, and inverters. Finally, a general formulation of UC models in microgrids was provided, discussing the objective function, equality and inequality constraints, and solution techniques.

In Chapter 3, conventional, transient, and angle droop controls were discussed. The performance of each control technique was evaluated through time domain simulations on a simple test system, and it was shown through simulation results that the transient droop control demonstrated better transient response, while angle droop control exhibited no steady-state deviation in the frequency response of the system. Following that, a new hybrid droop control was proposed based on the transient and angle droop control, showing that it has better transient and improved frequency response. In spite of the increased complexity in the tuning and implementation of the proposed controller, it has shown to have an overall superior performance that would justify its adoption instead of the other discussed controls.

In Chapter 4, a voltage-based frequency controller was proposed for isolated microgrids that makes use of the load voltage sensitivity to manipulate their consumption and thus compensate for power mismatches in the system. The performance of the proposed controller was evaluated using diesel-based and inverter-based isolated microgrids test systems. The simulation results showed that the VFC is efficient in controlling frequency and enhance the system damping, thus decreasing the system dependency on ESS.

In Chapter 5, a UC formulation was proposed for isolated microgrids that integrates in the mathematical formulation of different frequency controls, namely single unit, isochronous load sharing, and droop-based controls. The performance of the proposed UC was evaluated through various test scenarios. The simulation results showed that while the UC computation time is similar to the conventional UC, system dispatch is closer to reality resulting in more accurate and reduced operating costs.

The main conclusions of the presented work are:

- Manipulating loads consumption in an isolated microgrids through DERs voltage control is a viable solution for addressing the problem of frequency stability. Compared to large conventional systems, isolated microgrids are smaller, and hence it is possible to readily control DERs voltages throughout the system, given the relatively small voltage drops in the feeders.

- Eigenvalue studies show that the proposed VFC can improve system damping with proper controller tuning, as the dominant-poles of the system can be significantly affected by the controller.

- Time-domain simulations in PSCAD/EMTDC platform demonstrate the robust performance of the proposed VFC subject to various system disturbances. However, the VFC performance depends on the allowed voltage range and the loads voltage index.

- It is viable to have a 15% decrease in a residential load consumption by changing its operating voltage by 10%. Thus, the VFC can be seen as a virtual flywheel, with a capacity of up to 15% of the nominal load in the system. Hence, the VFC allows for a higher instantaneous penetration of renewable energies, thus saving fuel costs; the exact amount of fuel saved depends on the penetration of renewables, loading levels, and diesel engine efficiency.

- For isolated microgrids with a significant penetration of renewable energy, conventional UC either overestimates or underestimates the amount of energy for which DERs need to be optimized.

- The proposed UC, which accounts for the changes in the RES in the system in the UC problem, yields more accurate DERs dispatches, and alleviates the under/over estimation problem, for various frequency control techniques.

- The proposed UC reduces the operating cost of the system compared to a conventional UC; the exact savings depend on the system renewable penetration, system configuration, and renewable fluctuation.

6.2 Contributions

The main contributions of this thesis are the following:

- A state-of-the-art VFC has been developed for both diesel-based and inverter-based units in isolated micorgirds. The controller utilizes a load voltage regulation mechanism to manipulate the system demand, and consequently balance the power mismatch. The load voltage regulation is performed via diesel generator exciter systems and DER-based inverters, without the need for communication between different components of the system.

- A hybrid droop-based frequency controller has been designed for inverter-based isolated microgrids and the impact of various droop-based frequency control mechanisms on the transient response and stability of such systems has been studied and compared in detail.

- The impact of various frequency control mechanisms such as single unit control, droop control, or isochronous load sharing (ILS) control mode on optimal dispatch has been analyzed, using a novel UC model.

- A novel mathematical formulation of the frequency control mechanism integrated within a UC framework has been devised for isolated microgrids, yielding a more economical dispatch solution. The proposed formulation also allows to introduce a new reserve constraint in the UC model to represent the corresponding frequency control mechanism, considering intra-interval generation changes.

- A comprehensive dynamic and static simulation model of a CIGRE benchmark system for medium voltage distribution networks has been built to carry out time-domain and steady-state simulations to test and demonstrate the proposed frequency control techniques. Models of detailed voltage and frequency control systems, both for synchronous machines and inverters, have been developed.

The main contents of this thesis have been published in [94], [108], [109], [110], and [114].

6.3 Future Work

Future research may be carried out to address the following issues:

- The problem of voltage flickers during the VFC operation is not considered in the studies reported in this thesis; therefore, flickers during the VFC operation for a typical renewable energies output profile should be analyzed.

- The VFC proposed in this thesis compensates for steady-state frequency errors, essentially acting like an isochronous frequency controller; as a result, it cannot be used in parallel with another isochronous frequency controller. The use of a negative feedback loop added to the VFC control schematic, thus enabling it to work in parallel with another isochronous control unit, should be evaluated.

- A comprehensive study on the impact of the VFC on fuel saving in the system due to the higher renewable energies penetration should be carried out. Economic tools such as Homer or other developed codes would be suitable to perform such studies.

- Since the VFC is developed to avoid frequency instability in the system through voltage regulation, studies should be carried out to investigate the impact of different types of loads on the performance of the VFC, and the impact of the VFC on the protection scheme of the isolated microgrid.

- The proposed UC in this thesis does not include non-linear power flow constraints; thus, such constraints should be included to guarantee the feasibility of the optimal dispatch of DERs.

Bibliography

[1] R. H. Lasseter, C. M. A. Akhil, J. D. J. Stephens, R. Guttromson, A. Meliopoulous, and R. J. Yinger, "The CERTS microgrid concept," Transmission Reliability Program, Office of Power Technologies, US Department of Energy, Tech. Rep., 2002.

[2] R. H. Lasseter, J. H. Eto, B. Schenkman, J. Stevens, H. Vollkommer, D. Klapp, E. Linton, H. Hurtado, and J. Roy, "CERTS microgrid laboratory test bed," *IEEE Trans. Power Del.*, vol. 26, pp. 325–332, Jan. 2011.

[3] N. Hatziargyriou, H. Asano, R. Iravani, and C. Marnay, "Microgrids," *IEEE Power Energy Mag.*, vol. 5, no. 4, pp. 78–94, July 2007.

[4] World Energy Outlook. (2015) Electricity access database. [Online]. Available: http://www.worldenergyoutlook.org/resources/energydevelopment/energyaccessdatabase/

[5] M. Arriaga, C. Cañizares, and M. Kazerani, "Northern Lights: Access to Electricity in Canada's Northern and Remote Communities," *IEEE Power Energy Mag.*, vol. 12, no. 4, pp. 50–59, Aug. 2014.

[6] *IEEE Guide for Design, Operation, and Integration of Distributed Resource Island Systems with Electric Power Systems*, IEEE Std. 1547.4, 2011.

[7] J. M. Guerrero, F. Blaabjerg, T. Zhelev, K. Hemmes, E. Monmasson, S. Jemei, M. P. Comech, R. Granadino, and J. I. Frau, "Distributed generation: toward a new energy paradigm," *IEEE Ind. Electron. Mag.*, pp. 52–64, Mar. 2010.

[8] E. Barklund, N. Pogaku, M. Prodanovic, C. Hernandez-Aramburo, and T. C. Green, "Energy management in autonomous microgird using stability-constrained droop control of inverters," *IEEE Trans. Power Electron.*, vol. 23, no. 5, pp. 2346–2353, Sep. 2008.

[9] C. K. Sao and P. W. Lehn, "Control and power management of converter fed microgrids," *IEEE Trans. Power Syst.*, vol. 23, no. 3, pp. 1088–1098, Aug. 2008.

[10] G. Delille, B. Francois, and G. Malarange, "Dynamic Frequency Control Support by Energy Storage to Reduce the Impact of Wind and Solar Generation on Isolated Power System's Inertia," *IEEE Trans. Sustain. Energy*, vol. 3, no. 4, pp. 931–939, Oct. 2012.

[11] G. Lalor, A. Mullane, and M. O'Malley, "Frequency control and wind turbine technologies," *IEEE Trans. Power Syst.*, vol. 20, no. 4, pp. 1905–1913, Nov. 2005.

[12] C. Yuen, A. Oudalov, and A. Timbus, "The Provision of Frequency Control Reserves From Multiple Microgrids," *IEEE Trans. Ind. Electron.*, vol. 58, no. 1, pp. 173–183, Jan. 2011.

[13] K. Strunz, "Developing benchmark models for studying the integration of distributed energy resources," in *Proc. IEEE Power Eng. Soc. Gen. Meeting*, Montreal, QC, Jul. 2006.

[14] D. E. Olivares, A. Mehrizi-Sani, A. H. Etemadi, C. A. Cañizares, R. Iravani, M. Kazerani, A. H. Hajimiragha, O. Gomis-Bellmunt, M. Saeedifard, R. Palma-Behnke *et al.*, "Trends in Microgrid Control," *IEEE Trans. Smart Grid*, vol. 5, no. 4, pp. 1905–1919, May 2014.

[15] UCTE ad-hoc Group, "Frequency Quality Investigation," ENTSO-e, Brussels, Belgium, Tech. Rep., Aug. 2008, [Online]. Available: https://www.entsoe.eu/fileadmin/user_upload/_library/publications/ce/otherreports/090330_UCTE_FrequencyInvestigationReport_Abstract.pdf.

[16] P. Kundur, *Power System Stability and Control*. New York: McGraw Hill, 1994.

[17] Y. G. Rebours, D. S. Kirschen, M. Trotignon, and S. Rossignol, "A survey of frequency and voltage control ancillary services part I: Technical features," *IEEE Trans. Power Syst.*, vol. 22, no. 1, pp. 350–357.

[18] Z. Xu, M. Togeby, and J. Østergaard, "Demand as frequency controlled reserve: Final report of the PSO project," Technical University of Denmark, Tech. Rep., 2008.

[19] J. M. Guerrero, M. Chandorka, T. Lee, and P. C. Loh, "Advanced Control Architectures for Intelligent Microgrids–Part I: Decentralized and Hierarchical Control," *IEEE Trans. Ind. Electron.*, vol. 60, no. 4, pp. 1254–1262, Apr. 2012.

[20] J. M. Guerrero, P. C. Loh, T. Lee, and M. Chandorkar, "Advanced Control Architectures for Intelligent Microgrids–Part II: Power Quality, Energy Storage, and AC/DC Microgrids," *IEEE Trans. Ind. Electron.*, vol. 60, no. 4, pp. 1263–1270, Apr. 2012.

[21] F. A. Bhuiyan and A. Yazdani, "Multimode control of DFIG-based wind power unit for remote applications," *IEEE Trans. Power Del.*, vol. 24, no. 4, pp. 2079–2089, Sep. 2009.

[22] A. L. Dimeas and N. D. Hatziargyriou, "Operation of a multi-agent system for microgrid control," *IEEE Trans. Power Syst.*, vol. 20, no. 3, pp. 1447–1455, Aug. 2005.

[23] J. A. P. Lopes, C. L. Moreira, and A. G. Madureira, "Defining control strategies for microgrids islanded operation," *IEEE Trans. Power Syst.*, vol. 21, no. 2, pp. 916–924, May 2006.

[24] A. G. Tsikalakis and N. D. Hatziargyriou, "Centralized control for optimizing microgrids operation," *IEEE Trans. Energy Convers.*, vol. 23, no. 1, pp. 243–248, Feb. 2008.

[25] A. Mehrizi-Sani and R. Iravani, "Potential-Function based control of a microgrid in islanded and grid-connected modes," *IEEE Trans. Power Syst.*, vol. 25, no. 4, pp. 1883–1891, Oct. 2010.

[26] J. M. Carrasco, L. G. Franquelo, J. T. Bialasiewicz, E. Galvan, R. C. P. Guisado, M. A. M. Prats, J. I. Leon, and N. Moreno-Alfonso, "Power-electronic systems for the grid integration of renewable energy sources: A survey," *IEEE Trans. Ind. Electron.*, vol. 53, no. 4, pp. 1002–1016, Aug. 2006.

[27] N. Pogaku, M. Prodanovic, and T. C. Green, "Modeling, analysis and testing of autonomous operation of an inverter-based microgrid," *IEEE Trans. Power Electron.*, vol. 22, no. 2, pp. 613–625, March 2007.

[28] J. G. de Matos, F. S. F. e Silva, and L. A. de S. Ribeiro, "Power control in AC isolated microgrids with renewable energy sources and energy storage systems," *IEEE Trans. Ind. Electron.*, vol. 62, no. 6, pp. 3490–3498, June 2015.

[29] F. Katiraei and M. R. Iravani, "Power management strategies for a microgrid with multiple distributed generation units," *IEEE Trans. Power Syst.*, vol. 21, no. 4, pp. 1821–1831, Oct. 2006.

[30] M. . Marwali, J. W. Jung, and A. Keyhani, "Control of distributed generation systems - Part II: Load sharing control," *IEEE Trans. Power Electron.*, vol. 19, no. 6, pp. 1551–1561, Nov. 2004.

[31] M. C. Chandorkar, D. M. Divan, and R. Adapa, "Control of parallel connected inverters in standalone ac supply systems," *IEEE Trans. Ind. Appl.*, vol. 29, no. 1, pp. 136–143, Jan. 1993.

[32] M. N. Marwali, M. Dai, and A. Keyhani, "Robust stability analysis of voltage and current control for distributed generation systems," *IEEE Trans. Energy Convers.*, vol. 21, no. 2, pp. 516–526, Jun. 2006.

[33] ——, "Stability analysis of load sharing control for distributed generation systems," *IEEE Trans. Energy Convers.*, vol. 22, no. 3, pp. 737–745, Sep. 2007.

[34] G. F. Franklin, M. L. Workman, and D. Powell, *Digital control of dynamic systems*. Addison-Wesley Longman Publishing Inc., 1997.

[35] J. M. Guerrero, L. G. de Vecuna, J. Matas, M. Castilla, and J. Miret, "A wireless controller to enhance dynamic performance of parallel inverters in distributed generation systems," *IEEE Trans. Power Electron.*, vol. 19, no. 5, pp. 1205–1213, Sep. 2004.

[36] R. Majumder, B. Chaudhuri, A. Ghosh, R. Majumder, G. Ledwich, and F. Zare, "Improvement of stability and load sharing in an autonomous microgrid using supplementary droop control loop," *IEEE Trans. Power Syst.*, vol. 25, no. 2, pp. 796–808, Apr. 2010.

[37] Y. A.-R. I. Mohamed and E. F. El-Saadany, "Adaptive decentralized droop controller to preserve power sharing stability of paralleled inverters in distributed generation microgrids," *IEEE Trans. Power Electron.*, vol. 23, no. 6, pp. 2806–2816, Nov. 2008.

[38] J. Kim, J. M. Guerrero, P. Rodriguez, R. Teodorescu, and K. Nam, "Mode Adaptive Droop Control With Virtual Output Impedances for an Inverter-Based Flexible AC Microgrid," *IEEE Trans. Power Electron.*, vol. 26, no. 3, pp. 689–701, Nov. 2010.

[39] R. Majumder, G. Ledwich, A. Ghosh, S. Chakrabarti, and F. Zare, "Droop Control of Converter-Interfaced Microsources in Rural Distributed Generation," *IEEE Trans. Power Del.*, vol. 25, no. 4, pp. 2768–2778, March 2010.

[40] R. Majumder, A. Ghosh, G. Ledwich, and F. Zare, "Load sharing and power quality enhanced operation of a distributed microgrid," *IET Renew. Power Gener.*, vol. 3, no. 2, pp. 109–119, June 2009.

[41] K. D. Brabandere, B. Bolsens, J. V. den Keybus, A. Woyte, J. Driesen, and R.Belmans, "A voltage and frequency droop control method for parallel inverters," *IEEE Trans. Power Syst.*, vol. 22, no. 4, pp. 1107–1115, Jul. 2007.

[42] S. Chiang, C. Yen, and K. Chang, "A multimodule parallelable series-connected PWM voltage regulator," *IEEE Trans. Ind. Electron.*, vol. 48, no. 3, pp. 506–516, Aug. 2002.

[43] J. Zhao, X. Lyu, Y. Fu, X. Hu, and F. Li, "Coordinated microgrid frequency regulation based on DFIG variable coefficient using virtual inertia and primary frequency control," *IEEE Trans. Energy Convers.*, vol. 31, no. 3, pp. 833–845, Sep. 2016.

[44] M. F. M. Arani and E. F. El-Saadany, "Implementing virtual inertia in DFIG-based wind power generation," *IEEE Trans. Power Syst.*, vol. 28, no. 2, pp. 1373–1384, May 2013.

[45] F. C. Schweppe, R. D. Tabors, J. L. Kirtley, H. R. Outhred, F. H. Pickel, and A. J. Cox, "Homeostatic utility control," *IEEE Trans. Power App. Syst.*, vol. 99, no. 3, pp. 1151–1163, May 1980.

[46] D. J. Hammerstrom, J. Brous, D. P. Chassin, G. R. Horst, R. Kajfasz, P. Michie, T. Oliver, T. A. Carlon, C. Eustis, O. M. Jervegren *et al.*, "Part II. Grid Friendly™ appliance Project," Pacific Northwest National Laboratory, Richland, Washington, Tech. Rep. PNNL-17079, Oct. 2007.

[47] A. Molina-Garcia, F. Bouffard, and D. Kirschen, "Decentralized Demand-Side Contribution to Primary Frequency Control," *IEEE Trans. Power Syst.*, vol. 26, no. 1, pp. 411–419, Feb. 2011.

[48] K. Pamdiaraj, P. Taylor, N. Jenkins, and C. Robb, "Distributed load control of autonomous renewable energy systems," *IEEE Trans. Energy Convers.*, vol. 16, no. 1, pp. 14–19, Mar. 2001.

[49] J. A. Short, D. G. Infield, and L. L. Ferris, "Stabilization of grid frequency through dynamic demand control," *IEEE Trans. Power Syst.*, vol. 23, no. 3, pp. 1284–1293, Aug. 2007.

[50] G. Delille, J. Yuan, and L. Capely, "Taking advantage of load voltage sensitivity to stabilize power system frequency," in *Proc. IEEE PowerTech Conf.*, June 2013, pp. 1–6.

[51] G. Delille, L. Capely, D. Souque, and C. Ferrouillat, "Experimental validation of a novel approach to stabilize power system frequency by taking advantage of load voltage sensitivity," in *Proc. IEEE PowerTech Conf.*, June 2015, pp. 1–6.

[52] A. G. Expósito, A. J. Conejo, and C. A. Cañizares, *Electric Energy Systems: Analysis and Operation*. New York, US: CRC Press, 2008.

[53] C. A. H. Aramburo, T. C. Green, and N. Mugniot, "Fuel consumption minimization of a microgrid," *IEEE Trans. Ind. Appl.*, vol. 41, no. 3, pp. 673–681, June 2005.

[54] C. Chen, S. Duan, T. Cai, B. Liu, and G. Hu, "Smart energy management system for optimal microgrid economic operation," *IET Renew. Power Gener.*, vol. 5, no. 3, pp. 258–267, May 2011.

[55] E. F. Camacho and C. B. Alba, *Model Predictive Control*. London, UK: Springer-Verlag, 2013.

[56] R. Palma-Behnke, C. Benavides, F. Lanas, B. Severino, L. Reyes, J. Llanos, and D. Saez, "A microgrid energy management system based on the rolling horizon strategy," *IEEE Trans. Smart Grid*, vol. 4, no. 2, pp. 994–1006, Jan. 2013.

[57] D. E. Olivares, "Robust Energy Management Systems for Isolated Microgrids Under Uncertainty," Ph.D. dissertation, University of Waterloo, Waterloo, ON, 2014.

[58] D. E. Olivares, C. A. Cañizares, and M. Kazerani, "A centralized energy management system for isolated microgrids," *IEEE Trans. Smart Grid*, vol. 5, no. 4, pp. 1864–1875, April 2014.

[59] D. E. Olivares, J. D. Lara, C. A. Cañizares, and M. Kazerani, "Stochastic-predictive energy management system for isolated microgrids," *IEEE Trans. Smart Grid*, vol. 6, no. 6, pp. 2681–2693, Nov. 2015.

[60] J. D. Lara, "An Energy Management System for Isolated Microgrids Considering Uncertainty," Master's thesis, University of Waterloo, Waterloo, ON, 2014.

[61] B. V. Solanki, A. Raghurajan, K. Bhattacharya, and C. A. Cañizares, "Including smart loads for optimal demand response in integrated energy management systems for isolated microgrids," *IEEE Trans. Smart Grid*, no. pre-print, pp. 1–10, Dec. 2015.

[62] Y. C. Wu, M. J. Chen, J. Y. Lin, W. S. Chen, and W. L. Huang, "Corrective economic dispatch in a microgrid," *Int. J. Numer. Model. Electron. Netw. Devices Fields*, vol. 26, no. 2, pp. 140–150, June 2012.

[63] J. W. O'Sullivan and M. J. O'Malley, "A new methodology for the provision of reserve in an isolated power system," *IEEE Trans. Power Syst.*, vol. 14, no. 2, pp. 519–524, May 1999.

[64] G. W. Chang, C. Ching-Sheng, L. Tai-Ken, and W. Ching-Chung, "Frequency-regulating reserve constrained unit commitment for an isolated power system," *IEEE Trans. Power Syst.*, vol. 28, no. 2, pp. 578–586, Aug. 2012.

[65] A. H. Hajimiragha, M. R. D. Zadeh, and S. Moazeni, "Microgrids frequency control considerations within the framework of the optimal generation scheduling problem," *IEEE Trans. Smart Grid*, vol. 6, no. 2, pp. 534–547, March 2013.

[66] G. X. Guan, F. Gao, and A. J. Svoboda, "Energy delivery capacity and generation scheduling in the deregulated electric power market," *IEEE Trans. Power Syst.*, vol. 15, no. 4, pp. 1275–1280, Nov. 2000.

[67] Y. Yang, J. Wang, X. Guan, and Q. Zhai, "Subhourly unit commitment with feasible energy delivery constraints," *Appl. Energy*, vol. 96, pp. 245–252, Aug. 2012.

[68] G. Morales-Espana, A. Ramos, and J. Garcia-Gonzalez, "An MIP formulation for joint market-clearing of energy and reserves based on ramp scheduling," *IEEE Trans. Power Syst.*, vol. 29, no. 1, pp. 476–488, May 2013.

[69] H. Karimi, H. Nikkhajoei, and M. R. Iravani, "Control of an electronically-coupled distributed resource unit subsequent to an islanding event," *IEEE Trans. Power Del.*, vol. 23, no. 1, pp. 493–501, Jan. 2008.

[70] F. Katiraei, M. R. Iravani, and P. W. Lehn, "Micro-grid autonomous operation during and subsequent to islanding process," *IEEE Trans. Power Del.*, vol. 20, no. 1, pp. 248–257, Jan. 2005.

[71] P. Kundur, J. Paserba, V. Ajjarapu, G. Andersson, A. Bose, C. Cañizares *et al.*, "Definition and classification of power system stability IEEE/CIGRE joint task force on stability terms and definitions," *IEEE Trans. Power Syst.*, vol. 19, no. 3, pp. 1387–1401, Aug. 2004.

[72] P. Kundur, D. C. Lee, J. P. Bayne, and P. L. Dandeno, "Impact of turbine generator controls on unit performance under system disturbance conditions," *IEEE Trans. Power App. Syst.*, vol. 5, no. 6, pp. 28–29, July 2010.

[73] Y. A.-R. I. Mohamed and A. A. Radwan, "Hierarchical control system for robust microgrid operation and seamless mode transfer in active distribution systems," *IEEE Trans. Smart Grid*, vol. 2, no. 2, pp. 352–362, Jan. 2011.

[74] M. D. Ilic and S. X. Liu, *Hierarchical Power Systems Control: its value in a changing industry*. Springer Science & Business Media, 2012.

[75] J. M. Guerrero, J. C. Vasquez, J. Matas, L. G. de Vicuna, and M. Castilla, "Hierarchical control of droop-controlled AC and DC microgrids A general approach toward standardization," *IEEE Trans. Ind. Electron.*, vol. 58, no. 1, pp. 158–172, Dec. 2010.

[76] Y. Li and C. N. Kao, "An accurate power control strategy for power electronics-interfaced distributed generation units operating in a low-voltage multibus microgrid," *IEEE Trans. Power Electron.*, vol. 24, no. 12, pp. 2977–2988, Dec. 2009.

[77] H. Saadat, *Power System Analysis: Third Edition*. PSA Publishing, 2010.

[78] IEEE Committee Report, "Proposed excitation systems definitions for synchronous machines," *IEEE Trans. Power App. Syst.*, vol. 88, no. 8, pp. 1248–1258, Jan. 2007.

[79] ——, "Excitation system model for power system stability studies," *IEEE Trans. Power App. Syst.*, vol. 100, no. 2, pp. 494–509, Feb. 2007.

[80] J. Rocabert, A. Luna, F. Blaabjerg, and P. Rodriguez, "Control of power converters in AC microgrids," *IEEE Trans. Power Electron.*, vol. 27, no. 11, pp. 4734–4749, Nov. 2012.

[81] S. M. Ashabani and Y. A.-R. I. Mohamed, "New family of microgrid control and management strategies in smart distribution gridsanalysis, comparison and testing," *IEEE Trans. Power Syst.*, vol. 29, no. 5, pp. 2257–2269, Sep. 2014.

[82] J. C. Vasquez, J. M. Guerrero, A. Luna, P. Rodriguez, and R. Teodorescu, "Adaptive droop control applied to voltage-source inverters operating in grid-connected and islanded modes," *IEEE Trans. Ind. Electron.*, vol. 56, no. 10, pp. 4088–4096, Oct. 2009.

[83] J. M. Guerrero, J. Matas, L. G. de Vicuna, M. Castilla, and J. Miret, "Wireless-control strategy for parallel operation of distributed-generation inverters," *IEEE Trans. Ind. Electron.*, vol. 53, no. 5, pp. 1461–1470, Oct. 2006.

[84] J. T. Bialasiewicz, "Renewable energy systems with photovoltaic power generators: Operation and modeling," *IEEE Trans. Ind. Electron.*, vol. 55, no. 7, pp. 2752–2758, July 2008.

[85] A. K. Abdelsalam, A. M. Massoud, S. Ahmed, and P. N. Enjeti, "High-performance adaptive perturb and observe MPPT technique for photovoltaic-based microgrids," *IEEE Trans. Power Electron.*, vol. 26, no. 4, pp. 1010–1021, Apr. 2011.

[86] H. Kanchev, F. Colas, V. Lazarov, and B. Francois, "Emission reduction and economical optimization of an urban microgrid operation including dispatched pv-based active generators," *IEEE Trans. Sustain. Energy*, vol. 5, no. 4, pp. 1397–1405, July 2014.

[87] "IBM ILOG CPLEX V12.1 User's Manual for CPLEX," International Business Machines Corporation, Tech. Rep., 2009, [Online]. Available: ftp://public.dhe.ibm.com/software/websphere/ilog/docs/optimization/cplex/ps_usrmancplex.pdf.

[88] N. Padhy, "Unit commitment a bibliographical survey," *IEEE Trans. Power Syst.*, vol. 19, no. 2, pp. 1196–1205, May 2004.

[89] P. G. Lowery, "Generating unit commitment by dynamic programming," *IEEE Trans. Power App. Syst.*, vol. 85, no. 5, pp. 422–426, Jan. 2007.

[90] S. Virmani, E. C. Adrian, K. Imhof, and S. Mukherjee, "Implementation of a lagrangian relaxation based unit commitment problem," *IEEE Trans. Power Syst.*, vol. 4, no. 4, pp. 1373–1380, Aug. 2002.

[91] Z. Ouyang and S. M. Shahidehpour, "A hybrid artificial neural network-dynamic programming approach to unit commitment," *IEEE Trans. Power Syst.*, vol. 7, no. 1, pp. 236–242, Aug. 2002.

[92] R. Majumder, A. Ghosh, G. Ledwich, and F. Zare, "Angle droop versus frequency droop in a voltage source converter based autonomous microgrid," in *Proc. of IEEE Power Eng. Soc. gen. Meeting*, July 2009, pp. 1–8.

[93] *User's Guide on the use of PSCAD.* Winnipeg, MB, Canada: Manitoba HVDC Research Centre, 2010.

[94] M. Farrokhabadi, C. A. Cañizares, and K. Bhattacharya, "Evaluation of droop-based controls in an islanded microgrid with electronically interfaced distributed energy resources," in *Proc. IEEE PowerTech Conf.*, Eindhoven, Netherlands, June 2015, pp. 1–6.

[95] A. J. Collin, G. Tsagarakis, A. E. Kiprakis, and S. McLaughlin, "Development of Low-Voltage Load Models for the Residential Load Sector," *IEEE Trans. Power Syst.*, vol. 29, no. 5, pp. 2180–2188, Feb. 2014.

[96] E. Nasr-Azadani, C. A. Cañizares, D. E. Olivares, and K. Bhattacharya, "Stability Analysis of Unbalanced Distribution Systems With Synchronous Machine and DFIG Based Distributed Generators," *IEEE Trans. Smart Grid*, vol. 5, no. 5, pp. 2326–2338, Sep. 2014.

[97] H. Ghasemi, "On-Line Monitoring and Oscillatory Stability Margin Prediction in Power Systems Based on System Identification," Ph.D. dissertation, Univ. of Waterloo, Waterloo, ON, Aug. 2006.

[98] J. R. Smith, F. Fatehi, C. S. Woods, J. F. Hauer, and D. J. Trudnowski, "Transfer function identification in power system applications," *IEEE Trans. Power Syst.*, vol. 8, no. 3, pp. 1282–1290, Aug. 1993.

[99] *IEEE Recommended Practice for Excitation System Models for Power System Stability Studies*, IEEE Std. 421.5, 1992.

[100] J. Graf, *PID Control: Ziegler-Nichols Tuning.* CreateSpace Independent Publishing Platform, 2013.

[101] "Distributed Generation Technical Interconnection Requirements: Interconnections at Voltages 50kV and Below," Hydro One Networks INC., Toronto, Ontario, Tech. Rep. DT-10-015 R3, Mar. 2013.

[102] O. Tramblay, L. A. Dessaint, and A. I. Dekkiche, "A Generic Battery Model for the Dynamic Simulation of Hybrid Electric Vehicles," in *Proc. IEEE Vehicle Power and Propulsion Conf.*, Arlington, TX, Sep. 2007.

[103] A. A. Akhil, G. Huff, A. B. Currier, B. C. Kaun, D. M. Rastler, S. B. Chen, A. L. Cotter, D. T. Bradshaw, and W. D. Gauntlett, "DOE/EPRI 2013 Electricity Storage Handbook in Collaboration with NRECA," Sandia National Laboratories, Livermore, California, Tech. Rep. SAND2013-5131, July 2013.

[104] Z. Wang and J. Wang, "Review on implementation and assessment of conservation voltage reduction," *IEEE Trans. Power Syst.*, vol. 29, no. 3, pp. 1306–1315, May 2014.

[105] J. C. Erickson and S. R. Gilligan, "The effects of voltage reduction on distribution circuit loads," *IEEE Trans. Power App. Syst.*, vol. 101, no. 7, pp. 2014–2018, July 1982.

[106] V. J. Warnock and T. L. Kirkpatrick, "Impact of voltage reduction on energy and demand: Phase ii," *IEEE Trans. Power Syst.*, vol. 1, no. 2, pp. 92–95, May 1986.

[107] Z. Wang, M. Begovic, and J. Wang, "Analysis of conservation voltage reduction effects based on multistage svr and stochastic process," *IEEE Trans. Smart Grid*, vol. 5, no. 1, pp. 431–439, Jan. 2014.

[108] M. Farrokhabadi, C. A. Cañizares, and K. Bhattacharya, "Frequency control in isolated/islanded microgrids through voltage regulation," *IEEE Trans. Smart Grid*, no. pre-print, pp. 1–10, Oct. 2015.

[109] ——, "A voltage-based frequency controller for inverter-based systems in microgrids," in *Proc. IEEE Power Eng. Soc. Gen. Meeting*, Boston, MA, July 2016, pp. 1–5.

[110] ——, "Voltage-based Frequency Controller (VFC)," Invention Disclosure Form, Mar. 2016, Hatch Ltd., Canada.

[111] C. A. Floudas, *Nonlinear and Mixed-Integer Optimization: Fundamentals and Applications*. Oxford, UK: Oxford University Press, 1999.

[112] R. E. Rosenthal, *GAMS – A User's Guide*. Washington, DC, USA: GAMS Development Corporation, 2016.

[113] M. Arriaga and C. A. Cañizares, "Overview and analysis of data for microgrid at kasabonika lake first nation (KLFN)," Hatch Project Confidential Report, University of Waterloo, Tech. Rep., Sep. 2015.

[114] M. Farrokhabadi, C. A. Cañizares, and K. Bhattacharya, "Unit commitment for isolated microgrids considering frequency control," *IEEE Trans. Smart Grid*, no. pre-print, pp. 1–11, Oct. 2016.

APPENDIX

Test System Parameters

Table 1: Governor and AGC

Parameters	Value
Dead Band	0 pu
K_g	20 1/pu
τ_{SR}	0.1 s
τ_{SM}	0.2 s
P_{up}	0.40 pu/s
P_{down}	-0.5 pu/s
C_{max}	1.0 s
C_{min}	0 pu
K_{AGC}	1 pu
τ_{AGC}	1 s

Table 2: Synchronous Machine and AVR

Parameters	Value
R_a	0.0051716 pu
X_l	0.14 pu
X_d	1.014 pu
X_q	0.77 pu
X'_d	0.314 pu
X'_q	0.375 pu
$X"_d$	0.28 pu
$X"_q$	0.375 pu
T'_{d0}	6.55 s
T'_{q0}	0.85 s
$T"_{d0}$	0.039 s
$T"_{q0}$	0.071 s
ω_n	376.992 rad/s
H	3.117 s
K_F	0.03 pu
τ_E	0.8 s
τ_F	1.0 s
K_E	1 pu

Table 3: Line Parameters for the CIGRE Test System

Node From	Node To	R'_{ph} Ω/km	X'_{ph} Ω/km	B'_{ph} μS/km	R'_0 Ω/km	X'_0 Ω/km	B'_{ph} μS/km	l km
1	2	0.173	0.432	3.83	0.351	1.8	1.57	1.2
2	3	0.173	0.432	3.83	0.351	1.8	1.57	1
3	4	0.173	0.432	3.83	0.351	1.8	1.57	0.61
4	5	0.173	0.432	3.83	0.351	1.8	1.57	0.56
5	6	0.173	0.432	3.83	0.351	1.8	1.57	1.54
6	7	0.173	0.432	3.83	0.351	1.8	1.57	0.24
7	8	0.173	0.432	3.83	0.351	1.8	1.57	1.67
8	9	0.173	0.432	3.83	0.351	1.8	1.57	0.32
9	10	0.173	0.432	3.83	0.351	1.8	1.57	0.77
10	11	0.173	0.432	3.83	0.351	1.8	1.57	0.33
11	4	0.173	0.432	3.83	0.351	1.8	1.57	0.49
3	8	0.173	0.432	3.83	0.351	1.8	1.57	1.3
12	13	0.173	0.432	3.83	0.351	1.8	1.57	4.89
13	14	0.173	0.432	3.83	0.351	1.8	1.57	2.99
14	8	0.173	0.432	3.83	0.351	1.8	1.57	2

Table 4: Loads Apparent Power for the CIGRE Test System

(a) Phase a

Node	Residential	Commercial/Ind.
1	subnetwork*	—
2	100	200
3	—	80
4	200	—
5	200	50
6	50	—
7	—	100
8	100	—
9	100	—
10	150	—
11	50	150
12	subnetwork*	80
13	—	145
14	—	90

(b) Phase b

Node	Residential	Commercial/Ind.
1	—	100
2	500	200
3	200	80
4	100	—
5	subnetwork*	200
6	100	—
7	100	100
8	150	—
9	150	—
10	100	—
11	50	150
12	subnetwork*	80
13	—	145
14	—	90

(c) Phase c

Node	Residential	Commercial/Ind.
1	200	100
2	—	200
3	50	80
4	100	—
5	—	50
6	subnetwork*	—
7	—	100
8	—	200
9	100	—
10	250	—
11	—	150
12	—	80
13	—	145
14	subnetwork*	90

(d) Power Factor

Node	Residential	Commercial/Ind.
1	0.90	0.80
2	0.95	0.85
3	0.90	0.80
4	0.90	—
5	0.95	0.85
6	0.95	—
7	0.95	0.95
8	0.90	0.90
9	0.95	—
10	0.90	—
11	0.95	0.85
12	0.90	0.80
13	0.95	0.85
14	0.90	0.90

* Subnetwork demand is 172 kVA with a power factor of 0.95.